STATIC AND FATIGUE BEHAVIOUR OF THERMOPLASTIC COMPOSITE LAMINATES JOINED BY RESISTANCE WELDING

MARTINE DUBÉ
DEPARTMENT OF MECHANICAL ENGINEERING

McGILL UNIVERSITY, MONTRÉAL
SEPTEMBER 2007

A THESIS SUBMITTED TO McGILL UNIVERSITY IN PARTIAL FULFILMENT OF THE REQUIREMENTS OF THE DEGREE OF PHILOSOPHIAE DOCTOR

ACKNOWLEDGEMENTS

Je tiens tout d'abord à adresser mes sincères remerciements à mon superviseur, le Prof. Pascal Hubert qui m'a dispensé de précieux conseils tout au long de ce projet. Par-dessus tout, je voudrais le remercier pour son dynamisme et ses encouragements qui m'ont été d'un soutient moral essentiel à la réussite d'un tel projet. Merci Pascal!

I would like to gratefully acknowledge Dr. Ali Yousefpour for allowing me to collaborate with the Aerospace Manufacturing and Technology Centre. Dr. Yousefpour has been a thorough collaborator since the beginning of this project and his numerous technical advices were invaluable.

Je tiens également à remercier le Dr. Johanne Denault pour m'avoir permis d'établir une collaboration avec l'Institut des matériaux industriels il y a déjà plusieurs années. C'est en grande partie grâce au Dr. Denault que j'ai décidé d'entreprendre ce projet de doctorat et je lui en suis grandement reconnaissante.

I would also like to acknowledge my colleagues from the Design and Production of Composite Structures group in Delft University of Technology, particularly Jan Gallet, Dr. Harald E. N. Bersee and Darko Stavrov. Special thanks also go to the Composite Materials and Structure Laboratory of McGill University, the Polymer Composites group of Industrial Materials Institute and the Composites group of the Aerospace Manufacturing and Technology Centre.

Mes remerciements vont également à ma famille pour m'avoir supportée pendant ce projet ainsi qu'à Frédérick Gosselin pour m'avoir permis de vivre de nombreuses aventures et me donner l'opportunité de relever de nouveaux défis en Europe.

CONTRIBUTION OF AUTHORS

First manuscript (Chapter 3): "Resistance welding of thermoplastic composites skin/stringer joints", Dubé, M., Hubert, P., Yousefpour, A., Denault, J.

Second manuscript (Chapter 4): "Current leakage prevention in resistance welding of carbon fibre reinforced thermoplastics", Dubé, M., Hubert, P., Yousefpour, A., Denault, J.

Third manuscript (Chapter 5): "Fatigue failure characterisation of resistance-welded thermoplastic composites skin /stringer joints", Dubé, M., Hubert, P., Yousefpour, A., Denault, J.

Dubé, M.:

- Designed the resistance welding rig;
- Defined the welding parameters to be investigated;
- Proposed the ceramic-coating method for mesh insulation (2nd and 3rd manuscripts);
- Performed all the experimental work except the coating operation, which had to be done by a qualified technical officer;
- Analysed the results;
- Wrote the manuscripts.

Hubert, P.:

- Decided the general objectives of the work and suggested to investigate the skin/stringer configuration;
- Provided guidance to the general direction of the work;
- Assisted in the definition of the experimental work;
- Assisted in the understanding and analysis of the experimental results;
- Reviewed the manuscripts.

Yousefpour, A.: - Assisted in the design of the resistance welding rig;

- Explained the operation of the resistance welding set-up;
- Assisted in the definition of the welding parameters;
- Assisted in the understanding and analysis of the experimental results;
- Reviewed the manuscripts.

Denault, J.:

- Assisted in the definition of the general objectives of the work;
- Suggested to use ultrasonic inspection to evaluate the weld quality;
- Assisted in the understanding and analysis of the experimental results;
- Reviewed the manuscripts.

Fourth manuscript (Chapter 6): “Metal mesh heating element optimisation in resistance welding of thermoplastic composites”, Dubé, M., Hubert, P., Gallet, J.N.A.H., Bersee, H.E.N., Stavrov, D., Yousefpour, A.

Fifth manuscript (Chapter 7): “Fatigue performance characterisation of resistance-welded thermoplastic composites”, Dubé, M., Hubert, P., Gallet, J.N.A.H., Bersee, H.E.N., Stavrov, D., Yousefpour, A.

Dubé, M.:

- Contributed to the definition of the general objectives of the work;
- Contributed to the definition of the welding parameters to be investigated;
- Performed all the experimental work with CF/PEI and GF/PEI materials;
- Analysed the results;
- Wrote the manuscripts.

Hubert, P.: - Contributed to the definition of the general objectives of the work;
- Contributed to the definition of the welding parameters to be investigated;
- Assisted in the understanding and analysis of the experimental results;
- Reviewed the manuscripts.

Gallet, J.N.A.H.:- Contributed to the definition of the general objectives of the work;
- Contributed to the definition of the welding parameters to be investigated;
- Performed all the experimental work with the CF/PEKK material;
- Analysed the results;
- Assisted in writing the manuscripts.

Yousefpour, A.: - Initiated the project;
- Contributed to the definition of the general objectives of the work;
- Contributed to the definition of the welding parameters to be investigated;
- Assisted in the understanding and analysis of the experimental results;
- Reviewed the manuscripts.

Bersee, H.E.N.: - Contributed to the definition of the general objectives of the work;
- Contributed to the definition of the welding parameters to be investigated;

- Assisted in the understanding and analysis of the experimental results;
- Reviewed the manuscripts.

Stavrov, D.:

- Contributed to the definition of the general objectives of the work;
- Contributed to the definition of the welding parameters to be investigated;
- Assisted in the understanding and analysis of the experimental results;
- Reviewed the manuscripts.

ABSTRACT

This work investigates the mechanical behaviour of resistance-welded thermoplastic composites under both static and fatigue conditions for skin/stringer and lap shear welds. The first configuration was chosen in order to represent a typical reinforced aerospace composite structure. It consists of a flange laminate, representing a stringer or frame, welded onto a skin laminate. The effects of various resistance welding parameters on the weld quality and mechanical performance of a carbon fibre/poly-ether-ether-ketone (APC-2/AS4) composite skin/stringer are first investigated. The results show that the input power level and clamping distance, i.e., the distance between the connector to the power supply and the edge of the weld, have a significant influence on the weld quality. Then, the mechanical performance and the failure modes of the skin/stringer specimen are studied using the optimum welding conditions. Failure modes typically encountered with adhesively bonded thermosetting resin composites skin/stringer configuration are obtained. Diverse stress concentration reduction methods at the flange tip are also investigated. The most efficient one is to machine a taper angle at the flange tip after the welding operation. A novel solution to prevent current leakage in carbon fibre composites is developed where a ceramic (TiO_2) coating is applied to the heating element. Excellent electrical insulation is obtained which results in a more uniform temperature distribution at the weld interface. Furthermore, the coating does not affect the weld static mechanical performance. The fatigue properties are then investigated and the APC-2/AS4 skin/stringer joints present indefinite fatigue lives at 40% and 35% of their static damage initiation loads, for unidirectional and quasi-isotropic specimens, respectively. The previously developed ceramic coating does not affect the fatigue properties of the welds. The heating element mesh size is optimised for carbon fibre/poly-ether-ketone-ketone (CF/PEKK), carbon fibre/poly-ether-imide (CF/PEI) and glass fibre/poly-ether-imide (GF/PEI) lap shear composite joints. Indefinite fatigue lives are obtained between 20% and 25% of the reference static strength.

SOMMAIRE

Ce travail présente une étude de la performance mécanique statique et dynamique de matériaux composites à matrice thermoplastique assemblés par soudage par résistance pour des géométries de joints de type « revêtement/raidisseur » et « joint recouvrement ». La première géométrie représente une structure typique rencontrée dans l'industrie aérospatiale. Elle consiste en un laminé, représentant un raidisseur, soudé sur un autre laminé, représentant un revêtement. L'effet des différents paramètres de soudage sur la qualité des joints est d'abord étudié pour le joint revêtement/raidisseur composé de fibre de carbone/poly-éther-éther-kétone (APC-2/AS4). Les résultats montrent que la puissance électrique fournie à l'élément chauffant et la distance de connexion, soit la distance entre le connecteur et le côté du joint, ont des effets significatifs sur la qualité des joints produits. La condition de soudage optimale est ensuite utilisée pour étudier la performance mécanique et les modes de rupture des échantillons revêtement/raidisseur. Un mode de rupture semblable à des joints revêtement/raidisseur faits de composites thermodurcissables collés est observé. Diverses méthodes de réduction de la concentration de contraintes sur les côtés du raidisseur sont étudiées. La méthode la plus efficace consiste à machiner des angles de chaque côté du raidisseur après que l'opération de soudage soit complétée. Une solution, qui consiste en l'application d'un revêtement de céramique (TiO_2) sur l'élément chauffant est ensuite proposée pour contrer le problème de court circuit. Cette solution offre une bonne isolation électrique, améliore l'uniformité de la température à l'interface du joint et n'influence pas les propriétés mécaniques des joints sous chargement statique. Finalement, les propriétés des joints soudés en fatigue sont étudiées. Les échantillons revêtement/raidisseur faits de APC-2/AS4 ont une vie indéterminée à 40% et 35% de la charge de l'initiation de dommage sous chargement statique, pour les laminés unidirectionnels et quasi-isotropiques, respectivement. Le revêtement de céramique développé précédemment n'influence pas les propriétés des joints en fatigue. Après avoir optimisé la géométrie de l'élément chauffant pour les joints recouvrement faits de fibre de carbone/poly-éther-kétone-kétone (CF/PEKK), fibre de carbone/poly-éther-imide (CF/PEI) et fibre de verre/poly-éther-imide (GF/PEI), les propriétés mécaniques des joints recouvrement en fatigue sont étudiées. Des vies indéterminées sont rapportées entre 20% et 25% de la résistance des joints sous chargement statique.

TABLE OF CONTENTS

LIST OF TABLES

LIST OF FIGURES

LIST OF SYMBOLS

Symbol	Description	Unit
T	Temperature	°C
I	Input electrical current	A
V	Input Voltage	V
R	Heating element electrical resistance	Ω
t	Time	s
P	Power level	W
p	Power level per weld unit area	W/m^2
E	Energy supplied to the heating element	J

CHAPTER 1. INTRODUCTION

Continuous fibre reinforced thermoplastic composites (CFRTC) were first introduced in the industry because of their commonly-cited advantages over the more conventional thermosetting composites such as better toughness and impact resistance, unlimited shelf life, good solvent resistance and potential for rapid and low-cost mass production. Environmental concerns and new legislations in the areas of processing emission and end-of-life recycling have also made them ideal materials to replace their metallic or thermosetting composites counterparts [1]. However, these CFRTC materials also present a number of disadvantages among which a lack of drapability and formability induced by the continuous reinforcement, which limits the complexity of the parts that can be made out of them. Before CFRTC can be fully integrated to complex structural components in the transportation industries, rapid, reliable and cost effective joining methods are thus needed.

Conventional joining methods such as mechanical fastening and adhesive bonding have been developed. However, these two joining methods present some disadvantages such as the requirement of extensive surface preparation for adhesive bonding and mismatch of coefficients of thermal expansion, weight penalty and stress concentrations induced by the hole drilling process for mechanical fastening [2]. Another joining method, called either fusion bonding or welding, has thus been developed for CFRTC materials. Welding is a fast joining method that requires little or no surface preparation. It takes advantage of one of the most important properties of thermoplastic composites, which is their capability to be melted and cooled while retaining their physical and mechanical properties. In this method, the polymer at the surfaces of the parts to be joined, called weld interface, is heated above its glass-transition temperature, T_g (for amorphous polymers), or above its melting temperature, T_m (for semi-crystalline polymers). As a result of heating, the mobility of the polymer molecular chains increases. Under the application of pressure, the barriers associated with asperities disappear, allowing the polymer molecular chains to diffuse across the weld interface [1]. This leads to polymer chains entanglement and disappearance of the joint surfaces, which in turn promotes the ability of transferring loads through the welded area. The polymer is then cooled down, under the application of pressure, for solidification and consolidation purposes.

Heat can be generated at the weld interface by means of frictional work, thermal energy or electromagnetic field. These heat generation methods define the three categories of fusion bonding (Fig. 1-1). In friction welding, heat is generated at the weld interface by frictional work or polymer viscous dissipation. The two surfaces of the parts to be joined are rubbed against each other until the polymer at the weld interface is fully melted. The parts are then kept together, under the application of pressure. Friction welding methods can be divided into vibration welding, spin welding, ultrasonic welding and friction stir welding [1]. Thermal welding methods involve direct application of heat on the surfaces to be welded, followed by a forging step in which the surfaces are brought into contact, under the application of pressure. Heat can be applied to the surfaces to be joined using hot-gas, hot-tool, infrared lamp or laser [1]. The last category, electromagnetic welding, involves moulding or trapping powders or inserts such as iron oxide, stainless steel, ceramic, ferrite or graphite between the two surfaces of the parts to be joined. An electromagnetic field or electrical current is applied, causing the insert material at the interface to heat and melt the surrounding polymer. This category can be divided into induction welding, dielectric welding, microwave welding and resistance welding [1].

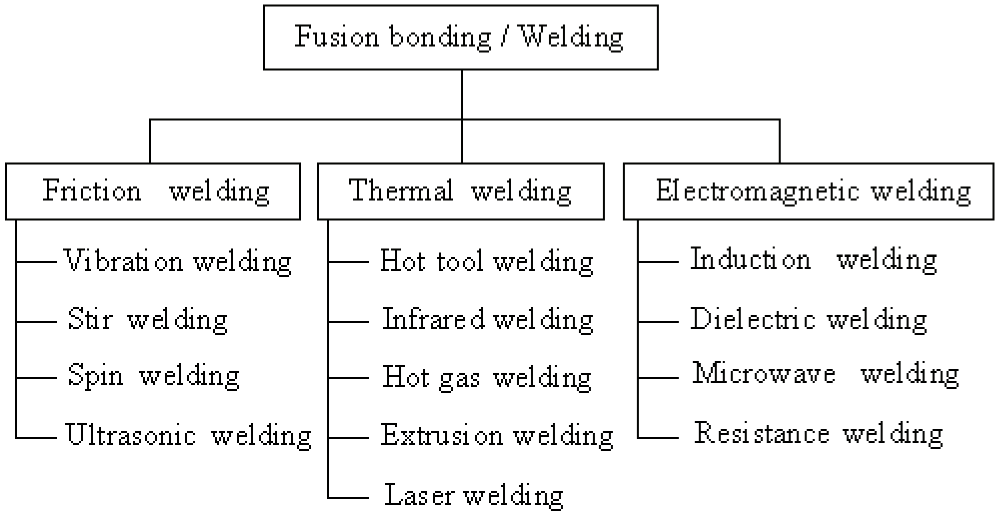

Fig. 1-1. Thermoplastic composites welding methods [1]

Among the various methods of joining thermoplastic composites, resistance welding appears to be an ideal welding technique. It can be applied to different joint configurations, is adaptable to automation and on-line inspection and provides joints with minimum surface preparation and cost [1]. The technique consists in applying an electrical conductive implant, called heating element, between two parts to be welded (adherends). As the current passes in the heating element, the temperature rises due to the Joule heating effect. When the polymer located at the weld interface melts (semi-crystalline polymers) or softens (amorphous polymers), the current is switched off and the weld interface is allowed to cool down, under the application of pressure, resulting in a weld. So far, resistance welding has found applications mostly in the aerospace industry. Its most commonly cited application is the welding of the glass fibre/poly-phenylene-sulfide (GF/PPS) J-nose leading edge of the Airbus A340-500/600 and A380 airplanes (Fig. 1-2).

Fig. 1-2. J-nose leading edge of Airbus A340/600 airplane, courtesy of Stork Fokker

A large number of experimental investigations were performed on resistance welding of thermoplastic composites [2]. The materials that are generally used are the carbon fibre/poly-ether-ether-ketone (CF/PEEK - APC-2/AS4), carbon fibre/poly-ether-imide (CF/PEI) and glass fibre/poly-ether-imide (GF/PEI) composites. The vast majority of the investigations focused on two specimen geometries: lap shear and double cantilever beam (DCB). These weld geometries are well suited to optimise the welding parameters or to evaluate the shearing (lap shear) and toughness (DCB) properties of the welds but are helpless to investigate the failure modes that are likely to occur in real aerospace structures, which in general, consist of reinforced skin panels. In addition, the studies raised some issues with the resistance welding technique among which is the current leakage problem [3, 4]. This problem occurs when electrically conductive adherends, such as carbon fibre reinforced thermoplastics, are welded. When the polymer located at the weld interface melts and flows, the heating element comes in contact with the carbon fibres, creating new electrical paths in the adherends. So far, the current leakage issue has limited the applications of resistance welding to glass fibre reinforced thermoplastics. Finally, the studies performed on resistance welding investigated the static behaviour of the welds, only. Since aerospace structures are subjected to cyclic loadings, the fatigue performance of the resistance-welded joints is an essential aspect to be investigated.

In light of the above, the objective of this work is to investigate the static and fatigue mechanical behaviour of resistance-welded thermoplastic composites. To achieve this goal, the following tasks are performed:

a) The effect of resistance welding parameters on the weld quality and the failure modes of an APC-2/AS4 skin/stringer specimen that represents a typical reinforced aerospace structure is presented in chapter 3 (1^{st} manuscript).
b) A solution to prevent current leakage in carbon fibre composite adherends is developed and the effect on the joint failure mode is presented in chapter 4 (2^{nd} manuscript).
c) The fatigue behaviour of the APC/AS4 skin/stringer specimen is presented in chapter 5 (3^{rd} manuscript).
d) The heating element mesh geometry is optimised for different fibre types and polymers, i.e., carbon fibre/poly-ether-ketone-ketone (CF/PEKK), CF/PEI and GF/PEI, for a lap shear weld geometry in chapter 6 (4^{th} manuscript).
e) The fatigue behaviour of the CF/PEKK, CF/PEI and GF/PEI lap shear joints is presented in chapter 7 (5^{th} manuscript).

1.1 References

1. Yousefpour, A., Hojjati, M., Immarigeon, J.-P., Fusion Bonding/Welding of Thermoplastic Composites. Journal of Thermoplastic Composite Materials, 2004;17(4):303-341.

2. Stavrov, D., Bersee, H.E.N., Resistance welding of thermoplastic composites - an overview. Composites Part A: Applied Science and Manufacturing, 2005;36(1):39-54.
3. Ageorges, C., Ye, L., Hou, M., Experimental investigation of the resistance welding for thermoplastic-matrix composites. I. Heating element and heat transfer. Composites Science and Technology, 2000;60(7):1027-1039.
4. Eveno, E., Gillespie, J.W.J., Resistance welding of graphite polyetheretherketone composites - An experimental investigation. Journal of Thermoplastic Composite Materials, 1988;1:322-338.

CHAPTER 2. LITERATURE REVIEW OF RESISTANCE WELDING OF THERMOPLASTIC COMPOSITES

This chapter presents a literature review covering both the experimental and modelling investigations on resistance welding of thermoplastic composites. The objective of the review is to provide insight into the main phenomena affecting the weld quality and mechanical performance.

2.1 Experimental work

The experimental work performed on resistance welding of thermoplastic composites investigated the effects of various welding parameters such as heating element type, input power level, welding pressure, etc. on the weld quality and mechanical performance. This section is a summary of the experimental investigations. Emphasis is put into the understanding of the main phenomena governing the weld quality and mechanical performance.

2.1.1 Resistance welding parameters

Fig. 2-1 presents a schematic of a typical resistance welding set-up. The main components of the welding set-up consist of the adherends, heating element, tooling materials, computer/data acquisition system, power supply, electrical connectors and pressure system. In general, a neat resin film is added to both sides of the heating element in order to create a resin rich region that facilitates diffusion of the molecular chains at the weld interface. Although resistance welding appears to be a relatively simple process, several processing parameters need to be optimised in order to obtain a good weld quality with optimal mechanical performance. These processing parameters and their effects on the weld quality are discussed in the next sections.

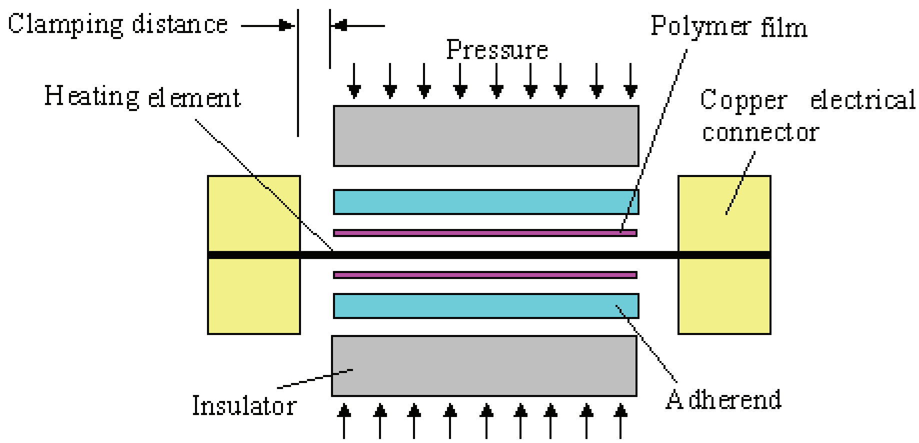

Fig. 2-1. Resistance welding schematic [1]

2.1.1.1 Heating element

The heating element is the source of heat generation at the weld interface and remains trapped in the joint after the welding operation. As such, it is probably the most important parameter in the resistance welding process. The material type, quality and size of the heating element all have a great influence on the quality and mechanical performance of the welded joints. So far, the investigators have used two main types of heating elements: carbon fibre prepreg plies and metal meshes. The carbon fibre heating elements generally consist of a unidirectional (UD) carbon fibre prepreg ply [2-7], a layer of carbon fibre fabric prepreg [2-4, 7] or a ply of UD commingled carbon fibre. These carbon fibre heating elements have the advantages of maintaining the compatibility with the adherends when carbon fibre reinforced thermoplastics are welded. Ageorges *et al.* and Stavrov *et al.* compared the electrical and thermal behaviours of the fabric and UD carbon fibre prepreg heating elements [2, 3, 7]. Their results show that carbon fibre fabric heating elements provide good thermal conductivities in both the length and width directions as opposed to the UD prepreg heating elements, which have poor thermal conductivity in the width direction. The carbon fibre fabric heating elements thus lead to better temperature uniformity and mechanical performance than the UD prepreg plies. Lap shear strength and mode I interlaminar fracture toughness improvements of 69% and 179%, respectively, were reported for CF/PEI adherends [3].

Although the carbon fibre fabric heating element leads to better results than a UD carbon fibre ply, some issues remain. In resistance welding, a direct electrical connection between the power supply and heating element is needed. In general, this electrical connection consists of copper electrical blocks, which are pressed against the heating element at a certain clamping pressure. The polymer matrix must be etched or burned away from the ends of the heating element in order to make the connection with the copper blocks. This etching or burning operation requires special care to avoid any damage to the carbon fibre heating elements. In addition, the required clamping pressure between the copper connectors and the heating element is reported to vary between 4 and 20 MPa [2]. Such a high clamping pressure often causes damage to the carbon fibre heating elements, which results in an inefficient connection. It is possible to improve the connection by coating the ends of the carbon fibre heating element with conductive silver but this method is expensive and does not prevent fibre damage [5, 8].

Fibre motion and distortion of the adherends are other problems encountered when using a carbon fibre heating element. As the weld interface temperature increases, the viscosity of the polymer decreases and fibre motion occurs within the adherends. To avoid this problem, a film of amorphous polymer can be co-consolidated with the adherends and both sides of the heating element. A good example of this is the Thermabond heating element that was developed by ICI Composite Structures [9, 10]. In Thermabond heating element, a PEI film is co-consolidated with the adherends and carbon fibre heating element. During the welding operation, the temperature is raised above T_g of PEI (215°C) but below T_m of PEEK (343°C). Since the PEEK matrix does not reach its melting temperature, the laminates remain intact and no fibre motion occurs in the adherends. The amorphous polymer used for this type of heating element must offer a good bond with the adherends. This can be achieved by the compatibility of the two thermoplastic polymers or by migration of the fibres from the adherends into the amorphous polymer film. The amorphous polymer should also have a glass-transition temperature lower than the melting point of the adherends' matrix. Thermabond heating element offers some advantages over conventional heating elements [11-14]. The lower temperature necessary to achieve fusion bonding reduces welding time and prevents any fibre motion in the adherends. Lap shear and double cantilever beam tests showed similar performances for both the Thermabond and conventional heating elements [14]. However, one of the main weaknesses of Thermabond is its reliance on an amorphous interlayer, which reduces the resistance to solvents. In addition, the disadvantages associated with carbon fibres heating element (connection inefficiency, fibre oxidation and non-uniform heating) remain an issue.

To eliminate the problems associated with carbon fibre heating elements, metal mesh (usually stainless steel meshes) heating elements are used in most of the recent investigations. Although the stainless steel mesh induces a loss of resistance to galvanic corrosion, it improves the temperature homogeneity over the weld area and is more resistant to pressure induced by the connectors, leading to a better joint performance and a wider processing window [7, 8, 15, 16]. Different sizes of wire diameters are available for stainless steel meshes. Care must be taken in the choice of proper metal mesh to assure a good impregnation of polymer in the mesh [16]. Fig. 2-2 shows the influence different types of heating elements on the lap shear strengths of resistance-welded APC-2/AS4 adherends. Mesh A has a wire diameter of 0.11 mm with open gap width, i.e., the distance between two wires, of 0.15 mm. Mesh B has a wire diameter of 0.04 mm with open gap width of 0.09 mm and mesh C has a wire diameter of 0.03 mm with open gap width of 0.04 mm. For APC-2/AS4 adherends, an optimal mechanical performance is obtained with mesh B [16]. Mesh A has a too large wire diameter while mesh C has a too small open gap width, which prevents the polymer from diffusing appropriately in the adherends.

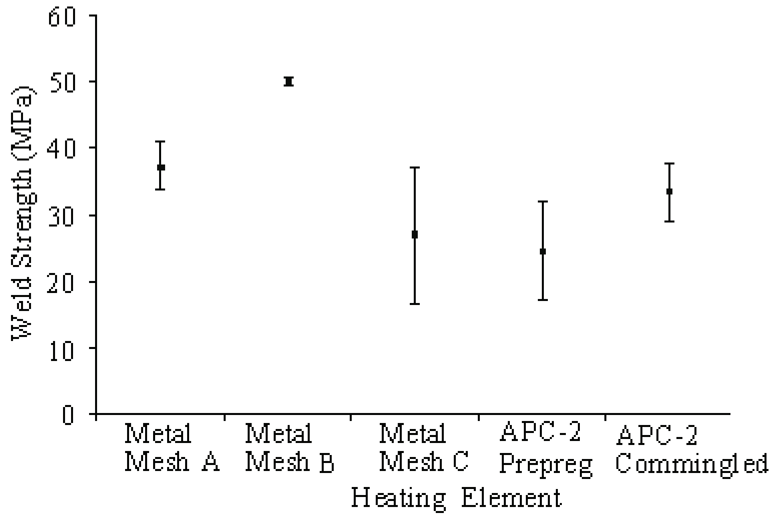

Fig. 2-2. Effect of different heating elements on lap shear strength of the welds

2.1.1.2 Current leakage issue

As mentioned in the introduction, one of the main concerns with resistance welding of electrically conductive adherends, such as carbon fibre reinforced thermoplastics, is current leaking from the heating element to the adherends [2, 3, 15, 17]. As the polymer matrix surrounding the heating element melts and flows, the heating element comes in contact with the carbon fibres of the adherends, creating new electrical paths across the weld interface. Current leakage leads to long welding times, due to power losses in the adherends, high temperature gradients along the length of the weld and a lack of controllability of the process. It is experimentally detected through on-line monitoring the electrical resistance of the heating element [2]. Fig. 2-3 shows the variations of the electrical resistance of various heating elements with time. The electrical resistances of the fabric and UD CF/PEI heating elements first decrease slowly with time. This behaviour is typical of carbon fibre heating elements since the electrical resistance of this material decreases with temperature increase. After approximately 20 and 50 seconds, an abrupt drop is seen in the electrical resistances of the fabric and UD CF/PEI heating elements, respectively. This abrupt reduction is due to establishment of new electrical paths in the adherends. To fix this problem, the carbon fibre heating elements can be insulated with a ply of GF/PEI prepreg. No current leakage is observed for these heating elements, showing the efficiency of the glass fibre electrical insulation [2-4, 15, 18]. The main drawback of this technique is the introduction a foreign material in the weld, which leads to mechanical performance penalty and thicker bondline.

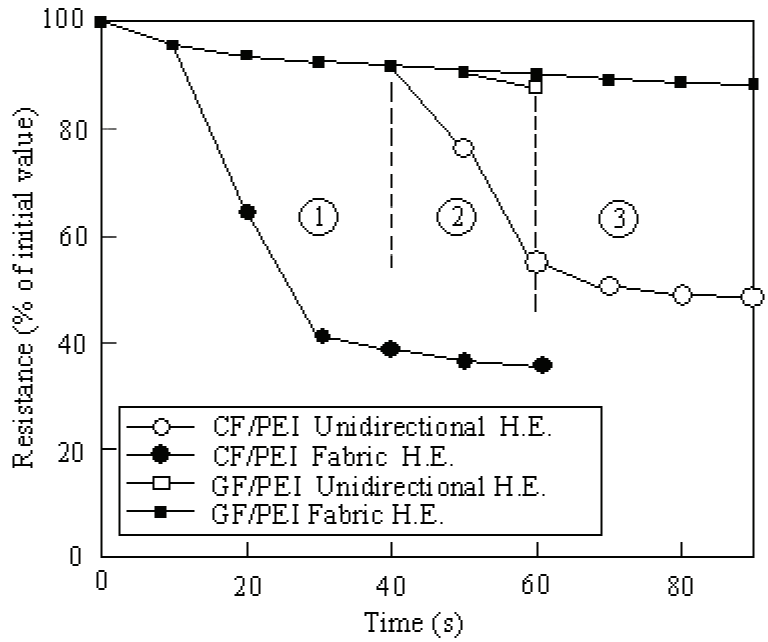

Fig. 2-3. Current leakage during resistance welding of CF/PEI [2]

Beukers *et al*. developed another solution to the current leakage problem [17]. In this solution, the heating element is coated with a high-temperature resistive paint, which is electrically resistive and thermally stabile up to 600°C [17]. CF/PEI adherends made of six plies of 5-harness satin weave configuration were welded with metal mesh heating element coated with this paint. No current leakage was observed with this method but lap shear strengths of only 15 MPa were reported [17].

2.1.1.3 Edge effect

Investigations on coupon size and large-scale specimens have shown that the non-uniform temperature distribution over the weld area is a major issue in resistance welding [19]. Preferential heating occurs in some parts of the welds because of damage to the heating element, poor electrical connection efficiency or current leakage in the laminates. Another phenomenon known as “edge effect” is observed during the resistance welding process. Edge effect is due to the poor heat transfer from the heating element into the air by natural convection as opposed to that in the weld stack by conduction [20-24]. The exposed part of the heating element becomes warmer than the embedded part and temperature rises rapidly at the specimen edges. Melting thus initiates at the edges and the melt front then propagates towards the middle of the specimen and finally spreads sideways (Fig. 2-4) [25].

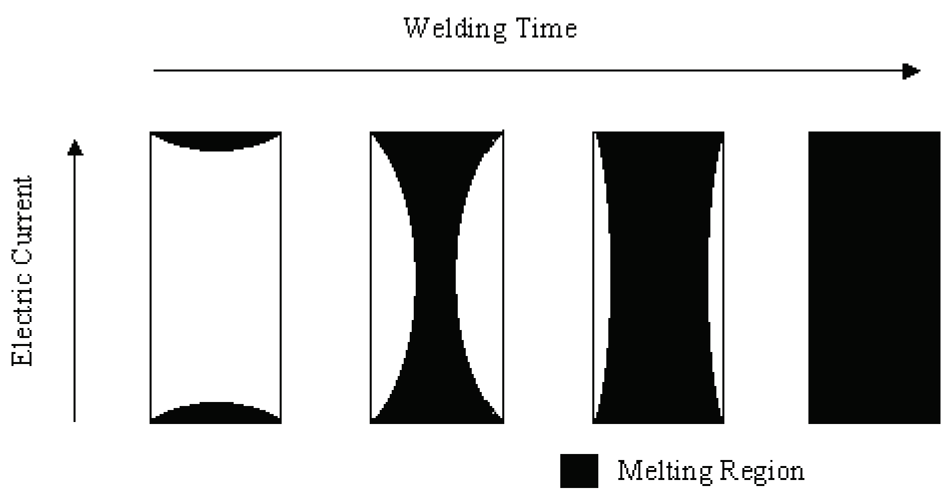

Fig. 2-4. Melt front propagation at bonding interface [25]

Stavrov *et al*. have shown that it is possible to reduce the edge effect by varying the distance between the connectors and the specimen (clamping distance) [26]. Temperature measurements were performed on GF/PEI lap shear configurations. The weld area was 25 mm wide and 200 mm long. Thermocouples were positioned along the length of the weld, as shown in Fig. 2-5.

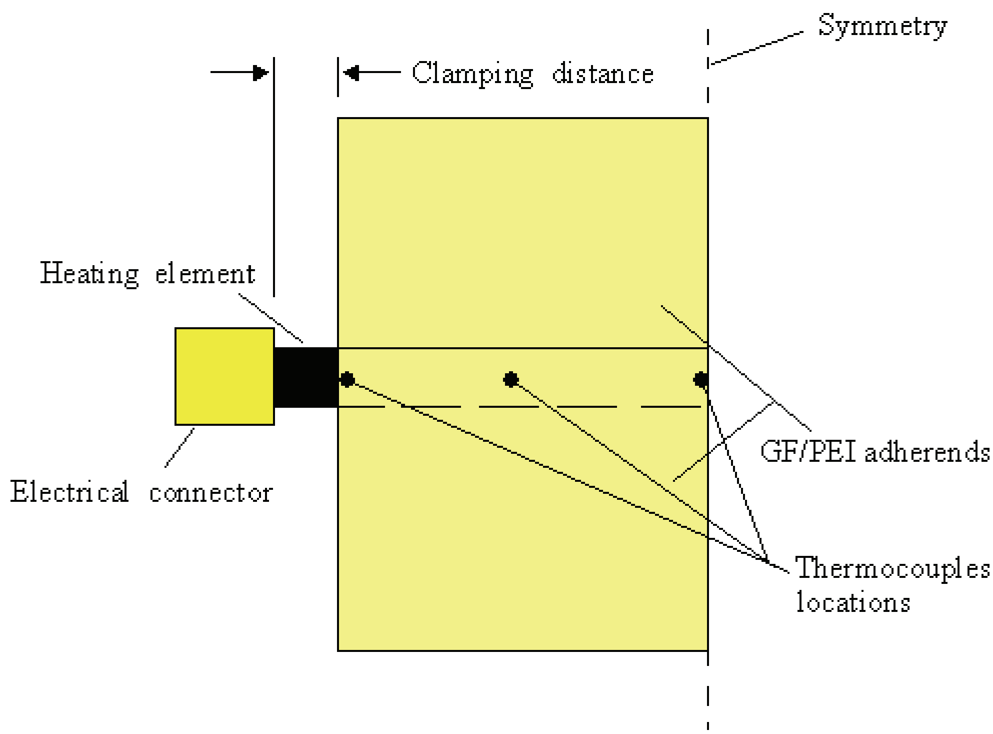

Fig. 2-5. Effect of clamping distance on temperature homogeneity

At a clamping distance of 10 mm, a temperature gradient of more than 100°C was observed between the edge and middle of the specimen, which is likely to cause polymer degradation because of the high temperature reached at the edge. At a clamping distance of 5 mm, a temperature gradient of 70°C was obtained. Finally, at a clamping distance of 0 mm (connectors touching the specimen), a temperature gradient of 20°C was observed. In this case, the lower temperature was detected at the edges of the weld, which means that the clamps were actually cooling the edges by conduction. Clamping distance is thus an effective method of improving the temperature distribution along the length of a specimen. However, it is important to mention that the optimum clamping distance changes depending on the material that is welded, heating element type, set-up, tooling material and input power level. Other methods for reducing the edge effect include cooling the heating element with gas flow during welding [27, 28].

2.1.1.4 Welding pressure

Two techniques can be used to apply the pressure to the adherends, i.e., the displacement control and pressure control [2]. In the displacement control technique, an initial pressure is applied to the weld stack using, for example, the two platens of an Instron machine. The platens remain fixed and the pressure can be monitored throughout the welding process. In the pressure control technique, an initial pressure is applied to the weld stack using a pneumatic system and the pressure remains constant throughout the welding operation. In this case, the displacement of the weld stack can be monitored during the welding. Monitoring the fluctuations of pressure or displacement during displacement control or pressure control, respectively, gives six distinct processing stages, namely, initial compaction, thermal expansion, melt-flow, melt-flow and cooling, solidification and contraction phases [13, 24, 29, 30] (Fig. 2-6). In the initial compaction stage (stage 1), load (or volume) increases due to thermal expansion of resin and then decreases when the polymer softens and fills the gaps between the heating element and adherends. In stage 2, volumetric expansion associated with melting of crystals and thermal expansion dominates. As the maximum load (P_m) is approached, thermal expansion is reduced due to absorption of the latent heat of fusion to melt the remaining crystals in the polymer. A rapid drop follows the maximum load because the entire polymer is melted and matrix squeeze flow occurs in the fibre transverse direction (stage 3). The polymer chains commence to inter-diffuse and mix at the weld interface under the applied pressure to form a weld. Once the electrical current is stopped (stage 4), the interface begins to cool down. Stages 5 and 6 of the curve represent solidification and contraction of the weld.

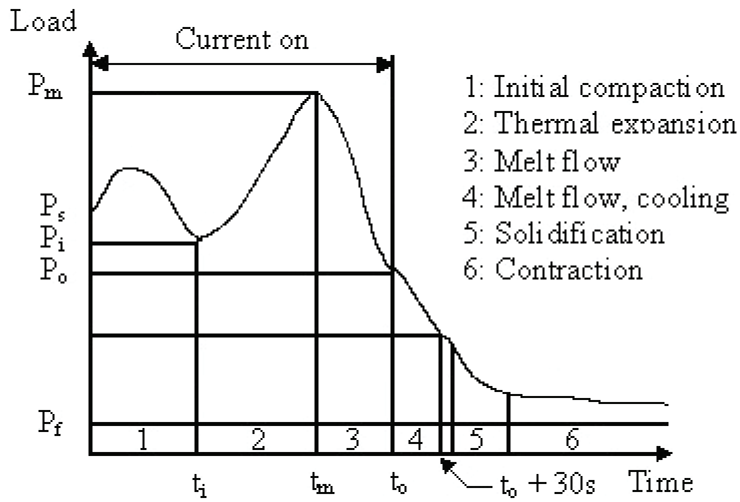

Fig. 2-6. Load curve for resistance welding at constant displacement [24, 29, 30]

For the constant displacement technique, Hou *et al.* reported an optimal initial pressure between 0.10 and 0.15 MPa for CF/PP. Lower initial pressures caused deconsolidation of the composite and higher initial pressures caused movement of the fibres at the weld interface. For APC-2/AS4 composites welded under the constant pressure technique, optimal welding pressures are in the range of 0.4 to 1.6 MPa [23].

2.1.1.5 Input power level

The input power level is a major contributor to weld quality and performance. It is defined as follows:

$$P(t) = I^2 R(t) \qquad \text{eq. 1}$$

where *P* is the power level (W), *t* is the time (s), *I* is the input electrical current (A) and *R* is the electrical resistance of the heating element (Ω). It is common to replace the power level defined in eq. 1 by the power level per weld unit area:

$$p(t) = \frac{I^2 R(t)}{lw} \qquad \text{eq. 2}$$

where p is the power level per weld unit area (W/m^2) and l (m) and w (m) are the length and width of the weld area, respectively. The energy supplied to the heating element per weld unit area (J/m^2) is then:

$$E = \int p(t)t \qquad \text{eq. 3}$$

where t is the period of time during which electrical current is applied (s). It has been shown in several investigations that the weld quality and the corresponding mechanical performance vary with the input power level, even though the input energy is the same [5, 6, 15, 25, 31]. For low input power levels, time to melt is longer due to heat losses from the weld stack to the environment and the input energy is higher [5, 25]. Heat losses also cause larger heat-affected-zones in the adherends, polymer squeeze out and deconsolidation of the adherends if insufficient pressure is applied [18, 32]. The result is a poor weld quality. At higher input power levels, welding time is shorter for the same input energy, which leads to a better weld quality [5, 25, 26]. However, too high power levels lead to severe thermal gradients throughout the weld area and complete melting of the polymer is not always achieved before deconsolidation or polymer degradation occurs in some parts of the weld [3, 6].

The input power level varies with material systems, heating element types and experimental set-up. The maximum and minimum power levels for a combination of material, heating element and tooling plates must be determined in order to have a good joint quality. Ageorges *et al.* and Hou *et al.* [3, 25] developed processing windows defining a combination of power levels and welding times corresponding to acceptable weld quality for CF/PEI composite material. The processing window obtained for CF/PEI adherends with carbon fibre fabric and metal mesh heating elements is shown in Fig. 2-7. The vertical axis represents the input power level per unit area and the horizontal axis represents the time during which current is applied. The weld quality was assessed by lap shear tests. A weld quality criterion of 90% of the lap shear strength of the compression-moulded laminates benchmark specimens was chosen. Five regions are distinguishable on the figure. Region 1 is the processing window. Laminates welded within this region lead to lap shear strengths of at least 90% of the benchmark value. Regions 2 and 3 represent limitations of the input power level. In region 2, it is impossible to soften the PEI polymer enough on the entire weld area before degradation occurs at some locations of the weld. Power levels in region 3 lead to excessive welding times. The boundary lines between the processing window and regions 4 and 5 represent the minimum and maximum welding times corresponding to each power levels. In region 4, the polymer at the interface cannot be softened enough to produce a good weld. Region 5 represents long welding times that lead to distortion of adherends.

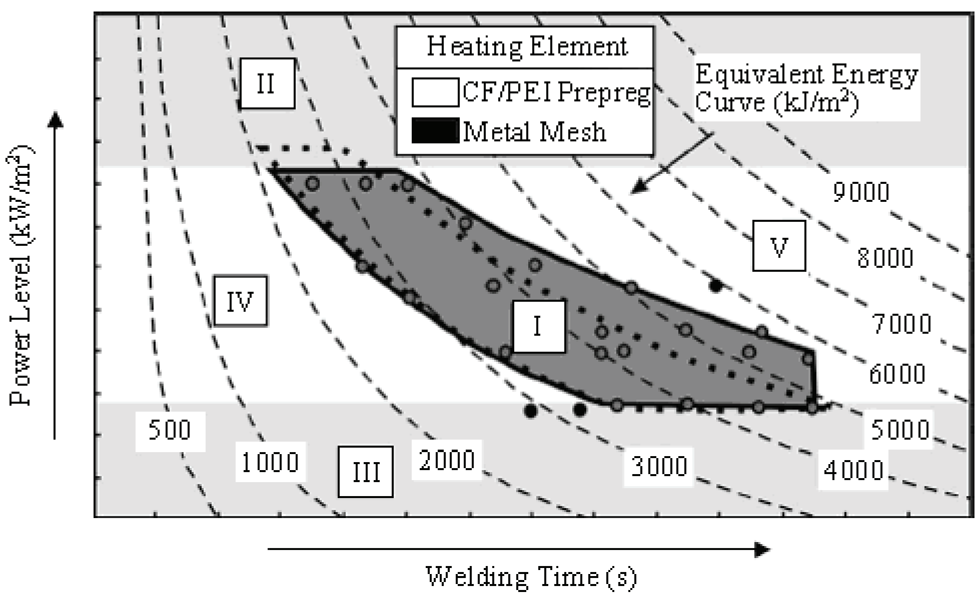

Fig. 2-7. Processing window for resistance-welded CF/PEI [25]

The power level can be introduced to the heating element using three different methods. In the first one, called the constant input voltage, a certain voltage is applied to the heating element and remains constant over the entire welding process. It is worth mentioning that, although the voltage is constant, the power level is not. The electrical resistance of the heating element varies with temperature and so does the power level. For a carbon fibre heating element, the electrical resistance decreases with temperature, which results in a power level increase. On the other hand, the electrical resistance of a stainless steel mesh heating element increases with temperature resulting in a power level decrease. A decaying heating rate is generally observed using the constant voltage method due to both the decreasing input power level (when metal mesh heating elements are used) and the heat losses in the environment.

The second method was proposed by Arias *et al.* and is called the impulse resistance welding (IRW) [33]. In this method, the input power is applied in the form of intense pulses up to 600 kW/m^2, followed by a pause of 1 to 3 seconds. The method requires less energy to melt the polymer due to lower heat losses [33, 34]. It was claimed that the pulsed nature of power signal improves the temperature distribution over the weld interface and provides better temperature uniformity in the joint.

The third method was introduced by Yousefpour *et al.* and is called the ramped voltage [35]. The ramped voltage method, i.e., voltage that is gradually increased with time, was used to weld UD 16-ply APC-2/AS4 adherends with a stainless steel mesh heating element [35]. A more uniform temperature distribution was obtained with this method and heat losses in the environment were reduced, leading to a more constant heating rate at the weld interface and lower input energy. However, no comparison between the lap shear strengths of the specimens welded using the constant and ramped voltage methods was presented.

2.1.2 Weld characterisation methods

The weld strength is evaluated using the lap shear and DCB mechanical testing methods. Other characterisation methods include observation of the weld interface by optical or scanning electron microscopy (SEM), differential scanning calorimetry (DSC) and non-destructive evaluation methods such as ultrasonic C-scan inspection.

2.1.2.1 Mechanical testing and failure modes

The mechanical performance of the resistance-welded specimens is usually evaluated using lap shear and DCB tests. The lap shear test is performed according to the ASTM D1002 standard test method. The weld area is 25.4 mm wide and 12.7 mm long. The specimens are produced one by one or cut from long welded areas. Lap shear strengths are calculated simply by dividing the maximum load by the weld area. Benchmark specimens can be produced in order to compare the weld strength with the parent material strength. The benchmark specimens can be fabricated using a mould having the same geometry as the lap shear specimens or by moulding laminates having twice the thickness of the lap shear specimens and then machining the laminates to the desired lap shear geometry. Table 2-1 and Table 2-1 present the reported lap shear strengths for APC-2/AS4, CF/PEI and GF/PEI adherends.

Table 2-1. Lap shear strengths of resistance-welded APC-2/AS4 adherends

Authors	Adherends material	Heating element	Laminate lay-up	Lap shear strength (MPa)
Silverman *et al.* [36]	APC-2/AS4	UD APC-2/AS4	UD 16-ply	25.5
Maguire *et al.* [37]	APC-2/AS4	UD APC-2/AS4	UD 25-ply	23.9
Bastien *et al.* [13]	Commingled NCS/PEEK	UD APC-2/AS4	Quasi-isotropic 16-ply	28.8
	Commingled NCS/PEEK	UD Thermabond	Quasi-Isotropic 16-ply	27.5
Don *et al.* [11]	APC-2/AS4	UD APC-2/AS4	UD 16-ply	37.1
	APC-2/AS4	UD Thermabond	UD 16-ply	34.2
Taylor *et al.* [8]	APC-2/AS4	UD APC-2/AS4	UD 16-ply	42.7
	APC-2/AS4	Stainless steel mesh	UD 16-ply	44.1
Don *et al.* [11]	APC-2/AS4	UD APC-2/AS4	Quasi-Isotropic 16-ply	30.4
	Commingled NCS/PEEK	UD APC-2/AS4	Quasi-Isotropic 16-ply	28.8
	Commingled NCS/PEEK	UD Thermabond	Quasi-Isotropic 16-ply	27.5
Xiao *et al.* [21]	APC-2/AS4	UD APC-2/AS4	Cross-ply 16-ply	33.9
Yousefpour *et al.* [16]	APC-2/AS4	UD APC-2/AS4	UD 16-ply	24.5
	APC-2/AS4	Commingled CF	UD 16-ply	33.0
	APC-2/AS4	Stainless steel mesh	UD 16-ply	50.1

Table 2-2. Lap shear strengths of resistance-welded CF/PEI and GF/PEI adherends

Authors	Adherends Material	Heating Element	Laminate Lay-Up	Lap Shear Strength (MPa)
Hou *et al.* [15]	CF fabric/PEI	Stainless steel mesh	Cross-ply 10-ply	34.5
Ageorges *et al.* [3]	CF fabric/PEI	CF/PEI	Cross-ply 10-ply	~ 25
	CF fabric/PEI	CF fabric/PEI	Cross-ply 10-ply	~ 30
Stavrov *et al.* [7, 17]	GF fabric/PEI	Stainless steel mesh	Fabric 6-ply	~ 31
	GF fabric/PEI	CF fabric/PEI	Cross-ply 6-ply	~ 23

The best lap shear strengths obtained are 50.1 and 30.4 MPa for UD and quasi-isotropic APC-2/AS4 adherends, respectively. Stainless steel mesh heating elements lead to better mechanical performance than carbon fibre heating elements for all types of adherends. This is due to the advantages of the stainless steel heating elements previously mentioned, e.g. a better temperature distribution and lower sensitivity to clamping pressure. In addition, the carbon fibre fabric heating elements lead to better results than the UD carbon fibre prepreg plies. In the UD prepreg heating elements, the main axial loads act on a direction perpendicular to the direction of the fibres. This is the worst possible loading case for a composite and explains the lower strength obtained with this heating element.

Fracture surfaces of welded specimens can reveal interfacial or interlaminar failure modes (Fig. 2-8). Interfacial failure occurs at the interface between the heating element and adherend (Fig. 2-8 – a) and leads to low lap shear strengths. This failure mode is caused by imperfect welding between the adherends heating element. The interlaminar failure modes, on the other hand, can be divided into cohesive failure of the heating element, tearing of the heating element and tearing of adherend [25, 38]. Cohesive failure of the heating element occurs when a crack propagates from one side of the heating element to the other side, in the length direction (Fig. 2-8 – b). This can be caused by deconsolidation in the heating element during the welding operation and leads to low lap shear strengths. Tearing of the heating element occurs when a crack propagates from one side of the heating element to the other side, involving damage (tearing) in the heating element (Fig. 2-8 – c). This failure mechanism may involve damage to the laminates (Fig. 2-8 – d) and then leads to high lap shear strengths due to the large amount of energy that is dissipated [25, 38].

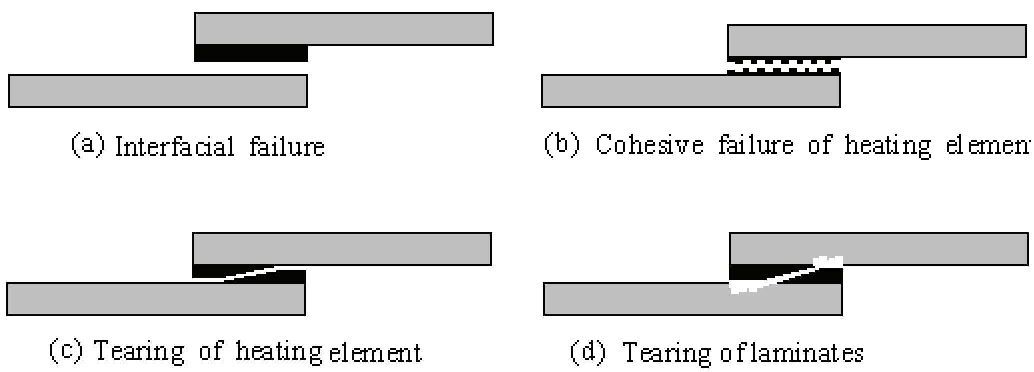

Fig. 2-8. Lap shear failure modes

DCB tests are performed according to the ASTM D5528 standard test method. The result of the test is the weld toughness under Mode I crack propagation (G_{IC}). Even though the standard is not well suited for resistance-welded specimens, it gives a supplement of information on the weld quality and is used to optimise the welding parameters. The Irwin-Kies equation states [39]:

$$G_{1C} = \frac{L^2 \partial C}{2b \partial a} \qquad \text{eq. 4}$$

where G_{IC} is the strain energy release rate (kJ/m^2), L is the load at crack initiation (N), C is the compliance (displacement/load ratio) (m/N), a is the crack length

(m) and b is the specimen width (m). The interlaminar fracture toughness can then be calculated with the modified beam theory:

$$G_{IC} = \frac{3L\delta}{2b(a+\Delta)} \quad \text{eq. 5}$$

where δ is the displacement at the load point (m) and Δ is the x-value at origin of the leasts squares plot of the cube root of compliance, $C^{1/3}$, as function of delamination length. Δ is determined experimentally (m). Interlaminar fracture toughness can also be calculated using the compliance calibration method:

$$G_{1C} = \frac{nP\delta}{2ba} \quad \text{eq. 6}$$

where n is the slope of log C as function of log a and is determined experimentally (m). DCB tests have been performed on CF/PP, GF/PP, CF/PEI and APC-2/AS4. The results indicate good results with fracture toughness approaching or exceeding the baseline value of the moulded laminates, which is around 1,5 kJ/m^2 for APC-2/AS4 composite material [3, 15]. However, the results of this test are not always reliable. The crack sometimes propagates in the laminate rather than in the joint and fibre bridging is a commonly observed problem with this test [3, 5, 6].

Arias *et al.* used the impulse resistance welding method to weld 8-ply quasi-isotropic APC-2/AS4 laminates with UD APC-2/AS4 heating element [33]. The short beam shear test method was used to calculate the interlaminar shear strength (ILSS) of the joint and an ILSS of 72.4 N/mm^2, which is around 89% of the reported benchmark value, was obtained.

2.1.2.2 Other characterisation methods

Evaluations of resistance-welded thermoplastic composites mainly focus on mechanical testing and thermal aspect rather than evaluation of the microstructure of the welds. However, some work has been done using DSC analyses, optical microscopy and SEM to shade light on the microstrucre and morphology of the welded joints. DSC is used to obtain the crystallinity level in the joints when semi-crystalline thermoplastic polymers are welded. Hou *et al*. reported that natural cooling of the welds leads to crystallinity levels between 40 and 42% for carbon fibre polypropylene (CF/PP) and glass fibre/polypropylene (GF/PP) composites with carbon fibre heating element [5, 6]. This crystallinity level was similar to the one of the compression-moulded laminates, showing that the weld operation had a negligible influence on the crystallinity level [5, 6]. However, the fracture surfaces revealed different polymer morphologies between the compression-moulded laminates and the welds [5, 6, 15]. Compression-moulded laminates showed very good fibre-matrix interface while the welded joints revealed a poor interface between the carbon fibres of the heating element and the PP polymer. It was believed that the input electrical current in the carbon fibre heating element damaged the interface and/or interphase between the matrix and fibres [5]. Contamination of the welded laminates may be another reason for this poor adhesion.

The processing temperature, residence time and cooling rate are the main parameters influencing a thermoplastic polymer morphology [40]. For a typical moulding cycle, increasing the moulding temperature or residence time reduces the number of surviving nuclei, which in turn reduces the number of spherulites in the matrix. A well-defined transcrystalline region can then be developed on the carbon fibres surfaces. In the resistance welding process, the weld interface is kept at the desired processing temperature for a very short period of time as compared to a typical moulding cycle. To assure a good impregnation of the heating element and entanglement of the polymer chains across the weld interface, it is thus essential to heat the polymer above its common moulding temperature. This welding temperature must be carefully chosen in order to avoid any thermal degradation (chain oxidation or cross-linking reaction).

A non-destructive evaluation method widely used to characterise the weld quality is ultrasonic C-scan inspection [5, 14, 25, 32, 41]. It provides information on the degree of bonding, melt flow propagation, non-welded zones and overall weld quality.

2.2 Modelling work

Process modelling has become very important for new manufacturing processes as it reduces the costs and time of experimental programs and facilitates optimisation of processing windows. Several authors have investigated process modelling of thermoplastic composites resistance welding. Investigations mainly include heat transfer, consolidation and crystallisation analyses. These analyses are summarised in this section.

2.2.1 Heat transfer modelling

Maffezzoli *et al.* [42] developed a one-dimensional mathematical heat transfer model of the resistance welding process. The model predicts heat conduction through the thickness (transverse direction) of the welded part taking into account kinetics of melting and crystallisation within the matrix. The model also predicts the degree of crystallinity as a result of different processing conditions as well as the effects of different boundary conditions arising from the use of different tool materials, such as steel or insulating ceramics.

Fig. 2-9 depicts the temperature profiles prediction at the centre of a APC-2/AS4 heating element (curve A) and at the interface between the amorphous PEEK film and the APC-2/AS4 adherends (curve B) when a ceramic tool is used. During the process, the temperature rises rapidly to the PEEK melting temperature of 343°C (curves A and B). The polymer crystallinity decreases gradually and the temperature remains almost constant until most of the crystals are melted. The temperature then rises to a new steady-state equilibrium around 400°C. Once the electrical current is stopped, the temperature drops due to heat conduction through the thickness and along the fibres of the adherends. During the cooling phase, the cooling rate decreases due to the lower thermal conductivity of ceramic tool at the boundaries, the decreasing thermal gradient between the joint and the environment and the heat generation during polymer crystallisation. Such a moderate cooling rate leads to a degree of crystallisation between 26% and 33%. As for steel tool, the temperature profile at the centre of the heating element (curve C) never reaches the polymer melting temperature, due to the high thermal conductivity of steel and carbon fibres. The steel tool acts as a heat sink and makes the welding process difficult.

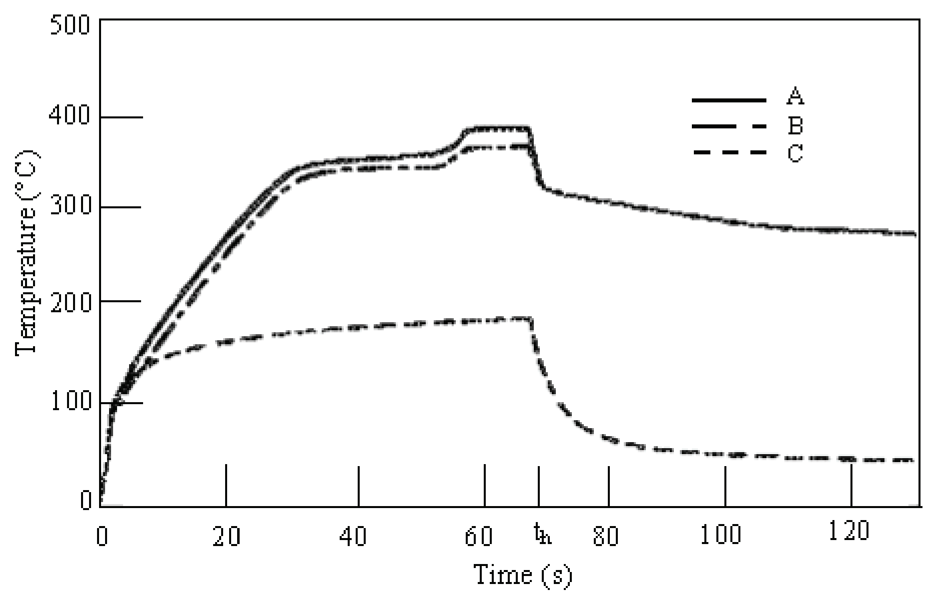

Fig. 2-9. Temperature profiles as a function of time using steel and ceramic tools [42]

In their work, Jakobson *et al*. [20] simulate the resistance welding process using a transient two-dimensional anisotropic thermal model, which is solved using the finite difference method. The model determines the time to melt, i.e., the time required for the temperature at the weld interface to reach the polymer melting temperature, the locations where preferential heating occurs and the effect of the melting through the thickness of the weld. The heat conduction equation (eq. 7) is coupled with the total heat generation/absorption as given in [20]. The model is summarised as below:

$$\rho c_p \frac{\partial T}{\partial t} = \dot{q} + k_{xx}\frac{\partial^2 T}{\partial x^2} + 2k_{xy}\frac{\partial^2 T}{\partial x \partial y} + k_{yy}\frac{\partial^2 T}{\partial y^2} \qquad \text{eq. 7}$$

$$\dot{q} = \dot{q}_{elec} - \dot{q}_{melt} + \dot{q}_{crys} \qquad \text{eq. 8}$$

where ρ is the density (kg/m^3), c_p is the heat capacity (J/(°C kg)), t is time (s), T is the temperature (°C), $\dot{q}$ is the total heat generation/absorption rate per unit volume (J/(m^{3}s)), $\dot{q}_{elec}$ is the electrical heat generation rate per unit volume (J/(m^{3}s)), $\dot{q}_{melt}$ is the heat absorption rate due to the endothermic melting process per unit volume (J/(m^{3}s)), $\dot{q}_{crys}$ is the heat generation rate due to the exothermic crystallisation process per unit volume (J/(m^{3}s)) and k_{xx}, k_{xy} and k_{yy} are the anisotropic thermal conductivity coefficients (W/(m°C)).

The internal heat generation/absorption (J/(m^{3}s)) can be expressed with the following equations [20]:

$$\dot{q}_{elec} = \frac{VI}{V_{HE}} \qquad \text{eq. 9}$$

$$\dot{q}_{melt} = X_{mr} H_f \rho_f X_{vci} \frac{dX_f}{dt} \qquad \text{eq. 10}$$

$$\dot{q}_{crys} = -X_{mr} H_f \rho_f \frac{dX_{vc}}{dt} \qquad \text{eq. 11}$$

where V_{HE} is the heating element volume (m^3), V is the voltage (V), I is the electrical current (A), X_{mr} is the mass fraction of polymer in the composite, H_f is the heat of fusion of polymer (J/kg), ρ_f is the crystalline density of polymer (kg/m^3), X_{vci} is the initial crystallinity of polymer, X_f is the degree of melting of polymer and X_{vc} is the polymer degree of crystallinity.

At t = 0, the total heat generation/absorption (eq. 8) is zero. The total heat generation becomes non-zero when the electrical power (eq. 9) is applied to the heating element. As the temperature of the polymer surrounding the heating element rises from the glass transition temperature to the melting temperature, the exothermic cold-crystallisation process of the amorphous polymer films starts (eq. 11). The semi-crystallised polymer films then start to absorb heat due to the endothermic effects of melting as the interface temperature approaches T_m (eq. 10). The melting process stops when the polymer at the interface is fully melted or the degree of melting X_f, is one. The electrical power is interrupted and the temperature begins to drop. When the temperature falls below $T_{m,}$ the exothermic crystallisation process starts again and the melted polymer re-crystallises. As a consequence of polymer re-crystallisation, heat is generated at the interface (eq. 11). When the temperature drops below $T_{g,}$ the total heat generation/absorption becomes zero (eq. 8) and the temperature continues to decrease according to the conduction equation (eq. 7) with appropriate boundary conditions. It should be noted that one of the main results of this analysis is that heat associated with the exothermic and endothermic processes of the polymer films surrounding the heating element is negligible as compared with the heat generation of the electrical current.

The parameters affecting the time to melt are the variations in the density of APC-2/AS4 composite during the heating process and the heating element electrical resistance [20]. The influence of the variations in density was found to be negligible. However, the electrical resistance of the APC-2/AS4 heating element has a considerable effect on the time to melt [20]. The model predicts that the time to melt can change from 50 to 140 seconds for a small variation of resistivity per thickness from 0.17 to 0.21 Ω. The variation in resistivity per thickness can be attributed to broken fibres, improper connections and variations in width, length, thickness and fibre content of the heating element. This shows, once again, the difficulties associated with the carbon fibre heating elements, which produce a high degree of scatter in the quality and mechanical performance of the welds. The effect of different tooling materials (convection coefficients *h* at the top and bottom boundaries of the welded parts) on the time to melt confirms the Maffezzoli's conclusions [42].

One- and two-dimensional heat transfer finite element models were developed by Holmes *et al.* to simulate large-scale welding assemblies [22]. In these models, the specific heat and density of the neat PEEK films associated with APC-2/AS4 heating element are considered temperature dependent. Latent heat of fusion is also considered in the models. The one-dimensional case simulates the thermal gradient through the thickness (z-direction), away from any edge effect. The weld stack contains insulators, adherends, APC-2/AS4 heating element and polymer films. The temperature gradients in the *X* and *Y* directions are zero, i.e., $\partial T/\partial X=0$ and $\partial T/\partial Y=0$. Fig. 2-10 shows the model and boundary conditions that are used for analysis.

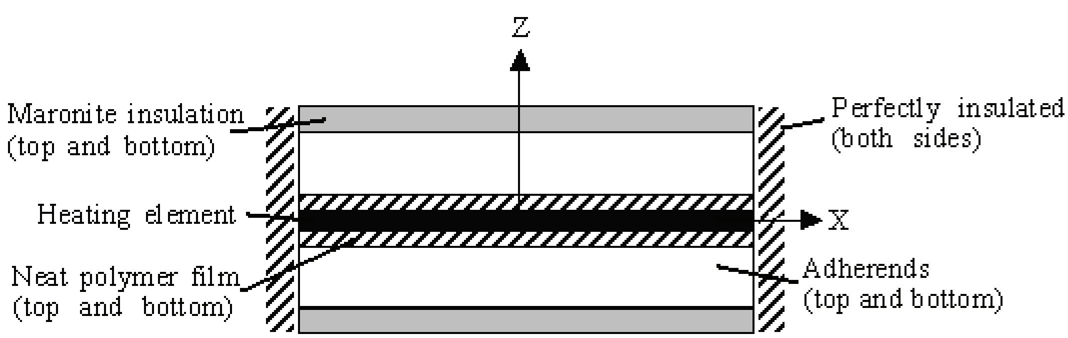

Fig. 2-10. One-dimensional model of the resistance welding process [22]

The two-dimensional model considers the influence of edge effect on the thermal gradient across the plane of the weld (Fig. 2-11). Convective and radiative losses are taken into account for the areas exposed to air. The thermal conductivities are assumed to be independent of temperature. A constant convection boundary condition is applied to represent the ceramic insulators. Heat generation is applied to the heating element at time zero and remains constant throughout the welding simulation.

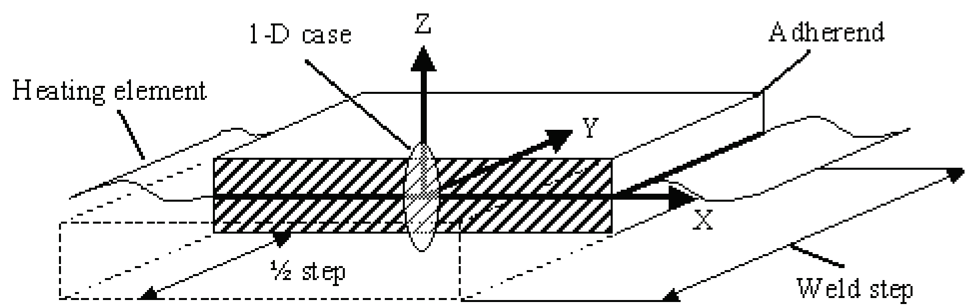

Fig. 2-11. Two-dimensional model of the resistance welding process [22]

The model is used to simulate resistance welding of APC-2/IM7 adherends using an APC-2/AS4 heating element sandwiched between two neat PEEK polymer films. The effects of convection and radiation on the areas of the heating element exposed to air are investigated [22]. The two-dimensional model shows the importance of the edge effect on the temperature distribution along the width of the weld. Insulation tooling is also shown to have an important influence on the time to melt, confirming the Maffezzoli's and Jakobson's conclusions.

Talbot *et al.* [1] developed one, two and three-dimensional transient heat transfer finite element models of resistance welding of APC-2/AS4 lap shear configuration using stainless steel mesh heating element. The one-dimensional model simulates the temperature gradient through the thickness of the weld, the two-dimensional model simulates the temperature gradient along the width of weld interface and the three-dimensional model is used to investigate the influence of conduction along the length of the adherends.

For the one-dimensional model, a constant volumetric power density of q = 2.0 GW/m^3 is applied to the heating element to account for Joule heating, calculated with $q = R \cdot I^2 / V_{HE}$, where q is the volumetric power density (W/m^3), R is the electrical resistance (Ω) of the heating element, I is the input current (A) and V_{HE} is the volume of the heating element (m^3). It was shown that including the latent heat in the one-dimensional model has a negligible influence on the weld interface thermal history, confirming Jakobson's results. The latent heat was thus neglected for the rest of the study [1].

The two-dimensional model shows the presence of a large thermal gradient at the edges of the welded parts for different heating times (Fig. 2-12). The changes in the heat transfer mechanism from convection and radiation to conduction cause localised overheating at the ends of the adherends and promote preferential heating at the edges of the weld. The temperature distribution is more uniform away from the edges where the edge effect is reduced.

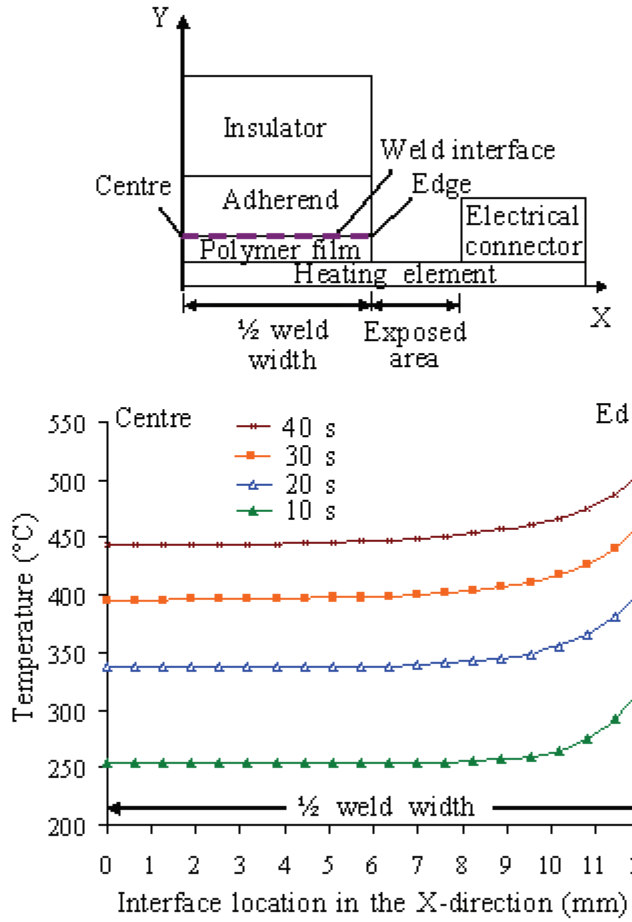

Fig. 2-12. Temperature profile along the weld interface [1]

An optimisation algorithm was developed for the two-dimensional model to identify the clamping distance that gives the most uniform temperature over the weld area. The objective was to reach a processing temperature of 390°C everywhere in the weld without having any degradation in the polymer. An optimum clamping distance of 0.65 mm was found. The temperature distribution for this clamping distance is shown in Fig. 2-13.

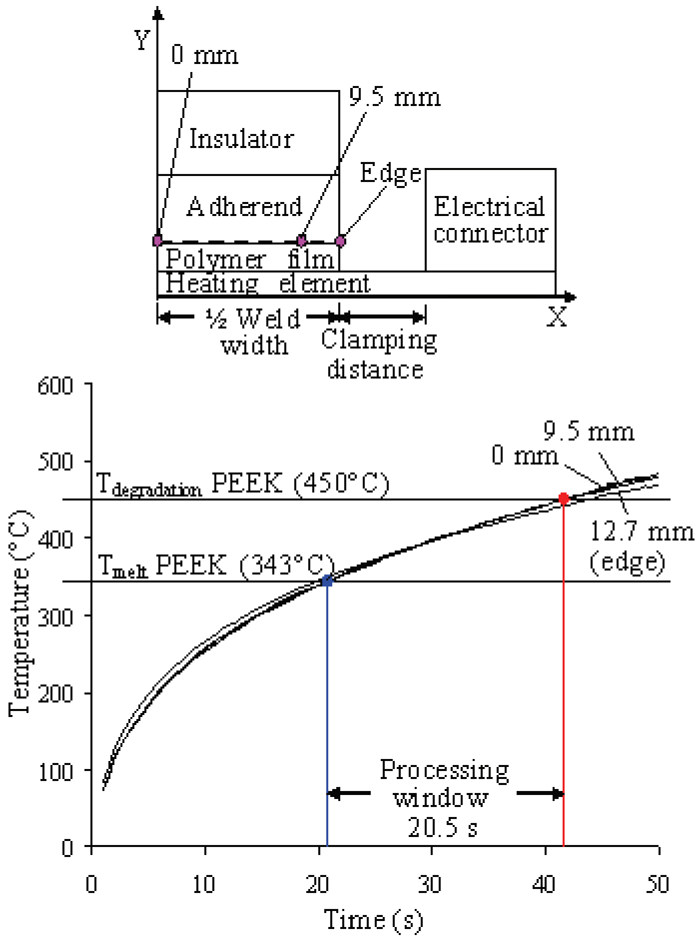

Fig. 2-13. Temperature profile at various locations in the weld, for a clamping distance of 0.65 mm [1]

The three-dimensional model simulates the temperature profile along the length of the laminates. The model was coupled with the optimisation algorithm to find the clamping distance that gives the best temperature uniformity in the weld. The optimum clamping distance was changed from 0.65 mm (from two-dimensional model) to 0.80 mm (from the three-dimensional model).

Ageorges *et al.* [43] developed a transient three-dimensional finite element model of resistance welding of lap shear specimen. The model includes orthotropic heat conduction in the composite parts, latent heat and edge effects. The model also accounts for surface roughness at the interfaces between the polymer neat films and the APC-2/AS4 heating element and between the polymer films and the adherends when temperature is below T_m. The heat conductivity at the interfaces, called thermal gap conductivity, k_{gap}, varies as the interface temperature rises. When the temperature at the interfaces is below T_g (or below T_m for semi-crystalline polymers), the gap conductivity at the interfaces can be calculated assuming that only portions of the surfaces are in contact with each other. In this case, k_{gap} is calculated using the thermal conductivities of the polymer and air:

$$k_{gap} = k_p A + k_{air}(1 - A) \qquad \text{eq. 12}$$

where k_{gap} is the thermal gap conductivity coefficient at the interface (W/°C kg), k_p is the thermal conductivity of polymer (W/°C kg), k_{air} is the thermal conductivity of air (W/°C kg) and A is the percentage of contact area at each interface. When temperature is above T_g (or above T_m for semi-crystalline polymers), the entire surface area is in contact and k_{gap} becomes k_p. The model also accounts for the non-uniform heating of the APC-2/AS4 heating element assuming that heat is generated in the fibre bundles rather than in the entire heating element. However, this effect was found to have a negligible influence on the time to melt.

2.2.2 Consolidation and crystallisation modelling

Ageorges *et al.* [44, 45] extended their three-dimensional transient heat transfer finite element model by coupling it with the intimate contact, autohesion and cystallisation kinetics models [43]. The intimate contact model describes the stages of surface rearrangement, surface approach and wetting of polymer at the interface and the autohesion model explains the molecular diffusion stages involved in a polymer/polymer interface healing [44]. The model predicts the degree of intimate contact (D_{ic}), the time to reach intimate contact (t_{ic}), the degree of bonding (D_b), the time to achieve full bonding (t_b) and the level of crystallinity in the weld. Mantell and Springer's [46] intimate contact and autohesion models have been used to calculate the degree of intimate contact (D_{ic}) and the degree of autohesion (D_{au}) based on the initial surface roughness. The degree of bonding can simply be defined as:

$$D_b = D_{ic} \times D_{au} \qquad \text{eq. 13}$$

Different crystallinity kinetic models developed by Ozawa [47], Velisaries *et al.* [48] and Choe *et al.* [49] were coupled to the three-dimensional finite element model of Ageorges *et al.* [45]. The crystallinity histories obtained from the different models are similar over a power range of 30 to 120 kW/m^2. It was also shown that natural cooling of the weld stack leads to a crystallinity level of 25% for APC-2/AS4 composite. The effect of the welding pressure on the development of intimate contact is illustrated in Fig. 2-14. The time to reach intimate contact decreases with the welding pressure. However, from a certain threshold, the effect of the welding pressure becomes negligible.

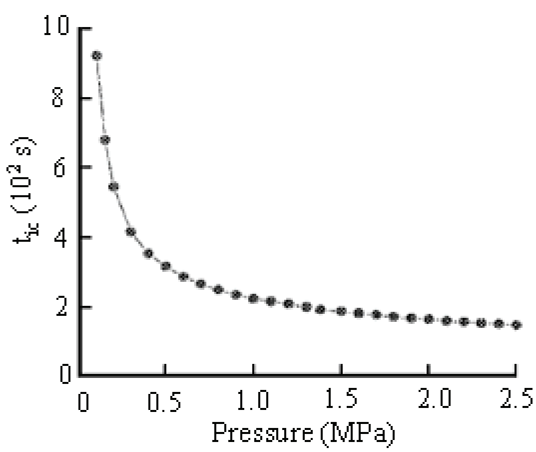

Fig. 2-14. Time to achieve intimate contact versus consolidation pressure for APC-2/AS4 [44]

2.3 Literature review summary

Resistance welding is a relatively new process that recently found applications in the aerospace industry. The process modelling efforts addressed the heat transfer, consolidation and crystallisation issues while the experimental investigations focused on the understanding of the effects of the welding parameters on the weld quality and mechanical performance. From the presented results, the following conclusions can be drawn:

1) The heating element has the most significant impact on the weld processing and mechanical performance. Stainless steel mesh heating elements are ideally suited to weld thermoplastic composites. APC-2/AS4, CF/PEI and GF/ PEI adherends all produced higher lap shear strengths when a stainless steel mesh heating element was used, as opposed to a carbon fibre heating element. A metal mesh size optimisation showed that a stainless steel mesh with a wire diameter of 0.04 mm and open gap width of 0.09 mm leads to the best lap shear strengths (50.1 MPa) for APC-2/AS4 adherends. However, no metal mesh size optimisation was performed for other polymers like PEKK and PEI.
2) The input power level and the clamping distance are two important parameters governing the welding process. They need to be adjusted for each welding set-up and adherends' material.
3) The weld mechanical performance was assessed using lap shear and DCB tests. Only the static mechanical behaviour of the welds was investigated.
4) Current leakage is a major issue with resistance welding of carbon fibre composites. Several solutions to this problem were proposed but they contaminated the weld interface with foreign materials, produced thicker bondline or reduced the weld strength.

Thus the present work was defined in order to fill some of the gaps indentified above. More specifically, a specimen geometry capable of representing a real aerospace structure is investigated; a new solution to the current leakage problem is proposed; the weld fatigue properties are investigated for APC-2/AS4 and other material systems like CF/PEKK, CF/PEI and GF/PEI.

2.4 References

1. Talbot, E. Manufacturing Process Modelling of Thermoplastic Composite Resistance Welding. M.Sc. Thesis, McGill University, Department of Mechanical Engineering, 2005.

2. Ageorges, C., Ye, L., Hou, M., Experimental investigation of the resistance welding for thermoplastic-matrix composites. I. Heating element and heat transfer. Composites Science and Technology, 2000;60(7):1027-1039.

3. Ageorges, C., Ye, L., Hou, M., Experimental investigation of the resistance welding of thermoplastic-matrix composites. II. Optimum processing window and mechanical performance. Composites Science and Technology, 2000;60(8):1191-1202.

4. Ye, L., Ageorges, C. Large scale resistance welding of thermoplastic composites: feasibility and limitations. Proceedings of the 9th European Conference (ECCM) Composites from Fundamentals to Exploitation, London, UK, 2000.

5. Hou, M., Friedrich, K., Resistance welding of continuous carbon fibre/polypropylene composites. Plastics Rubber and Composites Processing and Applications, 1992;18(4):205-213.

6. Hou, M., Friedrich, K., Resistance welding of continuous glass fibre reinforced polypropylene composites. Composites Manufacturing, 1992;3(3):153-163.

7. Stavrov, D., Bersee, H.E.N., Beukers, A. The Influence of the Heating Element on Resistance Welding of Thermoplastic Composite Materials. Proceedings of the ICCM-14 Conference, San Diego, USA, 2003.

8. Taylor, N.S., Davenport, R. The resistive implant welding of thermoplastic composite materials. Proceedings of the 49th Annual Technical Conference, Montreal, Canada, 1991.

9. Smiley, A.J., Halbritter, A., Cogswell, F.N., Meakin, P.J., Dual Polymer Bonding of Thermoplastic Composite Structures. Polymer Engineering and Science, 1991;31(7):526-532.

10. Cogswell, F.N., Meakin, P.J., Smiley, A.J., Harvey, M.T., Booth, C. Thermoplastic Interlayer Bonding for Aromatic Polymer Composites. Tomorrow's Materials: Today, Reno, USA, 1989.

11. Don, R.C., Bastien, L., Jakobsen, T.B., Gillespie, J.W., Fusion bonding of thermoplastic composites by resistance heating. SAMPE Journal, 1990;26(1):59-66.

12. Bastien, L., Howie, I., Don, R.C., Holmes, S., Gillespie, J.W.J., Lambing, C.L.T. Manufacture and Performance of Resistance Welded Graphite Reinforced Thermoplastic Composite Structural Elements. Fabricating Composites (Retroactive Coverage), Arlington, USA, 1990.

13. Bastien, L., Don, R.C., Gillespie, J.W. Processing and performance of resistance welded thermoplastic composites. Proceedings of the 45th Annual Conference, Washington DC, USA, 1990.

14. Don, R.C., Gillespie, J.W., Lambing, C.L.T., Experimental characterisation of processing-performance relationships of resistance welded graphite/PEEK [polyetheretherketone] composite joints. Polymer Engineering and Science, 1992;32(9):620-631.

15. Hou, M., Yang, M.B., Beehag, A., Mai, Y.W., Ye, L., Resistance welding of carbon fibre reinforced thermoplastic composite using alternative heating element. Composite Structures, 1999;47(1-4):667-672.

16. Yousefpour, A., Simard, M., Octeau, M.-A., Lamarée, M., Hojjati, M. Effects of Mesh Size on Resistance Welding of Thermoplastic Composites using Metal Mesh Heating Elements. SAMPE-Europe, Paris, France, 2004.

17. Stavrov, D., Bersee, H.E.N., Beukers, A. Experimental Investigation of Large-Scale Welding of Carbon Fiber Thermoplastic Composite Materials. Proceedings of the ICCM-14 Conference, San Diego, USA, 2003.

18. Yuan, Q., Mai, Y.W., Ye, L., Hou, M., Resistance welding of carbon fiber reinforced polyetherimide composite. Journal of Thermoplastic Composite Materials, 2001;14(1):2-19.

19. Talbot, E., Yousefpour, A., Hubert, P., Hojjati, M. Thermal Behavior During Thermoplastic Composites Resistance Welding. Annual Technical Conference (ANTEC) of the Society of Plastics Engineers, Boston, USA, 2005.

20. Jakobsen, T.B., Don, R.C., Gillespie, J.W., Two-dimensional thermal analysis of resistance welded thermoplastic composites. Polymer Engineering and Science, 1989;29(23):1722-1729.

21. Xiao, X.R., Hoa, S.V., Street, K.N., Processing and Modelling of Resistance Welding of APC-2 Composite. Journal of Composite Materials, 1992;26(7):1031-1049.

22. Holmes, S.T., Gillespie, J.W.J., Thermal Analysis for Resistance Welding of Large-Scale Thermoplastic Composite Joints. Journal of Reinforced Plastics and Composites, 1993;12(6):723-736.

23. Stavrov, D., Bersee, H.E.N., Resistance welding of thermoplastic composites - an overview. Composites Part A: Applied Science and Manufacturing, 2005;36(1):39-54.

24. Eveno, E., Gillespie, J.W.J., Resistance welding of graphite polyetheretherketone composites - An experimental investigation. Journal of Thermoplastic Composite Materials, 1988;1:322-338.

25. Hou, M., Ye, L., Mai, Y.W., An experimental study of resistance welding of carbon fibre fabric reinforced polyetherimide (CF fabric/PEI) composite material. Applied Composite Materials, 1999;6(1):35-49.

26. Stavrov, D., Bersee, H.E.N. Thermal Aspects in Resistance Welding of Thermoplastic Composites. ASME Summer Heat Transfer Conference, Las Vegas, USA, 2003.

27. McKnight, S.H., Holmes, S.T., Gillespie, J.W.J., Lambing, C.L.T., Marinelli, J.M., Scaling issues in resistance-welded thermoplastic composite joints. Advances in Polymer Technology, 1997;16(4):279-295.

28. Lambing, C.L.T., Don, R.C., Andersen, S.M., Holmes, S.T., Leach, B.S., Gillespie, J.W. Design and manufacture of an automated resistance welder for thermoplastic composites. Proceedings, 49th Annual Technical Conference, Montréal, Canada, 1991.

29. Eveno, E., Gillespie, J.W., Vinson, J.R. Resistance welding of graphite polyetheretherketone composites. SPE Technical Papers, Proceedings of the 47th Annual Technical Conference, New York, USA, 1989.

30. Eveno, E.C. Experimental investigation of resistance and ultrasonic welding of graphite reinforced polyetheretherketone composites. M.Sc. Thesis, University of Delaware, 1988.

31. Wahab, M.M.A., Ashcroft, I.A., Crocombe, A.D., Hughes, D.J., Shaw, S.J., The effect of environment on the fatigue of bonded composite joints. II. Fatigue threshold prediction. Composites Part A: Applied Science and Manufacturing, 2001;32A(1):59-69.

32. Dubé, M., Hubert, P., Yousefpour, A. Mechanical Performance of Resistance-Welded Thermoplastic Composite Skin/Stringer Specimen. SAMPE Fall Technical Conference, Seattle, USA, 2005.

33. Arias, M., Ziegmann, G. Impulse resistance welding: a new technique for joining advanced thermoplastic composite parts. Proceedings of the 41st International SAMPE Symposium and Exhibition, Anaheim, USA, 1996.

34. Ageorges, C., Ye, L., Simulation of impulse resistance welding for thermoplastic matrix composites. Applied Composite Materials, 2001;8(2):133-147.

35. Yousefpour, A., Simard, M., Octeau, M.-A., Hojjati, M. Process Optimization of Resistance-Welded Thermoplastic Composites Using Metal Mesh Heating Elements. SAMPE, Long Beach, USA, 2005.

36. Silverman, E.M., Griese, R.A., Joining Methods for Graphite/PEEK Thermoplastic Composites. SAMPE Journal, 1989;25(5):34-38.

37. Maguire, D.M., Joining Thermoplastic Composites. SAMPE Journal, 1989;25(1):11-14.

38. Yousefpour, A., Hojjati, M., Immarigeon, J.-P., Fusion Bonding/Welding of Thermoplastic Composites. Journal of Thermoplastic Composite Materials, 2004;17(4):303-341.

39. Perrin, F. Rupture interlaminaire en mode I dans les composites unidirectionnels polypropylène/fibres de verre. École Polytechnique de Montréal, Department of physic and material engineering, 2000.

40. Denault, J., Vu-Khanh, T., Crystallization and Fiber/Matrix Interaction During the Molding of PEEK/Carbon Composites. Polymer Composites, 1992;13(5):361-371.

41. Dubé, M., Hubert, P., Yousefpour, A., Denault, J., Wadham-Gagnon, M. Resistance Welding of Thermoplastic Composites Skin/Stringer Specimens. SAMPE, Long Beach, USA, 2006.

42. Maffezzoli, A.M., Kenny, J.M., Nicolais, L., Welding of PEEK/carbon fibre composite laminates. SAMPE Journal, 1989;25(1):35-39.

43. Ageorges, C., Ye, L., Mai, Y.W., Hou, M., Characteristics of resistance welding of lap shear coupons. Part I. Heat transfer. Composites Part A: Applied Science and Manufacturing, 1998;29(8):899-909.

44. Ageorges, C., Ye, L., Mai, Y.W., Hou, M., Characteristics of resistance welding of lap shear coupons. Part II. Consolidation. Composites Part A: Applied Science and Manufacturing, 1998;29(8):911-919.

45. Ageorges, C., Ye, L., Mai, Y.W., Hou, M., Characteristics of resistance welding of lap-shear coupons. Part III. Crystallinity. Composites Part A: Applied Science and Manufacturing, 1998;29(8):921-932.

46. Mantell, S., Springer, G., Manufacturing process models for thermoplastic composites. Journal of Composite Materials, 1992;26(16):2348-2377.

47. Ozawa, T., Kinetics of non-isothermal crystallization. Polymer, 1971;12:150-158.

48. Velisaris, C.N., Seferis, J.C., Crystallization Kinetics of Polyetheretherketone (PEEK) Matrices. Polymer Engineering and Science, 1986;26(22):1574-1581.

49. Choe, C.R., Lee, K.H., Non-isothermal Crystallization Kinetics of Polyetheretherketone. Polymer Engineering and Science, 1989;29:801-805.

CHAPTER 3. FIRST MANUSCRIPT

3.1 Preface

This chapter presents an investigation of the effects of the input power level and clamping distance on the skin/stringer weld quality and mechanical performance. Specimens welded with optimised conditions are characterised through mechanical testing in order to understand their failure modes under static loading. Finally, methods to reduce the stress concentration at the flange tip are investigated.

Resistance welding of thermoplastic composites skin/stringer joints*

*Composites Part A: Applied Science and Manufacturing, 2007, doi: 10.1016/j.compositesa.2007.07.014

Dubé, M. and Hubert, P.
McGill University, CREPEC, Department of Mechanical Engineering
817 Sherbrooke Street West, Montréal, Québec, H3A 2K6, Canada

Yousefpour, A.
Aerospace Manufacturing Technology Centre, National Research Council Canada
5145 Decelles Avenue, Montréal, Québec, H3T 2B2, Canada

Denault, J.
Industrial Materials Institute, National Research Council Canada
75 de Mortagne, Boucherville, Québec, J4B 6Y4, Canada

3.2 Abstract

An experimental investigation of resistance welding of APC-2/AS4 PEEK/carbon fibre composite using a stainless steel mesh heating element is presented. A special specimen geometry, the skin/stringer configuration, was used to represent a typical reinforced aerospace structural joint. The specimens consisted of a flange, representing a stringer or frame, welded onto a skin laminate. The effects of the welding parameters such as the input power level and clamping distance on the weld quality and performance were investigated. The welding parameters were optimised using short beam shear tests, ultrasonic C-scan inspection and optical microscopy. The mechanical performance of the resistance-welded skin/stringer configuration was investigated using three- and four-point bending tests and the failure mechanisms were characterised by optical and scanning electron microscopy. Two methods were used to reduce the stress concentration at the flange tip. The first method was to machine a 20° taper angle at the edge of the flange and the second one was to create a resin fillet at the flange tip. No mechanical performance improvement was obtained with the resin fillet method but the taper angle method showed 25% mechanical performance improvement when the taper angles were machined after the welding operation.

Keywords: Resistance welding; A. Polymer-matrix composites (PMCs); B. Mechanical properties; B. Debonding; E. Welding/joining

3.3 Introduction

Continuous carbon fibre thermoplastic composites are increasingly being used for structural components in automotive, marine and aerospace industries [1]. These materials present the general advantages of thermoplastic composites with respect to environmental resistance and damage tolerance but are limited to the manufacture of relatively simple components due to deformation restrictions associated with the use of continuous reinforcements. In order to use these materials in complex structures, joining methods such as adhesive bonding and mechanical fastening have been developed. In the case where thermoplastic composites are to be joined, fusion bonding or welding is an alternative joining method.

Welding consists of heating the surfaces of the parts to be joined above the polymer glass transition temperature (for amorphous polymers) or melting temperature (for semi-crystalline polymers) and then allowing the weld interface to cool down, under the application of pressure [2]. Various welding techniques are available for thermoplastic composites. Depending on the heat generation method at the weld interface, these techniques are usually classified into three main categories [2, 3]: friction welding, thermal welding and electromagnetic welding. Among different electromagnetic welding techniques, resistance welding was the focus of many investigations in the last decade because of its simplicity and cost-effectiveness [2, 4]. Resistance welding involves trapping an electrical conductive implant, called heating element, between the two parts to be welded (adherends). An electrical current is applied to the heating element and its temperature rises by Joule heating effect. As temperature reaches the polymer glass-transition temperature or melting temperature, the adjoining polymer matrix melts and flows. When a predetermined processing temperature is reached, the current is stopped and the weld interface cools down, under the application of pressure. Resistance welding has shown performance and cost benefits over other joining techniques and is now being used in current applications like the welding of glass fibre/poly-phenylene-sulfide (GF/PPS) J-nose leading edges of the Airbus 340-500/600 and 380 airplanes [5].

In the literature, the experimental investigations about resistance welding are limited to two different types of joint geometry, i.e., lap shear and double cantilever beam (DCB) configurations [4, 6-13]. These welded samples are usually characterised using ultrasonic C-scan inspection, optical and scanning electron microscopy, lap shear tests (lap shear configuration) and Mode I fracture toughness tests (DCB configuration). Different types of heating element were investigated over the past years. Don *et al.* [9] used a carbon fibre prepreg ply heating element to weld carbon fibre/poly-ether-ether-ketone (CF/PEEK) laminates. Lap shear strengths of 37 MPa were obtained. Ageorges *et al.* [13, 14] used a carbon fibre fabric heating element to weld carbon fibre/poly-ether-imide (CF/PEI) and glass fibre/PEI (GF/PEI). It was shown that a fabric heating element provides better temperature uniformity and mechanical performance than a UD prepreg ply. More recently, another type of heating element consisting of a stainless steel mesh was introduced [6, 8, 15, 16]. Stainless steel meshes improved the weld quality and reliability with lap shear strengths up to 50 MPa for APC-2/AS4 (CF/PEEK) composites [8, 16].

The lap shear and DCB weld configurations mentioned above have the advantages of being very simple geometries that are well suited to evaluate and optimise the resistance welding parameters. However, since the resistance welding process is foreseen to have applications in the aerospace industry, a specimen geometry that would represent a typical aerospace structure is needed in order to better represent the loading cases of a real-life situation. For example, aerospace structures such as fuselages are subjected to out-of-plane loading caused by the internal pressure of the passengers cabin. Since the structures supporting this out-of-plane loading are generally made of reinforced skin panels, an investigation of the failure mechanisms of this type of structure is essential. Specimens cut from full-size reinforced panels were investigated at NASA Langley Research Centre for adhesively bonded thermosetting composite materials [17]. However, these full-size panels were rather expensive to produce and there was a need for a simpler configuration that would allow the study of the failure modes at a lower cost [17]. A simplified specimen configuration, called skin/stringer configuration, was developed to represent the specimens cut from the full-size panels [17]. This simplified configuration consisted of a composite flange laminate, representing a stringer or stiffener, bonded onto a composite skin laminate. The experiments revealed that the failure mechanisms of both types of specimens were the same [17, 18]. Benefiting from this result, the failure modes of the specimens cut from the full-size panels can be studied using a simple skin/stringer specimen that is easier and less expensive to manufacture.

A taper angle is generally used at the edges of the flange in order to reduce the stress concentration at flange tip. A comparison between square-ended and tapered flanges revealed that a 20° taper angle reduced the stress concentration at the flange tip and improved the mechanical performance of the specimens by 30% [17]. Stress concentration at the flange tip is thus an important issue that needs to be further investigated, especially if other joining methods, such as resistance welding, are used.

In this paper, an investigation of resistance-welded skin/stringer specimens consisting of quasi-isotropic 16-ply APC-2/AS4 composite is presented. The main objectives of this work are to investigate the effects of the power level and clamping distance on the weld quality and mechanical performance of the specimens, to characterise the failure behaviour of the resistance-welded skin/stringer specimens under monotonic loading and to analyse two methods of reducing the stress concentration at the flange tip. The first method was to manufacture a taper angle at the flange tip and the second one was to create a resin fillet at the edges of the flange.

3.4 Experimental

3.4.1 Material

The laminates to be welded were provided by CYTEC Engineered Materials Inc. and were made of quasi-isotropic $[\pm45/90/0]_{2S}$ APC-2/AS4 material. The laminates were compression-moulded under a standard PEEK moulding condition, i.e., a processing temperature of 390°C, a residence time of 20 min., a moulding pressure of 0.7 MPa and a cool down rate of approximately 7°C/min. The geometries of the welded skin/stringer specimens are shown in Fig. 3-1. Two different flange configurations, square-ended (θ = 90°) and tapered (θ = 20°), were considered.

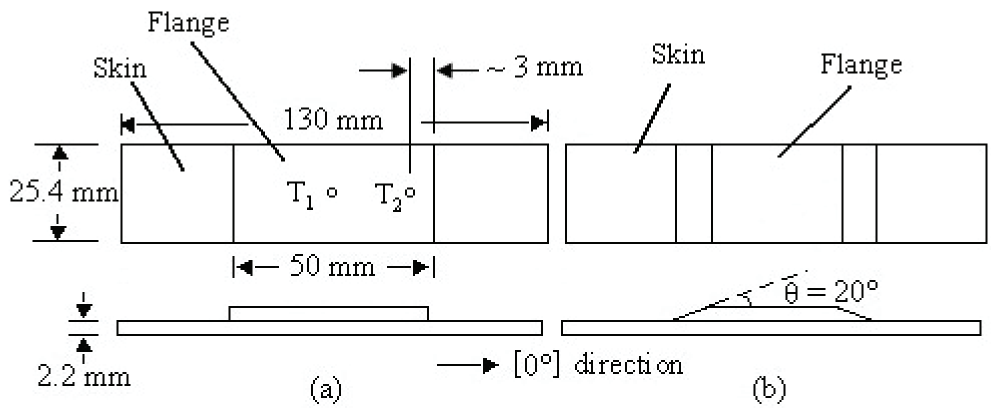

Fig. 3-1. Specimen geometry: square-ended (a) and tapered (b) flanges

3.4.2 Resistance welding

An experimental set-up was developed for the resistance welding and consisted of a DC power supply with maximum output of 40 A and 80 V, a pneumatic pressure system, a computer/data acquisition system and a resistance welding rig. The computer/data acquisition system was used to monitor the temperature at the weld interface and the applied current and voltage into the heating element. This system was utilised with a control system in order to adjust and control the input power. The control system was designed to stop the electrical current when the temperature at the weld interface reached a pre-determined welding temperature. The heating element was a stainless steel mesh with a wire diameter of 40 μm, an open gap of 90 μm and a thickness of 80 μm. A neat PEEK polymer film was placed on each side of the heating element in order to provide a resin rich region at the weld interface. The thickness of the films was 127 μm. The ends of the heating element were clamped between the copper electrical connectors and the skin laminate. To prevent possible current leakage to the conductive skin adherend, a layer of Kapton film (thickness of 30 μm) was placed between the skin laminate and the heating element under each electrical connector (Fig. 3-2).

The electrical current was then introduced to the heating element through the copper electrical connectors. A ceramic block was placed on the flange laminate to provide thermal insulation and facilitate uniform pressure distribution on the weld surface. All welds were conducted under a constant pressure of 1.0 MPa [19, 20]. The temperature during the welding operation was monitored using two K-type thermocouples with wire diameter of 0.25 mm. One thermocouple was located at the centre of the weld (T_1) and the other one was placed at approximately 3 mm from the edge of the flange (T_2). Both thermocouples were positioned at the weld interface, between the top neat PEEK film and the flange laminate (see Fig. 3-1 and Fig. 3-2).

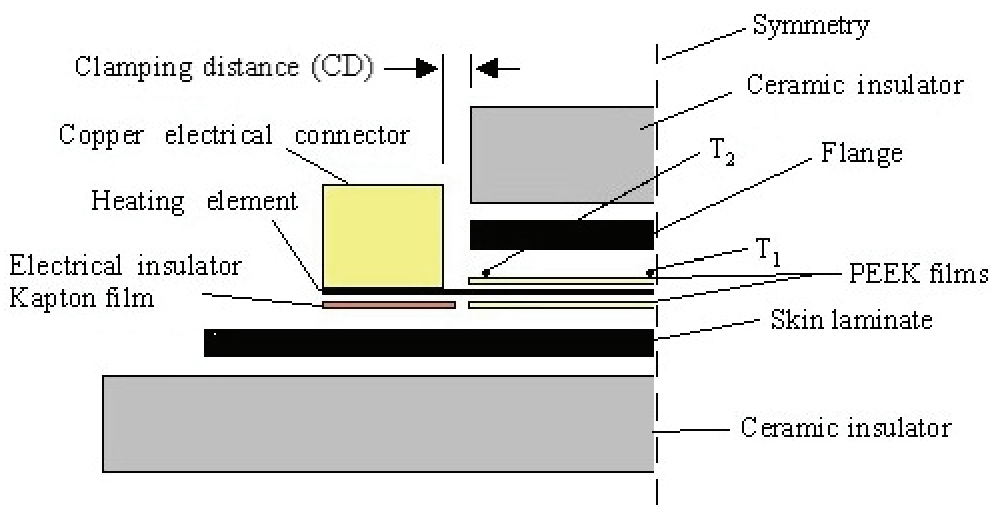

Fig. 3-2. Weld stack [19]

As mentioned in the introduction, a skin/stringer configuration with a 90° angle at the flange tip is subjected to stress concentration at the edges of the flange. To remedy this problem and improve the mechanical performance of the joined parts, two general methods are applicable: to machine a taper angle at the flange tip and to create a resin fillet at the edges of the flange. These two stress concentration reduction methods have shown good results in the past for adhesive bonding of thermosetting composites without major manufacturing issues [17]. Although the taper angle machining time is costly, no other difficulties usually appear in the bonding operation. However, the influences of these methods on fusion bonding process and mechanical performance of the welded parts have not been investigated. It was thus believed that, even though the stress concentration reduction methods are well known and established for adhesive bonding, they should be investigated for resistance welding of thermoplastic composites. In this study both methods were investigated. For the taper angle method, two approaches were taken. In the first one, the flange was machined at 20° taper angles prior to the welding operation. The tapered flange was then welded to the skin. In order to apply pressure on the inclined edges of the flange, the top ceramic block shown in Fig. 3-2 was machined with 20° angles to fit the geometry of the tapered flange. The welding operation was then conducted. In the second approach, the square-ended flange was welded to the skin (see Fig. 3-2) and the taper angles were then machined. For the other stress concentration reduction method, i.e., the resin fillet at the edges of the flange, the copper electrical connectors were machined to a 2.6 mm radius and placed very close to the edges of the weld (Fig. 3-3). This was to ensure that the resin squeezing out of the weld would mould in the cavity between the connectors and the edges of the flange in order to form a fillet. More resin was needed at the interface so that enough polymer would squeeze out of the weld and fit the radius of the connectors. Two polymer films were thus placed on each side of the heating element.

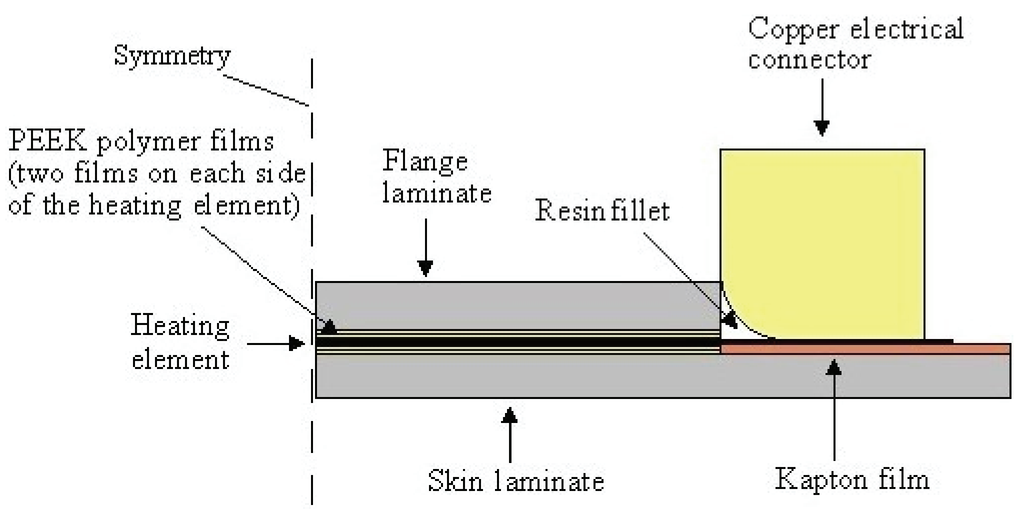

Fig. 3-3. Modified copper electrical connectors for the resin fillet method

Two schemes were used to apply the electricity into the heating element, i.e., the constant and ramped voltage methods. In the first scheme, a constant voltage was applied to the heating element until the polymer at the interface reached the desired welding temperature. Two constant voltages of 9.0 V and 9.5 V (corresponding to average area power levels of 249 kW/m^2 and 282 kW/m^2, respectively) were used for the constant voltage method. For the second scheme, i.e., the ramped voltage, the input voltage was increased at a predetermined rate. As reported by Yousefpour *et al.* [8], a more constant heating rate can be obtained with this method. Three ramped voltage rates (1.5 V/min., 3.0 V/min. and 6.0 V/min.) were used in this investigation.

In addition to the input power methods, another welding parameter, the clamping distance, was shown to be critical in resistance welding [21, 22]. The clamping distance, which is the distance between the edge of the specimen and the electrical connector (Fig. 3-2), was found to have a significant influence on the temperature distribution at the weld interface. When a large section of the heating element is exposed to air, the edges of the specimen tend to burn (local heating) before the temperature in the middle of the weld reaches the welding temperature. The problem of local over-heating arises from a sudden change in the heat transfer mechanism from convection and radiation to conduction at the edges of the weld [23]. The areas of the heating element exposed to air have poor heat transfer properties caused by free convection. As a result, the exposed areas reach a higher temperature faster than the areas of the heating element in contact with the weld interface. From preliminary tests at different clamping distances, two clamping distances of 1.5 mm and 2.0 mm were selected for the constant voltage technique and one clamping distance of 2.0 mm was used for the ramped voltage technique. It is worth mentioning that these two clamping distances could not be used for the samples welded using the resin fillet method. For these samples, the connectors were placed very close to the edges of the weld (approximately 0.5 mm) in order for the resin to mould into the cavity.

3.4.3 Methodology, mechanical testing and characterisation methods

As presented in Table 3-1, seven welding conditions were first investigated. The samples welded using these conditions were characterised by short beam shear tests, ultrasonic inspection and optical microscopy in order to determine the best welding conditions that should be further investigated. The two best welding conditions selected from these initial evaluations were then subjected to further characterisation under three- and four-point bending tests. From the results of the three- and four-point bending tests, one optimal welding condition was selected to investigate the stress concentration reduction methods at the flange tip.

Table 3-1. Welding parameters and their characterisation methods

Welding parameters		Evaluation methods				
Voltage or ramped voltage rate	**Clamping distance (mm)**	**Short beam shear test**	**Ultrasonic inspection**	**Optical microscopy**	**Three-point bending test**	**Four-point bending test**
9.0 V	1.5	X	X	X	X	X
9.0 V	2.0	X		X		
9.5 V	1.5	X	X	X		
9.5 V	2.0	X		X		
1.5 V/min.	2.0	X	X	X		
3.0 V/min.	2.0	X	X	X	X	
6.0 V/min.	2.0	X	X	X		

The short beam shear tests were conducted according to the ASTM D2344M standard test method. The samples were 4.6 mm thick and 8.5 mm wide and were cut off from a welded area as shown in Fig. 3-4. A support span of 18 mm and a crosshead speed of 1.0 mm/min. were used for all tests. Five replicated samples were tested for each welding condition. The interlaminar shear strengths (ILSS) were obtained from the first peak of the load-deflection curves. The fractured specimens were then analysed by optical microscopy. Non-destructive ultrasonic inspection was performed on welded samples as indicated in Table 3-1. Both C-scan and B-scan images were obtained. To confirm the results of the ultrasonic inspection, the specimens were cut at different locations of the weld area and the weld interface was analysed by optical microscopy. The two best welding conditions selected from the previous evaluations were then characterised using three- and four-point bending tests. These two mechanical test configurations were selected to represent the loading cases that are likely to occur in a real-life situation. For example, reinforced fuselages are subjected to a pressure differential between the cabin and the outside atmosphere. Under such loading, deformation of the skin is observed between each stringer. This local out-of-plane deformation then creates flexural loads in the skin that in turn create peel and shear stresses on the bondline between the skin and flange [17]. These peel and shear stresses were simulated using the three- and four-point bending tests. For the three-point bending test, a support span varying between 70 and 100 mm was used with the central load applied on the backside of the skin laminate. For the four-point bending test, the upper support had a 55 mm span and the bottom support had a span varying between 95 and 125 mm. Again, the load was applied on the backside of the skin laminate. Specimens were tested at 23°C and at a relative humidity of 50% under a crosshead speed of 2.0 mm/min. Five replicated samples were welded and tested for each welding condition. Optical and scanning electron microscopy were used to observe the failure mechanisms of the specimens.

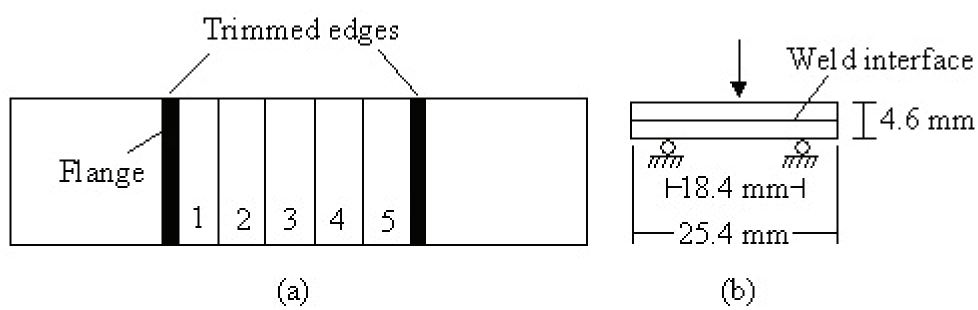

Fig. 3-4. Location of short beam samples on the specimen (a) and schematic of the short beam shear test (b)

3.5 Results and discussion

3.5.1 Thermal behaviour

The thermal behaviour of the square-ended specimens is discussed in this section. The temperature vs. time curves obtained for the constant voltage of 9.0 V and the two clamping distances of 1.5 mm and 2.0 mm are shown in Fig. 3-5. For a clamping distance of 2.0 mm, a large temperature gradient of 35°C was measured between the centre and the edge of the weld. This large temperature gradient was due to local heating at the edges of the weld as a larger section of the heating element was exposed to air. For the smaller clamping distance of 1.5 mm, T_1 was closer to T_2, showing a small temperature gradient of 7°C between the centre and the edge of the weld. These observations are in agreement with previous analytical and experimental studies; it was shown that reducing the clamping distance leads to lower temperature at the edges of the welds, because of the heat transfer in the copper connectors by conduction [21, 22]. The same type of temperature profile was observed for the constant voltage of 9.5 V, but the welding time was reduced from 60 to 45 seconds because of the higher power applied to the heating element. The temperature profile of the specimens welded under the ramped voltage rate of 3.0 V/min. is shown in Fig. 3-6. The welding time of these specimens was 210 seconds, which was 150 seconds longer than the specimens welded under the constant voltage of 9.0 V. This longer welding time was due to gradual increase of the applied power into the heating element using the ramped voltage scheme. Fig. 3-6 also shows that, as opposed to the constant voltage scheme, the ramped voltage scheme led to a lower temperature at the edges of the welds ($T_2 < T_1$). This was attributed to the initial low input voltage that was applied at the beginning of the process. The initial low input voltage did not over-heat the exposed region of the heating element, as was the case for the constant voltage method with initial high input voltage. The exposed region of the heating element started to over-heat only at the end of the process, when the voltage reached higher values. The edge effect was thus strongly reduced and the conduction in the connectors was the main reason explaining the lower temperature at the edges (temperature gradient of 35°C). This behaviour was present even though the larger clamping distance (2.0 mm) was used. The same type of temperature profile was monitored for the ramped voltage rates of 1.5 V/min. and 6.0 V/min. but the welding times were 323 and 120 seconds, respectively.

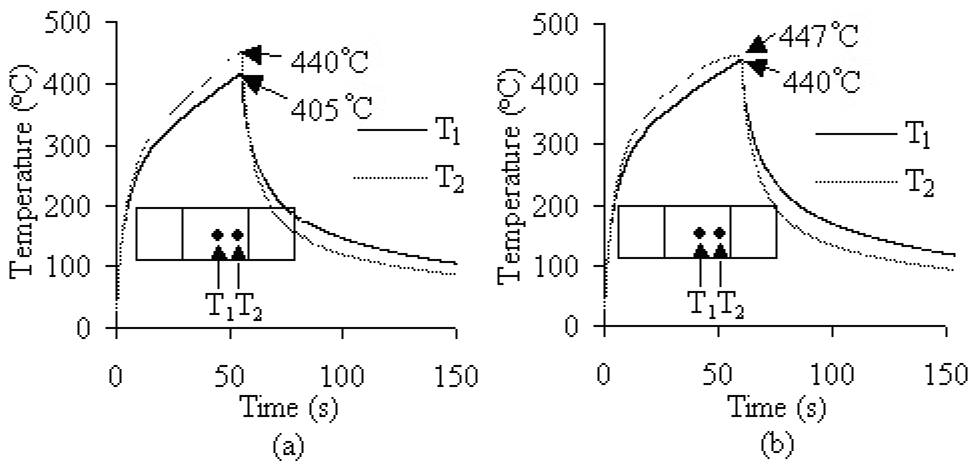

Fig. 3-5. Temperature profiles of the specimens welded under a constant input voltage of 9.0 V and clamping distances of 2.0 mm (a) and 1.5 mm (b)

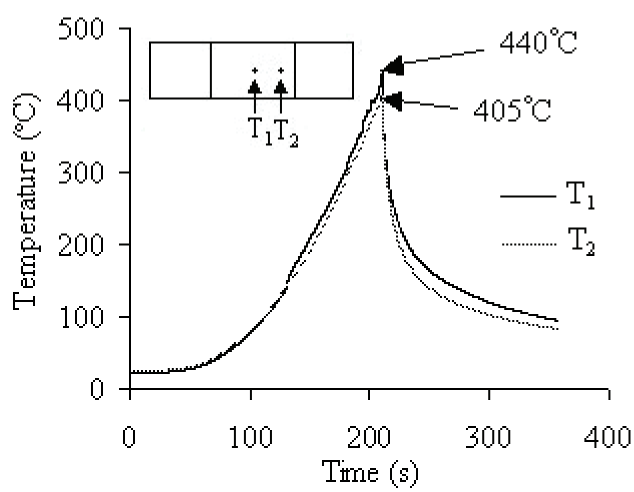

Fig. 3-6. Temperature profile of the specimens welded under the ramped voltage rate of 3.0 V/min.

3.5.2 Resistance welding process optimisation

The short beam shear strengths of the specimens welded using the various welding conditions are presented in Fig. 3-7. The error bars in this figure correspond to two standard deviations. The best ILSS (between 87.0 and 88.9 MPa) were obtained for three welding conditions: the ramped voltage rate of 3.0 V/min. and the constant voltages of 9.0 V and 9.5 V with a clamping distance of 1.5 mm. These three welding conditions showed small standard deviations (less than 5%). Larger standard deviations were obtained for the constant voltage method using a clamping distance of 2.0 mm. These larger standard deviations were expected since it was shown in the previous section that a clamping distance of 2.0 mm provided larger temperature gradients over the weld area (Fig. 3-5). For the ramped voltage of 3.0 V/min., the temperature profile also showed a large temperature gradient of 45°C between the centre and the edge of the weld (Fig. 3-6). However, the effect of this large temperature gradient was not reflected in the short beam shear test results as large standard deviations. In this case, it is possible that the tested samples were cut slightly closer to the centre of the weld and that the low-temperature-area was not part of the tested samples. However, in all cases, the extremities of the welds (approximately the first millimetre of the flange) were not part of the tested short beam samples (see Fig. 3-4 – a). The weld quality at this particular location could thus not be evaluated by the short beam shear tests.

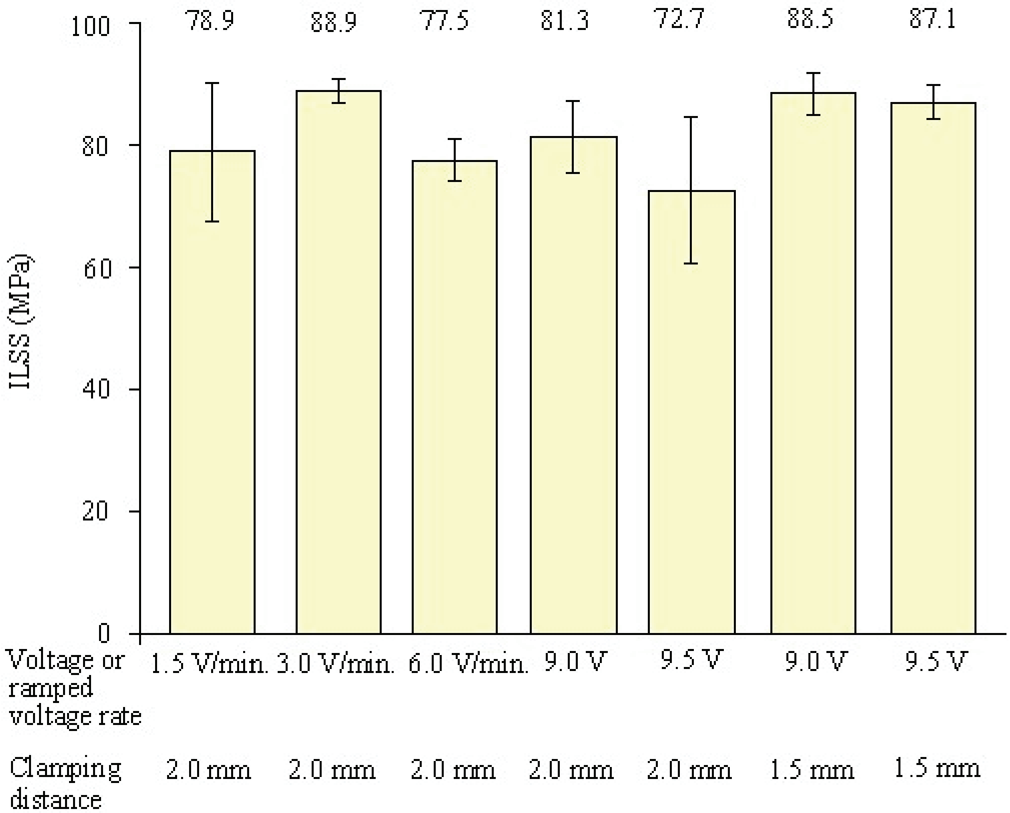

Fig. 3-7. Short beam shear strengths for different welding conditions

The two thermocouples that were placed in the welds were located at the centre of the short beam samples 1 or 5 (T_2) and short beam sample 3 (T_1) (see Fig. 3-4). It was thus possible to relate the ILSS of short beam samples 1, 3 and 5 to the temperatures measured at those particular locations. The resulting graph is shown in Fig. 3-8 as a plot of the ILSS vs. temperature. Three regions can be observed on this graph. At low welding temperatures (below 440°C), the ILSS increased with temperature. Two failure modes were present in this range. The first one was called laminate failure and was defined as a failure in the flange or skin laminates. In this case, a crack initiated and propagated at the interface between two plies, as is generally observed for the short beam shear tests on composite laminates. The second failure mode was called weld interface failure and was defined as a crack initiating and propagating at the weld interface. The weld interface failure was observed only for two samples and occurred between the weld interface and the skin or flange laminate (Fig. 3-9 – a). Between 440°C and 450°C, the ILSS reached a maximum and all the samples failed in the flange or skin laminates, between the 0° and the 90° or 45° plies (Fig. 3-9 – b). At temperatures higher than 450°C, the ILSS decreased with temperature but the samples still failed within the laminates. The lower ILSS values were attributed to deconsolidation in the laminates, due to the high temperatures involved.

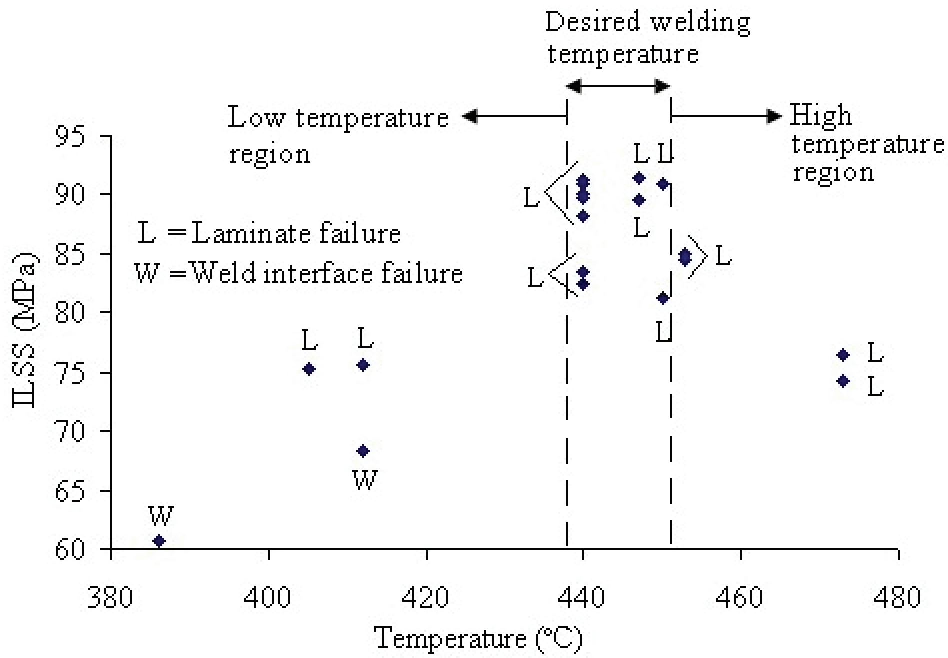

Fig. 3-8. ILSS vs. weld interface temperature and corresponding failure modes

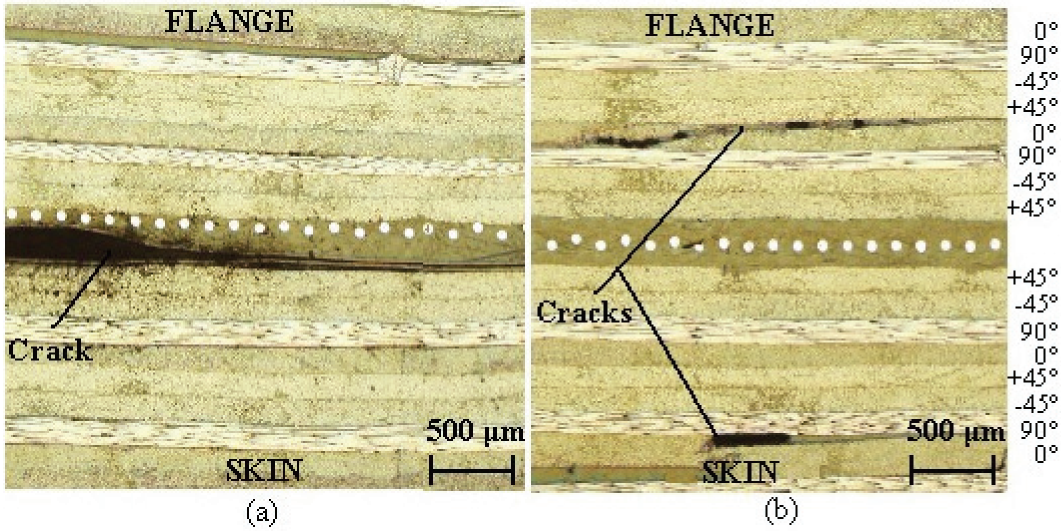

Fig. 3-9. Short beam shear tests failure modes: weld interface failure (a) and laminate failure (b)

Fig. 3-10 presents the C-scan images of five different welding conditions of the square-ended specimens. The figure shows that the weld quality is uniform in the centre of the specimens for all presented welding conditions. However, defects and porosities were observed at the edges of the welds. No significant difference was observed between the various welding conditions, except for the constant voltage of 9.0 V, where fewer defects were present at the edges. This more uniform quality over the weld area explained the small standard deviation obtained with this condition (Fig. 3-7). For the other welding conditions, where porosities were found at the edges of the weld, the B-scan images revealed that the porosities were not only located at the weld interface but also in the adherends. An example is given in Fig. 3-11 for the ramped voltage rate of 1.5 V/min. Optical microscopy was used to shade more light on the nature of the defects detected by the C-scan and B-scan images. Fig. 3-12 shows the weld interfaces at the centre and edge of a specimen welded using a constant voltage of 9.5 V. A good weld quality was observed at the centre of the welds (Fig. 3-12 – a) while defects were observed at the edges (Fig. 3-12 – b). The defects at the edges consisted of voids at the weld interface and in the skin and flange laminates. The voids at the weld interface were created during the welding operation, when the polymer melting temperature was reached and the polymer began to flow and squeeze out of the weld. Not enough resin was left behind to fill up the gaps between the metal mesh wires at the edges. This squeeze out phenomenon was thus responsible for the voids created at the weld interface. As for the deconsolidation and voids located in the skin and flange laminates, another phenomenon came into play. When the polymer squeezed out of the welds, only the remaining polymer, i.e., the polymer located at the centre of the welds, could sustain the applied welding pressure. The parts of the skin and flange laminates located at the edges thus experienced a reduced welding pressure, which was responsible for the deconsolidation and voids at the edges of the adherends.

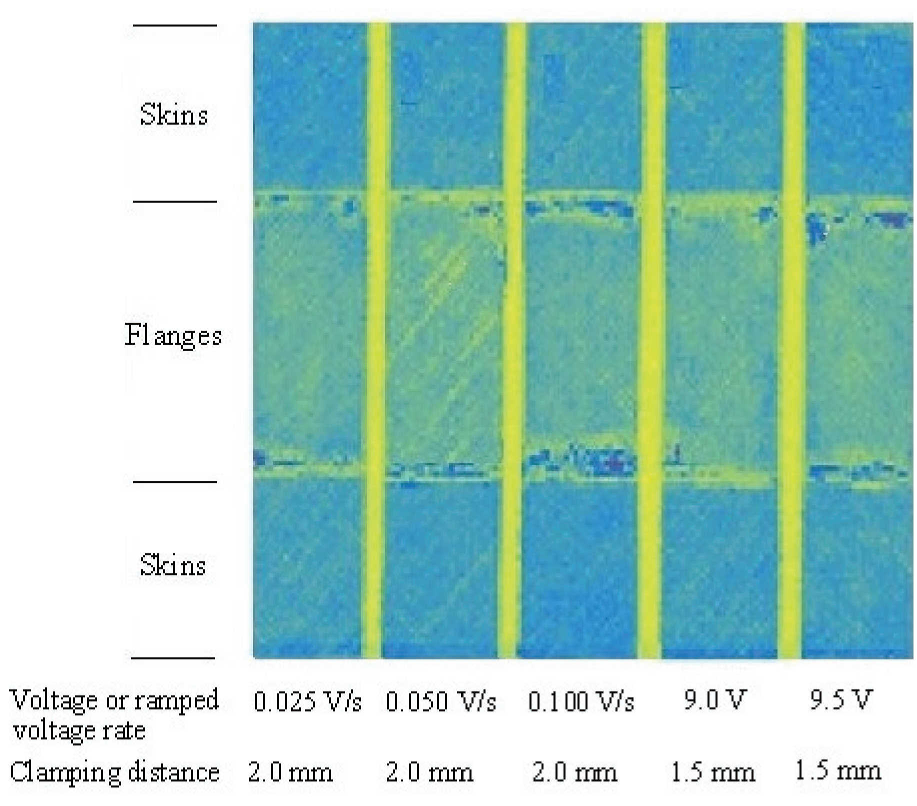

Fig. 3-10. C-scan of square-ended specimens for various welding conditions

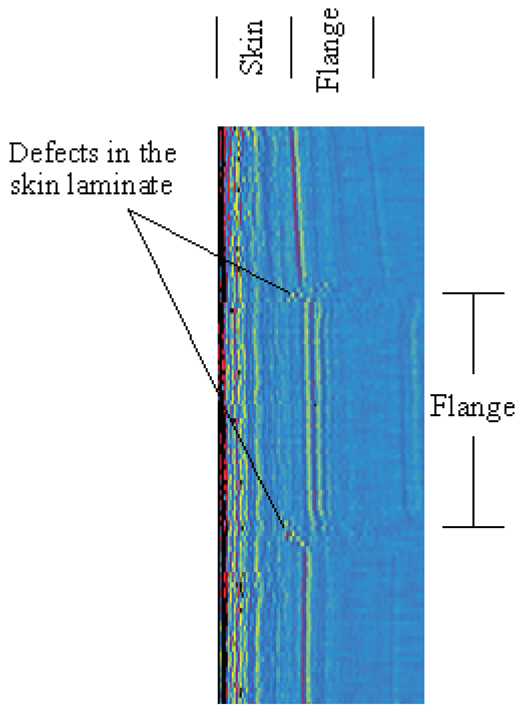

Fig. 3-11. B-scan of a square-ended specimen welded using the ramped voltage rate of 1.5 V/min.

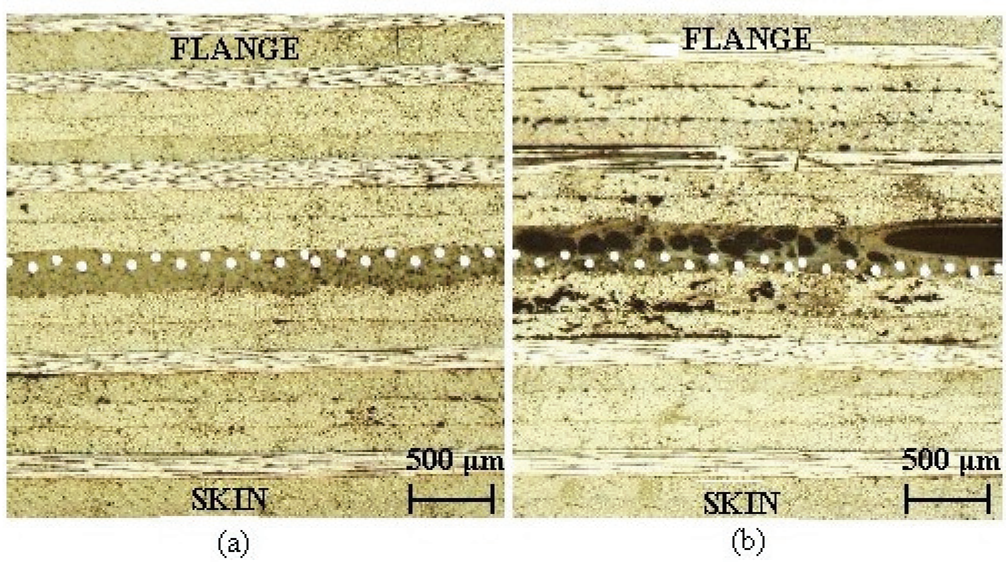

Fig. 3-12. Weld interfaces at the centre (a) and edge (b) of the specimens welded using a constant voltage of 9.5 V and a clamping distance of 1.5 mm

3.5.3 Mechanical performance

From the initial evaluation, two welding conditions, i.e., the constant voltage of 9.0 V with a clamping distance of 1.5 mm and the ramped voltage rate of 3.0 V/min., were selected (Table 3-1). Inadvertently, two of the five specimens welded at a ramped voltage rate of 3.0 V/min. experienced a higher processing temperature of 460°C in the centre of the weld. For those specimens, polymer squeeze out and distortion of the laminates were observed. For the proper intended processing temperature of 440°C, laminates remained intact. Three-point bending tests using a support span of 80 mm were performed on all specimens, including the over-heated specimens. The results are shown in Table 3-2. Unexpectedly, for the ramped voltage rate of 3.0 V/min., the specimens that were over-heated showed a better performance than the specimens that were welded under the intended temperature of 440°C. This unexpected result can be explained as follows. Cracks in the three-point bending test always started at the flange tip. The temperature reached in this region during the welding process is thus very important. For the over-processed specimens, the temperature at the flange tip was around the optimal temperature of 440°C when the temperature in the centre of the weld was 460°C. Specimens welded under this condition exhibited a better performance because of the optimal temperature reached at the flange tip, which delayed crack initiation. In the case of the specimens welded at the intended temperature of 440°C (in the centre), one can see in Fig. 3-6 that the temperature at the flange tip was around 405°C only. This low temperature at the flange tip could explain why cracks formed earlier in the test. These results are in good agreement with the ILSS vs. temperature relationship that was presented in Fig. 3-8. Even though the mechanical performance of the over-heated specimens was better, distortion of the specimens was unacceptable and the high temperature involved in the centre of the weld would probably cause polymer degradation and reduce the toughness of the welds. Scanning electron microscopy was used to observe the fracture surfaces of both specimens, in the centre of the weld (Fig. 3-13). As expected, good fibre/matrix adhesion was observed at the optimum processing temperature of 440°C, while a weaker adhesion was seen at the higher processing temperature of 460°C. The lower matrix ductility observed at the higher processing temperature was also an indication of polymer degradation. As reported by Denault and Dumouchel [24], PEEK undergoes chemical bonding during degradation, which leads to brittle fractures.

Table 3-2. Three-point bending performance

Welding condition	Maximum load (N)	Maximum bending moment (N-mm)
3.0 V/min. (over-heated)	1780 ± 69	13 350
3.0 V/min. (proper temperature)	1456 ± 35	10 920
9.0 V	1989 ± 20	14 918

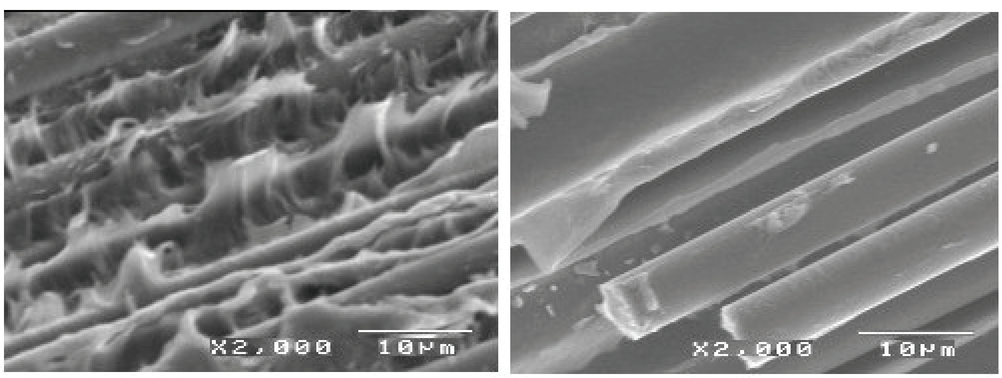

(a) (b)

Fig. 3-13. Fracture surfaces for processing temperatures of 440°C (a) and 460°C (b) [20]

Although the two selected welding conditions have shown similar results under short beam shear tests (Fig. 3-7), the specimens welded at the constant voltage of 9.0 V showed better performance under 3-point bending test than the specimens welded at the ramped voltage of 3.0 V/min. (Table 3-2). This can be attributed to higher sensitivity of the three-point bending test to the weld quality at the flange tip. The bending moment at the flange tip creates a peel stress, which leads to crack opening, similarly to a mode I crack propagation. This crack opening mechanism is very sensitive to voids and porosities at the tip of the flange. When preparing the short beam samples, the edges of the welds were trimmed (Fig. 3-4 – a). The defects that were located in this region were thus not present in the short beam samples and their effect on the weld performance could not be assessed. Since better temperature uniformity was obtained with the constant voltage of 9.0 V, the weld quality at the flange tip was better (see C-scan Fig. 3-10), explaining the better performance of the specimens welded with this condition under three-point bending.

In a three-point bending test, the weld interface experiences both shear forces and bending moment. In previous studies on adhesive bonding of thermosetting composites skin/stringer configurations, it was shown that the main mechanism contributing to debonding was the bending moment at the flange tip [17]. This was proved by testing samples under three- and four-point bending tests with various spans [17]. The same study was performed here on the specimens welded under the constant voltage of 9.0 V. Table 3-3 presents the comparison between the tests. Considering the standard deviations, the bending moments obtained from three- and four-point bending tests were comparable. This indicates that the main failure mechanism responsible for delamination is the bending moment at the flange tip. This is in agreement with the previous study on adhesively bonded skin/stringer specimens [17]. The specimens welded under the ramped and constant voltage exhibited the same failure behaviour. In both cases, two failure modes were observed. In the first one, a crack initiated at the flange tip, between the weld and the skin laminate. This crack then started to propagate at the weld interface, towards the centre of the flange. A matrix crack branching was then observed, going from the weld interface to the ±45° ply interface of the skin laminate. From this point, another delamination occurred, which was followed by another matrix crack branching to the -45°/90° ply interface of the skin. This first failure mode is schematically depicted in Fig. 3-14 – a. In the second failure mode, a first crack initiated at the flange tip, at the ±45° ply interface of the skin laminate. This crack then propagated in the skin laminate, towards the centre of the weld. At some point, a matrix crack branching was observed and a second delamination propagated at the weld interface. This failure mode is illustrated in Fig. 3-14 – b. SEM micrographs were taken to shade more light on the failure behaviour of the welds (Fig. 3-15). No adherence was observed between the wires of the heating element and the PEEK polymer, which means that the weld relied on mechanical interlocking rather than interfacial bonding.

Table 3-3. Three- and four-point bending tests results for specimens welded under a constant voltage of 9.0 V

	Three-point bending tests				Four-point bending tests			
Upper support span (mm)	-	-	-	-	55	55	55	55
Bottom support span (mm)	70	80	90	100	95	105	115	125
Maximum load (N)	2873	1989	1703	1326	2392	1454	1147	1045
Maximum bending moment (N-mm)	14365	14918	17030	16575	23322	17812	16918	18026
Average bending moment (N-mm)	17 003 ± 1282				19 020 ± 2908			

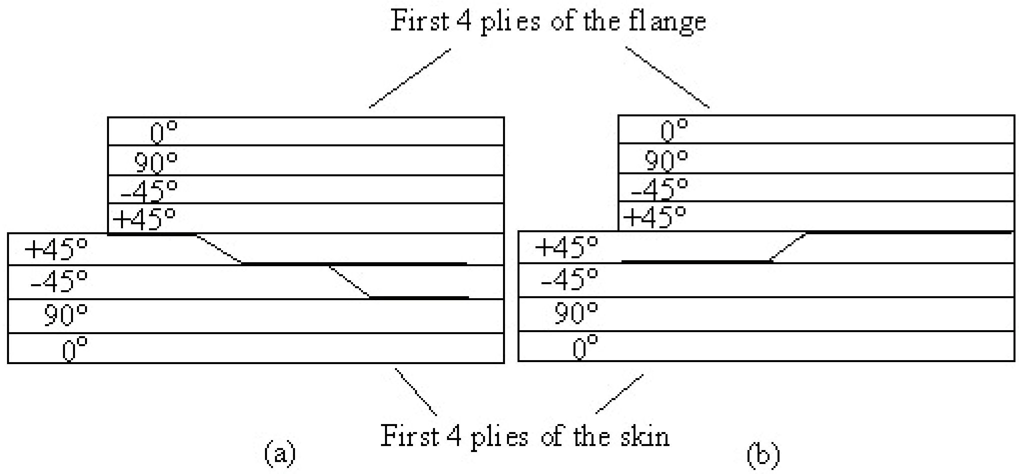

Fig. 3-14. Failure modes of the square-ended specimens under three-point bending

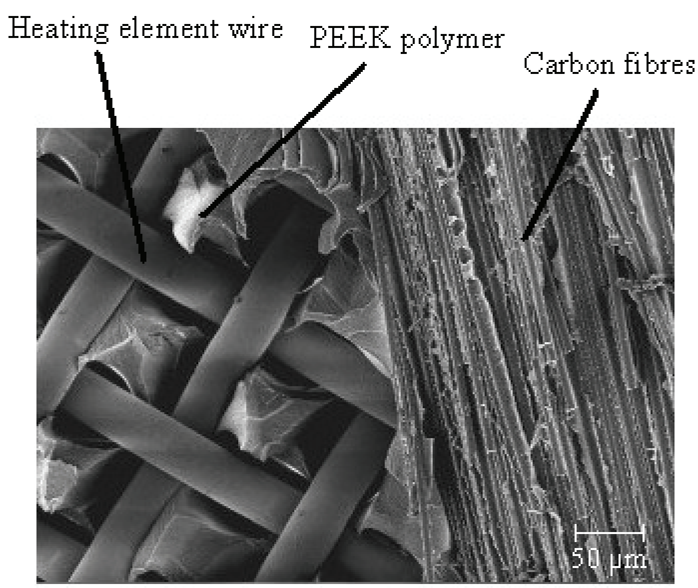

Fig. 3-15. SEM micrograph of a square-ended specimen tested under three-point bending

3.5.4 Stress concentration reduction

From the previous section, an optimal welding condition has been identified, i.e., a constant voltage of 9.0 V with a clamping distance of 1.5 mm. This welding condition provided a better weld quality at the edges of the flange, which led to an overall better mechanical performance than all the other welding conditions. This condition was thus selected to investigate the last aspect of the study, which is the stress concentration reduction at the flange tip.

Table 3-4 presents the results of the three-point bending tests for the stress concentration reduction methods described in the experimental section. The tapered specimens that were machined before the welding operation did not show any mechanical performance improvement in comparison to the square-ended specimens. This lack of improvement was due to lower pressure distribution at the inclined edges of the flange, which resulted in weak bond at the edges of the weld. It is possible that the machined ceramic bloc did not match the flange tapered surface adequately, causing an incomplete pressure transfer to the weld interface. As mentioned before, the flange tip is a critical location of the specimens where cracks first initiate. Since the welding pressure was low at this location, the cracks formed earlier during the mechanical tests, even though the stress concentration was reduced. The second reason for the lack of improvement was overheating of the edges due to the inclined edges. It was shown before that a uniform temperature distribution over the weld area is difficult to obtain and very sensitive to the boundary condition at the flange tip. With the tapered edge, a uniform temperature is even harder to obtain. In some of the welded specimens, the edges of the weld experienced distortion caused by the high temperature in the thin part of the flange. The intended taper angle was thus deformed and stress concentration at the flange tip was no longer controllable. The second approach was to weld the square-ended specimens and then machining the taper angle. This approach showed 25% mechanical performance improvement over the square-ended specimens (Table 3-4). This was attributed to better temperature and pressure control during the welding operation. This 25% mechanical performance improvement is comparable to what was reported for adhesively bonded tapered skin/stringer specimens [17]. The disadvantage of this method is that special care had to be taken not to damage the skin laminate when machining the taper angles after the welding operation.

Table 3-4. Maximum loads under three-point bending

Square-ended specimens	Tapered specimens (machined before welding)	Tapered specimens (machined after welding)	Resin fillet specimens
1989 ± 80 N	1858 ± 98 N	2486 ± 107 N	1710 ± 64 N

The resin fillet method did not exhibit any mechanical performance improvement. The reason for the lower performance in this case was the fact that a very small clamping distance had to be used during the welding. The small clamping distance induced a cold edge, which was responsible for a weaker bond in this area. Cracks thus initiated at the flange tip earlier in the mechanical tests. It was tried to increase the welding temperature in order for the edges of the specimen to reach the optimal temperature of 440°C. But even at a very high processing temperature of 500°C (at the centre of the weld), the temperature at the edges remained low (below 400°C) and the mechanical performance of the specimens could not be improved.

Two failure behaviours were observed for the tapered specimens. For the specimens that were machined prior to the welding operation, the crack started at the flange tip at the weld interface and then propagated in the skin laminate at the ±45° plies interface and between the -45° and 90° plies. This failure mode was the same as the first failure mode of the square-ended specimens (Fig. 3-14 – a). The specimens that were machined after the welding operation showed a crack initiation in the flange laminate, at the ±45° ply interface. The crack then propagated in the flange and skin laminates, after tearing the heating element (Fig. 3-16). The specimens welded using the resin fillet method exhibited a different failure mode. The crack initiated at the weld interface and then propagated in the skin laminate at the ±45° plies interface.

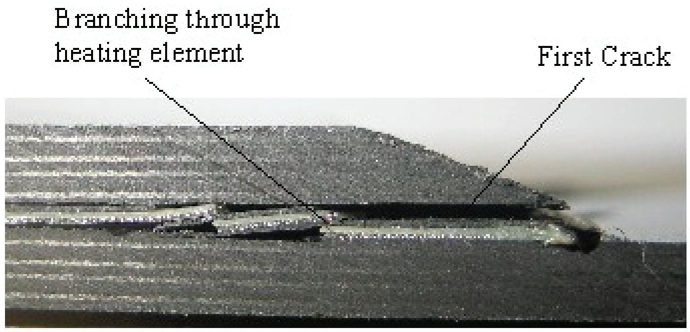

Fig. 3-16. Failure mechanism of tapered specimens machined after welding

Among different methods attempted to reduce the stress concentration at the flange tip, only one showed a substantial mechanical performance improvement. Machining the taper angle before the welding operation was simpler from a machining point of view but it complicated the welding task and no mechanical performance improvement could be obtained. The resin fillet method did not show any mechanical performance improvement due to the lower welding temperature involved at the edges of the welds. It is thus believed that the best way to reduce the stress concentration and improve the mechanical performance is to machine the taper angles after the welding operation. This method required more machining time and precautions but was the most efficient one in reducing the stress concentration.

3.6 Summary and conclusions

In this study, quasi-isotropic APC-2/AS4 composite skin/stringer specimens were resistance-welded using a stainless steel mesh heating element. Different constant and ramped voltages were used to apply power to the heating element and the quality of the welds was analysed using short beam shear tests, ultrasonic inspection, optical and scanning electron microscopy and three- and four-point bending tests. ILSS of 88 MPa was obtained and the following conclusions were drawn from the investigation:

1) Ultrasonic C-scan inspection and optical microscopy showed that weld quality is uniform over the weld area, except at the specimens' edges where voids and porosities were observed. This was caused by polymer squeeze-out during the welding operation as well as a reduced pressure at the edges of the welds.
2) Short beam shear tests showed that the temperature reached at the weld interface has an important effect on the strength of the welds. An optimum processing temperature of 440°C was determined.
3) For the particular specimen geometry presented, the constant voltage method is the best way to apply power to the heating element. An optimal clamping distance of 1.5 mm with a constant voltage of 9.0 V (corresponding to an average area power level of 249 kW/m^2) led to the best mechanical performance. This is due to the better temperature uniformity obtained with this reduced clamping distance, as opposed to a larger clamping distance of 2.0 mm.
4) The main mechanism contributing to flange debonding is the bending moment at the flange tip. No difference in the bending moment at the flange tip was observed between the three- and four-point bending tests. The same failure modes were also observed.
5) A 20° taper angle improved the mechanical performance by 25%. This improvement was obtained for the specimens that were machined after the welding operation. The flanges that were machined prior to welding did not show any mechanical performance improvement. This was due to the difficulties associated with the temperature distribution at the flange tip as well as the reduced welding pressure on the inclined edges. The polymer fillets at the edges of the flange did not improve the mechanical performance either because of the small clamping distance that had to be used, which prevented the edges of the welds from heating properly.

The taper angle is a common method used in aerospace industry to reduce the stress concentration in adhesively bonded skin/stringer configurations. In resistance welding, the taper angle method induces extra difficulties because of the over-heating at the edges of the flange. Machining the angles after the welding operation led to better results but this method required more machining time and precautions. Future work should thus focus on other methods to reduce the stress concentration at the flange tip. In addition, since resistance welding finds applications in the aerospace industry, where parts are subjected to cyclic loading, fatigue analysis of the skin/stringer configuration is essential and should be the subject of future investigations.

3.7 Acknowledgements

This work was supported by funding from the Natural Sciences and Engineering Research Council of Canada. The authors also greatly acknowledge Mr. Christian Néron from Industrial Materials Institute for his help concerning the ultrasonic inspection and Mr. David Leach from Cytec Engineered Materials Inc. for providing the materials used in this study.

3.8 References

1. Hou, M., Ye, L., Mai, Y.W. An experimental study of resistance welding of carbon fibre fabric reinforced polyetherimide (CF fabric/PEI) composite material. Applied Composite Materials 1999;6(1):35-49.

2. Yousefpour, A., Hojjati, M., Immarigeon, J.-P. Fusion Bonding/Welding of Thermoplastic Composites. Journal of Thermoplastic Composite Materials 2004;17(4):303-341.

3. Stokes, V.K. Joining methods for plastics and plastic composites: an overview. Polymer Engineering and Science 1989;29(19):1310-1324.

4. Stavrov, D., Bersee, H.E.N. Resistance welding of thermoplastic composites - an overview. Composites Part A: Applied Science and Manufacturing 2005;36(1):39-54.

5. Gardiner, G. Thermoplastic composites gain leading edge on the A380. High-Performance Composites - Design and Manufacturing Solutions for Industry 2006:50-55.

6. Stavrov, D., Bersee, H.E.N. Experimental Investigation of Resistance Welding of Thermoplastic Composites with Metal Mesh Heating Element. SAMPE-Europe, Paris, France, 2004.

7. Stavrov, D., Bersee, H.E.N., Beukers, A. The Influence of the Heating Element on Resistance Welding of Thermoplastic Composite Materials. International Conference on Composite Materials, San Diego, USA, 2003.

8. Yousefpour, A., Simard, M., Octeau, M.-A., Hojjati, M. Process Optimization of Resistance-Welded Thermoplastic Composites Using Metal Mesh Heating Elements. SAMPE, Long Beach, USA, 2005.

9. Don, R.C., Gillespie, J.W., Lambing, C.L.T. Experimental characterisation of processing-performance relationships of resistance welded graphite/PEEK [polyetheretherketone] composite joints. Polymer Engineering and Science 1992;32(9):620-631.

10. Hou, M., Friedrich, K. Resistance welding of continuous carbon fibre/polypropylene composites. Plastics Rubber and Composites Processing and Applications 1992;18(4):205-213.

11. Hou, M., Friedrich, K. Resistance welding of continuous glass fibre reinforced polypropylene composites. Composites Manufacturing 1992;3(3):153-163.

12. Xiao, X.R., Hoa, S.V., Street, K.N. Processing and Modelling of Resistance Welding of APC-2 Composite. Journal of Composite Materials 1992;26(7):1031-1049.

13. Ageorges, C., Ye, L., Hou, M. Experimental investigation of the resistance welding of thermoplastic-matrix composites. II. Optimum processing window and mechanical performance. Composites Science and Technology 2000;60(8):1191-1202.

14. Ageorges, C., Ye, L., Hou, M. Experimental investigation of the resistance welding for thermoplastic-matrix composites. I. Heating element and heat transfer. Composites Science and Technology 2000;60(7):1027-1039.

15. Hou, M., Yang, M.B., Beehag, A., Mai, Y.W., Ye, L. Resistance welding of carbon fibre reinforced thermoplastic composite using alternative heating element. Composite Structures 1999;47(1-4):667-672.

16. Yousefpour, A., Simard, M., Octeau, M.-A., Lamarée, M., Hojjati, M. Effects of Mesh Size on Resistance Welding of Thermoplastic Composites Using Metal Mesh Heating Elements. SAMPE-Europe, Paris, France, 2004.

17. Minguet, P.J., O'Brien, T.K. Analysis of test methods for characterizing skin/stringer debonding failures in reinforced composite panels. Composite Materials: Testing and Design, Proceedings of the 12th Symposium, Montréal, Canada, 1996.

18. Minguet, P.J., O'Brien, T.K. Analysis of composite skin/stringer bond failure using a strain energy release rate approach. Tenth International Conference on Composite Materials. I. Fatigue and Fracture, Whistler, Canada: Woodhead Publishing Limited, 1995.

19. Dubé, M., Hubert, P., Yousefpour, A., Denault, J. Mechanical Performance of Resistance-Welded Thermoplastic Composite Skin/Stringer Specimen. SAMPE Fall Technical Conference, Seattle, USA, 2005.

20. Dubé, M., Hubert, P., Yousefpour, A., Denault, J., Wadham-Gagnon, M. Resistance Welding of Thermoplastic Composites Skin/Stringer Specimens. SAMPE, Long Beach, USA, 2006.

21. Stavrov, D., Bersee, H.E.N. Thermal Aspects in Resistance Welding of Thermoplastic Composites. ASME Summer Heat Transfer Conference, Las Vegas, USA, 2003.

22. Talbot, E., Yousefpour, A., Hubert, P., Hojjati, M. Thermal Behavior During Thermoplastic Composites Resistance Welding. Annual Technical Conference (ANTEC) of the Society of Plastics Engineers, Boston, USA, 2005.

23. Eveno, E., Gillespie, J.W.J. Resistance welding of graphite polyetheretherketone composites - An experimental investigation. Journal of Thermoplastic Composite Materials 1988;1:322-338.

24. Denault, J., Dumouchel, M. Consolidation Process of PEEK/Carbon Composite for Aerospace Applications. Advanced Performance Materials 1998;5:83-96.

CHAPTER 4. SECOND MANUSCRIPT

4.1 Preface

In the previous chapter, the mechanical behaviour of resistance-welded skin/stringer specimens was investigated. The adherends were made of quasi-isotropic APC-2/AS4 composite. No major problems were detected when welding these quasi-isotropic laminates. However, the welding of UD laminates is more complicated because of the current leakage issue. This chapter focuses on a new solution to the current leakage problem and its impact on the joint static mechanical properties.

Current leakage prevention in resistance welding of carbon fibre reinforced thermoplastics*

*Composites Science and Technology, 2007, doi: 10.1016/j.compscitech.2007.09.008

Dubé, M. and Hubert, P.
McGill University, CREPEC, Department of Mechanical Engineering
817 Sherbrooke Street West, Montréal, Québec, H3A 2K6, Canada

Yousefpour, A.
Aerospace Manufacturing Technology Centre, National Research Council Canada
5145 Decelles Avenue, Montréal, Québec, H3T 2B2, Canada

Denault, J.
Industrial Materials Institute, National Research Council Canada
75 de Mortagne, Boucherville, Québec, J4B 6Y4, Canada

4.2 Abstract

Current leakage is a concern with resistance welding of carbon fibre reinforced thermoplastic composites. This phenomenon is particularly important when unidirectional adherends, with the carbon fibres parallel to the electrical current direction, are welded. In this investigation, a new electrically-insulated heating element consisting of a ceramic-coated (TiO_2) stainless steel mesh was developed to prevent current leakage. A special specimen geometry, called a skin/stringer configuration, was welded with this newly developed heating element to represent typical reinforced aerospace structures. The adherends were made of APC-2/AS4 (carbon fibre/PEEK) composites. Unidirectional specimens, which represent the most critical case, were first welded using the new heating element. The insulated heating element successfully prevented current leakage and showed great improvement in temperature homogeneity over the weld area. The impact of the new heating element on the mechanical performance of the welds was then assessed by welding quasi-isotropic specimens. The mechanical performances of quasi-isotropic specimens welded using the new insulated heating elements and conventional (non-insulated) ones were compared under short beam and three-point bending tests. No mechanical performance drawback was observed with the new heating element; however, the failure mode of the welded quasi-isotropic specimens was changed from a delamination in the skin laminate failure to a weld interface debonding failure.

Keywords: Resistance welding; A. Polymer-matrix composites (PMCs); A. Coating; B. Mechanical properties; E. Welding/joining; Heating element.

4.3 Introduction

Joining has been identified as one of the major issues in the implementation of continuous fibre reinforced composite structures in industry [1]. As the complexity of the components made of composite materials increases, efficient, reliable and low-cost joining methods are needed [2]. Conventional joining methods such as adhesive bonding and mechanical fastening have been developed for composite materials. In the case of thermoplastic-matrix composites, fusion bonding, or welding, is an advantageous joining method, since no extensive surface treatment is required and no stress concentrations are induced by the holes drilling process. Among the various available welding methods, resistance welding has been shown to be an efficient, simple and low-cost technique [3]. This welding process requires the application of a heating element between two thermoplastic composite parts to be welded (adherends). An electrical current is applied to the heating element and its temperature rises due to the Joule heating effect. As temperature rises, the surrounding polymer softens (amorphous polymers) or melts (semi-crystalline polymers). When the desired welding temperature is reached, the electrical current is stopped and the polymer cools down, under the application of pressure, resulting in a weld.

The experimental studies performed on the resistance welding process shed light on some critical issues that need to be addressed before this technique can be fully implemented in industry [1, 4-12]. Current leakage has been expressed as a major concern when electrically conductive adherends, such carbon fibre reinforced thermoplastics, are welded [1, 4, 5, 13]. When the polymer at the weld interface melts and flows, the heating element can get in contact with the carbon fibres of the adherends and as a result, new electrical paths are created in the adherends. Current leakage is an uncontrollable variable that results in long welding times, due to power losses in the adherends, and non-homogenous temperature distribution over the weld area. To remedy this problem, Don *et al.* [14] used two polymer films on each side of the heating element in order to prevent the heating element from touching the carbon fibres. This solution shows very limited success in preventing current leakage mostly because the melted polymer tends to squeeze out of the weld and thus no longer offers a barrier against current leakage. Another proposed solution was the use of a glass fibre ply on each side of the heating element [5, 9]. This solution can successfully prevent the current leakage; however, it adds a foreign material in the weld, which reduces the weld strength and leads to a thicker specimen [9, 13]. Another solution that has been developed is spraying of a high-temperature resistive paint on the heating element [9]. The paint is electrically resistive and thermally stabile up to 600°C. Good electrical insulation can be obtained with this method but the paint has to undergo a three-step curing cycle after it is applied on the heating element. This operation prolongs the resistance welding, which had the advantage of being a simple and fast technique. Current leakage thus remains an issue that needs to be addressed. So far, this problem has limited the applications of the resistance welding technique to glass fibre reinforced polymers.

In a previous study, resistance welding of a special specimen geometry, called a skin/stringer specimen, was investigated [15]. The specimens were made of a flange laminate, representing a stringer or frame, welded onto a skin laminate. This particular specimen geometry was selected as it represents a typical reinforced aerospace structure [16]. Both the flange and skin laminates were made of quasi-isotropic APC-2/AS4 (carbon fibre/PEEK) composite. The welding parameters, mechanical performance and failure modes of the specimens were investigated [15]. The present study uses the same skin/stringer geometry and pursues two main objectives: to develop a new insulated heating element that prevents current leakage and to analyse the effects of this insulated heating element on the mechanical performance and failure modes of the welded skin/stringer specimens.

4.4 Experimental procedures

4.4.1 Materials and specimen geometry

The adherends used in this study were made of 16 plies of unidirectional (UD) and quasi-isotropic $[\pm 45/90/0]_{2S}$ APC-2/AS4 composite laminates. The APC-2/AS4 laminates were provided by CYTEC Engineered Materials Inc. and were compression-moulded under a standard PEEK moulding condition, i.e., a processing temperature of 390°C, a residence time of 20 minutes, a moulding pressure of 0.7 MPa and a cool down rate of approximately 7°C/minute. The laminates were 2.2 mm thick. In order to evaluate the efficiency of the current leakage solutions, specimens made of non conductive material, which consisted of UD 16 plies glass fibre/PEEK (GF/PEEK) adherends, were also welded, as a benchmark reference. The considered specimen geometry in all cases was the skin/stringer configuration with square-ended (θ = 90°) flanges (Fig. 4-1) [6, 17-19]. The skin laminate was 130 mm long and 25.4 mm wide and the flange was 50 mm long and 25.4 mm wide.

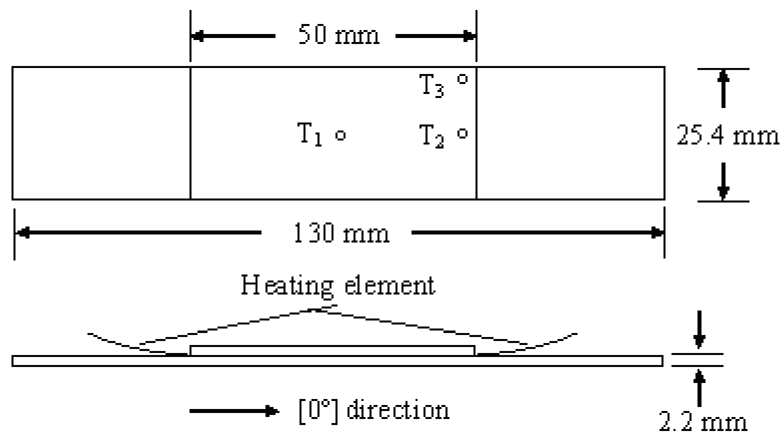

Fig. 4-1. Specimen geometry

4.4.2 Resistance welding set-up

The resistance welding set-up consisted of a DC power supply with maximum output of 40 A and 80 V, a pressure system, a computer/data acquisition system and a resistance welding rig. The computer/data acquisition system was used to monitor the temperature, current and voltage in the welds. The current and voltage were monitored at the copper connectors. A control system was developed using National Instruments Labview software to control the input power. The control system was designed such a way that when temperature at the weld interface reached a pre-determined welding temperature of 440°C, the electrical current was turned off [15].

The resistance welding rig that was used to weld the skin/stringer specimens was described in [15]. The heating element was placed between the skin and flange laminates. The ends of the heating element were clamped between the copper electrical connectors and the skin laminate (Fig. 4-2). A ceramic block was placed on the flange laminate to provide thermal insulation and facilitate a uniform pressure distribution on the weld surface. Two side ceramic blocks were used to prevent lateral movement of the flange during the welding process. All welds were conducted under a constant pressure of 1.0 MPa. Temperature during the welding operation was monitored using three K-type thermocouples. One thermocouple was located at the centre of the weld (T_1), one was placed at the edge of the flange (T_2) and the last one was placed at the corner of the flange (T_3). All three thermocouples were positioned at the weld interface, between the top neat PEEK film and the flange laminate (Fig. 4-1 and Fig. 4-2).

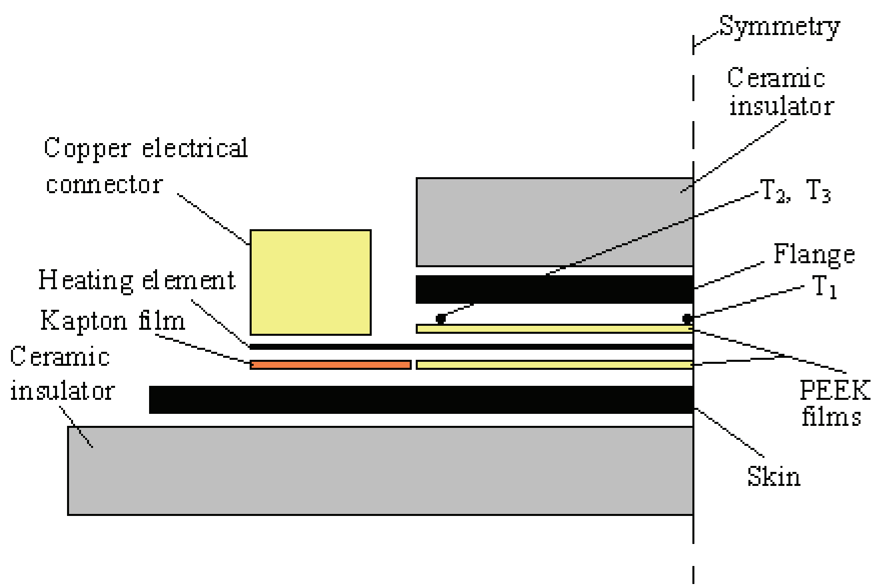

Fig. 4-2. Weld stack [15, 17]

The input power was applied to the heating element using the constant voltage method [11]. A constant voltage of 9.0 V was applied until the polymer reached the desired welding temperature of 440°C. It is worth noting that, although the voltage was constant in this method, the input power varied. Since the electrical resistance of the stainless steel heating element increased with temperature, the input current, and thus the power, decreased accordingly. The monitored current and voltage data were used to calculate the electrical resistance according to the simple formula $R = V/I$ where R is the electrical resistance (Ω), V is the voltage (V) and I is the current (A). Plots of the electrical resistance as a function of the weld interface temperature were obtained from these data. Since the voltage was measured at the copper connectors' terminals, the calculated resistance was the summation of the copper connectors' resistances, the contact resistances between the heating element and connectors and the resistance of the heating element itself. All these resistances were considered to be in series. If current leakage occurred, then new electrical paths were created in the adherends and the new created electrical resistances were considered to be in parallel with the heating element resistance. In order to reduce the impact of the contact resistance between the connectors and heating element, a torque wrench was used to apply a clamping pressure of 16.3 MPa for each weld [5]. The contact resistance was constant since a constant clamping pressure was applied. Thus, the variations of electrical resistance were caused by the heating element or current leakage only.

4.4.3 Heating element preparation

The heating element was a stainless steel mesh with a wire diameter of 40 μm and an open gap width of 90 μm. The thickness of the mesh was 80 μm. A neat PEEK polymer film (thickness of 127 μm) was applied on each side of the mesh to provide a resin-rich region at the weld interface. This heating element, sandwich between these two polymer films, is referred to in the text as the conventional heating element (conventional HE). Two methods were elaborated to prevent current leakage to the adherends. The first method was similar to the one used by Don *et al*. [14] and consisted in applying a second polymer film to each side of the stainless steel mesh. That is, two films of a thickness of 127 μm were placed on each side of the mesh. This heating element is referred to as the two-films HE. The second insulation method was to coat the stainless steel mesh with a layer of nanostructured titanium oxide (TiO_2) powders. This powder was produced by Altair Nanomaterials Inc. and was deposited on the mesh using the high velocity oxy-fuel (HVOF) thermal spraying method. It was shown in a previous investigation that the nanostructured TiO_2 coating is tougher and more ductile than the conventional TiO_2 coating and provides a better interfacial bonding with the stainless steel substrates [20]. These characteristics explain the choice of the nanostructured TiO_2 coating for this investigation. The meshes were cut to the desired dimensions, cleaned with acetone and placed on an aluminium plate. HVOF spraying was then conducted on the meshes with special care not to coat the edges, which have to be connected to the copper electrical connectors. The TiO_2 layer applied on the heating element was 2 μm thick (Fig. 4-3). The TiO_2-coated heating elements are referred to as TiO_2 HE in the text.

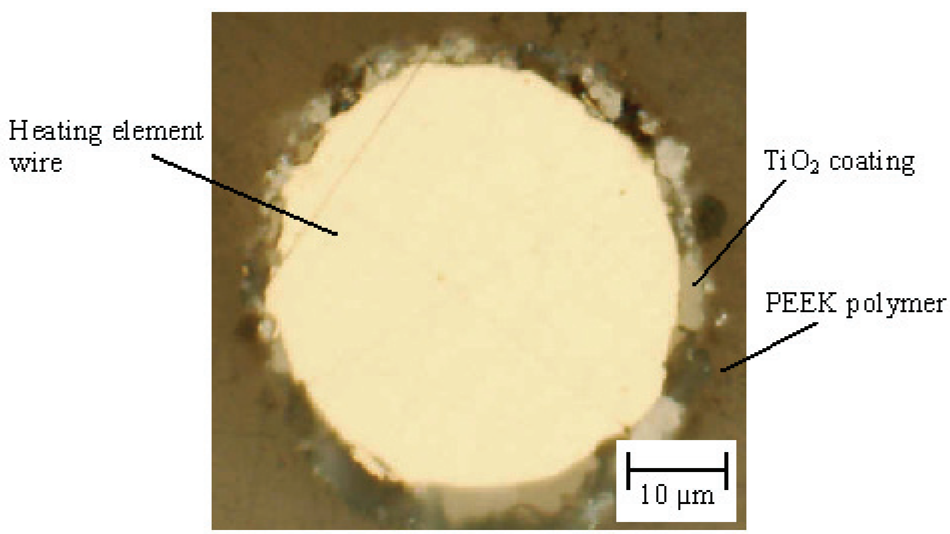

Fig. 4-3. TiO_2 coating on a stainless steel wire

4.4.4 Mechanical testing and characterisation methods

Short beam shear test was used to evaluate the interlaminar shear strength (ILSS) of the welded samples. These tests were carried out according to the ASTM D2344M standard test method. The samples were 4.6 mm thick and 9.0 mm wide. For the quasi-isotropic specimens, the samples were cut from the welded area according to Fig. 4-4 - a. In order to have the fibres in the length direction, the samples of the UD specimens were cut as shown in Fig. 4-4 - b. A support span of 18 mm and a crosshead speed of 1.0 mm/min were used for all tests. For each welding condition, five replicated samples were tested for the quasi-isotropic specimens and four replicated samples were tested for the UD specimens. The ILSS was obtained from the first peak of the load-deflection curves. The fractured specimens were analysed by optical microscopy.

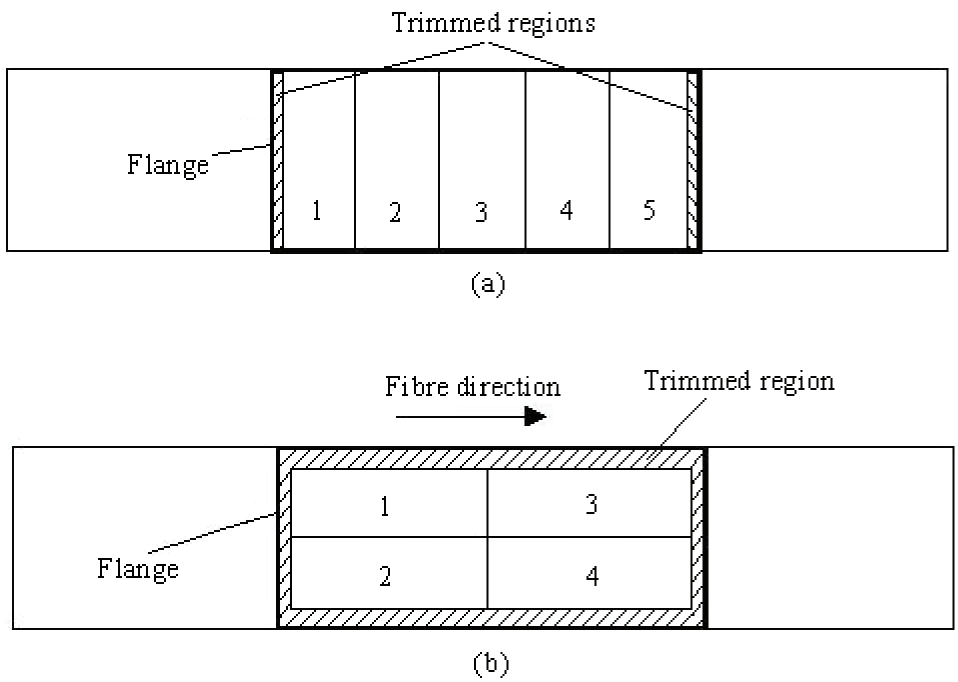

Fig. 4-4. Short beam samples of quasi-isotropic (a) and UD (b) specimens

The mechanical performance of the welded skin/stringer configuration was evaluated using three-point bending tests. It was shown before that this test can represent the typical load case experienced by a reinforced aerospace structure, for example a fuselage, under the application of internal pressure [15, 16]. A support span of 80 mm was used with a central load applied on the backside of the skin laminate. Specimens were tested at 23°C and at relative humidity of 50% under a crosshead speed of 2.0 mm/min. The reported results are average of at least five replicated samples and the error bars correspond to two standard deviations.

The various welding conditions and characterisation methods are summarised in Table 4-1.

Table 4-1. Welding conditions and characterisation methods

Welding conditions		Characterisation methods			
Adherend	**Heating element**	**Electrical resistance monitoring**	**Temperature monitoring**	**Short beam shear test**	**Three-point bending test**
UD APC-2/AS4	Conventional		X		
UD APC-2/AS4	Two-films	X	X		
UD APC-2/AS4	TiO_2	X	X	X	X
UD GF/PEEK	Conventional	X	X		
Quasi-isotropic APC-2/AS4	Conventional	X	X	X	X
Quasi-isotropic APC-2/AS4	TiO_2	X	X	X	X

4.5 Results and discussion

4.5.1 Electrical resistance

Current leakage can be detected through online monitoring the heating element electrical resistance during the welding process. Ageorges *et al*. [5] showed that when current leakage occurs, an electrical resistance drop is observed, due to the new electrical paths created in the adherends, mostly after the polymer melting temperature is reached. Fig. 4-5 presents the electrical resistance measured during welding of the UD and quasi-isotropic specimens as a function of the weld interface temperature. The standard deviation of the presented data is 5%. The electrical resistance of the GF/PEEK specimens, which did not allow any current leakage, is also shown for reference. As observed before by Don *et al.* [14], the two-films HE did not show any success in preventing current leakage. Initially, the electrical resistance increased with temperature (as expected for a stainless steel heating element) but started to decrease right after the PEEK melting temperature was reached. This reduction was due to melting of the polymer, which allowed the heating element mesh to come in contact with the carbon fibres of the adherends. New electrical paths were created in the adherends, reducing the overall electrical resistance of the system. Since the power supply was controlled by the voltage, the input electrical current kept increasing in order to match the reduced electrical resistance. When the power supply reached its maximum output current (40 A), it could no further maintain the constant targeted voltage. A reduction of voltage was then observed and the welding process was no longer controllable. Since it did not prevent current leakage, the two-films HE was not further investigated in this study.

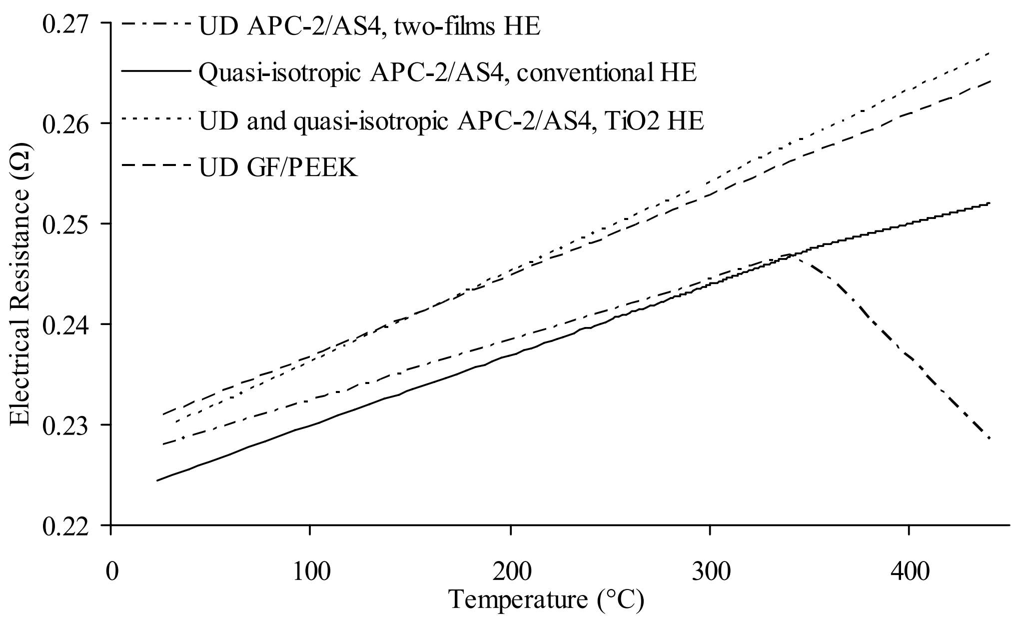

Fig. 4-5. Electrical resistance as a function of the weld interface temperature

In Fig. 4-5, it can also be observed that the specimens welded using the TiO_2 HE behaved as it is expected for a virgin stainless steel heating element, i.e., a constant electrical resistance increasing rate with temperature. No resistance drop was observed, showing the good electrical insulation provided by the TiO_2 coating. When comparing the APC-2/AS4 specimens welded using the TiO_2 HE with the GF/PEEK reference specimens, a 5% slope difference is observed. However, this slight difference was within the standard deviation of the measured data and was thus neglected. From the two attempted methods to reduce or eliminate current leakage in the UD specimens, the TiO_2 HE thus provided the best insulation.

In the case of the quasi-isotropic specimens, the 45° angle ply between the fibres next to the heating element and the electrical current direction increased the electrical resistance of the adherends, as no fibre was directly in contact with both ends of the heating element. Due to this 45° angle, it was expected that current leakage in the quasi-isotropic adherends would be reduced, even though no electrical insulation was used. However, some discrepancies were observed between these specimens and the GF/PEEK specimens or the ones welded using the TiO_2 HE. Fig. 4-5 shows that the slope of the quasi-isotropic specimens welded using the conventional HE started to decay after the PEEK melting temperature was reached. Current leakage, though reduced, was the reason for this behaviour. After the polymer melted, the combined effects of the stainless steel mesh (in which most of the current passed) and the carbon fibres of the adherends (in which an undetermined part of the current leaked) explained this lower slope. However, the controllability of the welding process was not affected due to the limited amount of current passing in the carbon fibres. As opposed to the UD specimens, it was still possible to weld the quasi-isotropic specimens with a good process control and accuracy, even without any electrical insulation.

The effect of current leakage was observed using optical microscopy. Dark areas existed at the edges of the UD specimens welded using the two-films HE, due to the damaged carbon fibres and polymer degradation in the first plies of the laminates. These dark areas were observed at both specimens ends, showing that current passed from one extremity of the specimens to the other, in the carbon fibres of the adherends (Fig. 4-6). These observations could be made only for the UD specimens. It was assumed that the reduced current leakage in the quasi-isotropic specimens did not damage the carbon fibres of the adherends nor induced polymer degradation, even when no electrical insulation was used.

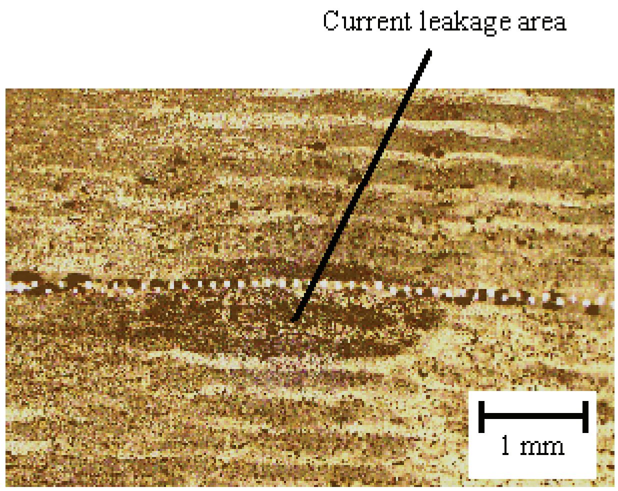

Fig. 4-6. Micrograph of the edge of a UD specimen welded using the two-films HE. The dark section represents the current leakage region, in which damaged fibres and polymer degradation were observed.

4.5.2 Thermal behaviour

The UD specimens welded without insulation produced non-repeatable temperature profiles. Large temperature gradients and long welding times, caused by power losses in the adherends, were observed. Fig. 4-7 shows a comparison between the UD specimens welded with conventional and TiO_2 HE. It should be noted that due severe current leakage, it was hard to obtain consistent results for the specimens welded with the conventional HE. Therefore, the curve presented in Fig. 4-7 – a is a simple example of all the tests performed. The welding time without insulation was long and variable (130 seconds for the presented test) with non-uniform temperature distribution over the weld area, variable heating rate and temperatures up to 550°C at the edges of the weld. The high temperatures reached at the edges of the welds led to polymer melting in these areas, which explain the fact that current leakage started right at the edges of the welds rather than in the middle (Fig. 4-6). In addition to these problems, many UD specimens could not be welded as current leakage prevented enough current from passing in the heating element. Fig. 4-7 – a shows that the large temperature gradients observed for the UD specimens initiated around the PEEK melting temperature of 343°C, when the PEEK polymer melted and flowed, allowing the heating element to touch the carbon fibres. The same type of curve was obtained with the two-films HE, showing, once again, the insufficient electrical insulation of this method. However, using the TiO_2 HE successfully prevented energy losses in the adherends and reduced the welding time from 130 seconds to 45 seconds. Temperature uniformity was also greatly improved with small temperature gradients (10°C) between the edges and the centre of the welds. Since the TiO_2 coating was also applied on the exposed surfaces of the heating element, it acted as a thermal insulation on these areas, preventing the metal mesh from over-heating and thus, reducing the edge effect.

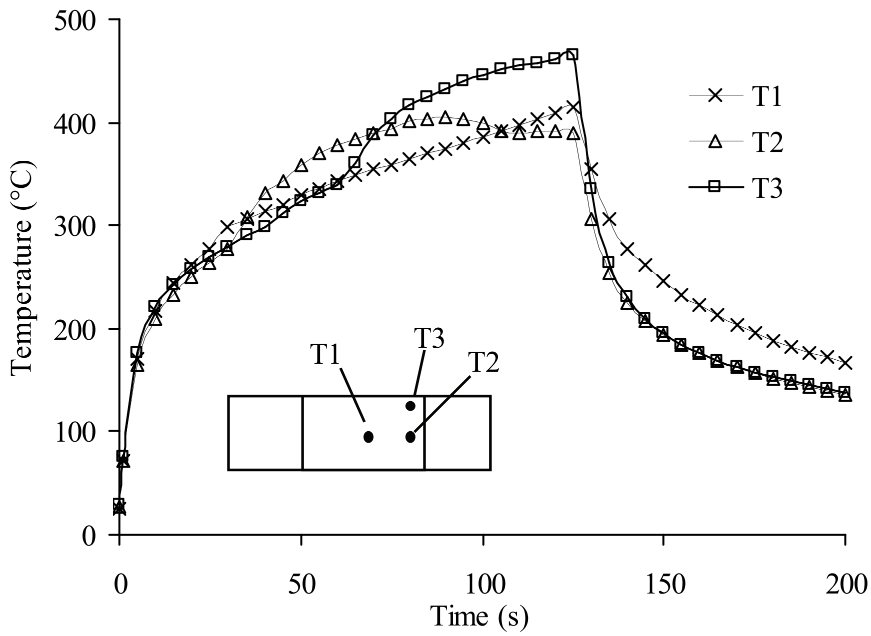

(a)

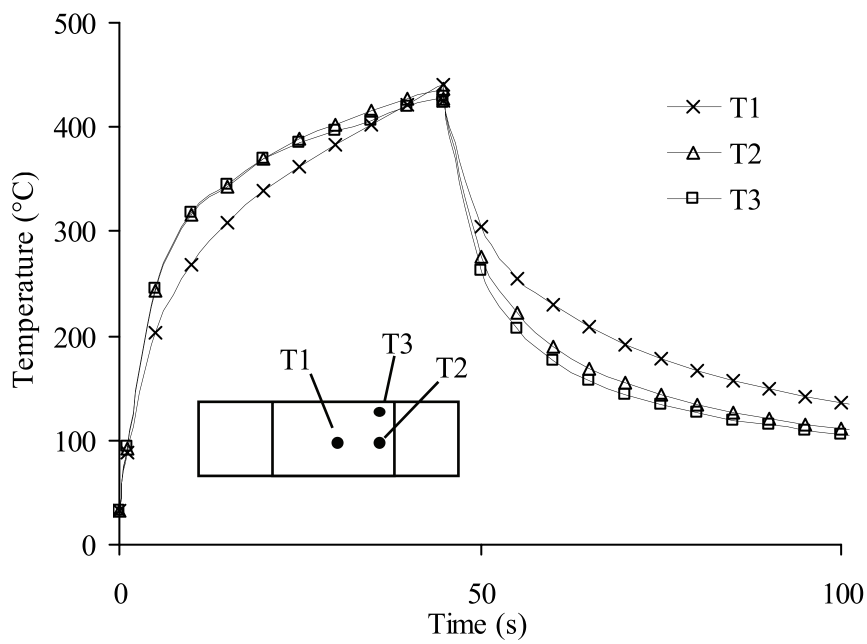

(b)

Fig. 4-7. Temperature profiles of UD APC-2/AS4 specimens welded using the conventional (a) and TiO_2 (b) HE

Fig. 4-8 – a shows the temperature profile of the quasi-isotropic specimens welded with the conventional HE. No major temperature gradient was observed after the polymer melted, as opposed to the UD specimens welded using the conventional or two-films HE. The temperature gradient observed was simply due to the different thermal boundary conditions (edge effect). However, it was observed that the welding time of the quasi-isotropic specimens (60 seconds) was longer than the welding time of the UD specimens welded with the TiO_2 HE (45 seconds). The welding time of the quasi-isotropic specimens was reduced from 60 seconds to 40 seconds when using the TiO_2 HE (Fig. 4-8 – b). This confirmed the previous observations about current leakage in the quasi-isotropic adherends. Even though a larger electrical resistance existed in the adherends due to the 45° angle ply between the fibres next to the heating element and the electrical current direction, an undetermined part of the current leaked in the laminates. Using the TiO_2 HE reduced the welding time and provided better temperature homogeneity over the weld area. The temperature gradient between the edges and the centre was only 10°C. As for the UD specimens, it was assumed that the TiO_2 coating on the exposed parts of the heating element acted as a thermal insulation and reduced the edge effect.

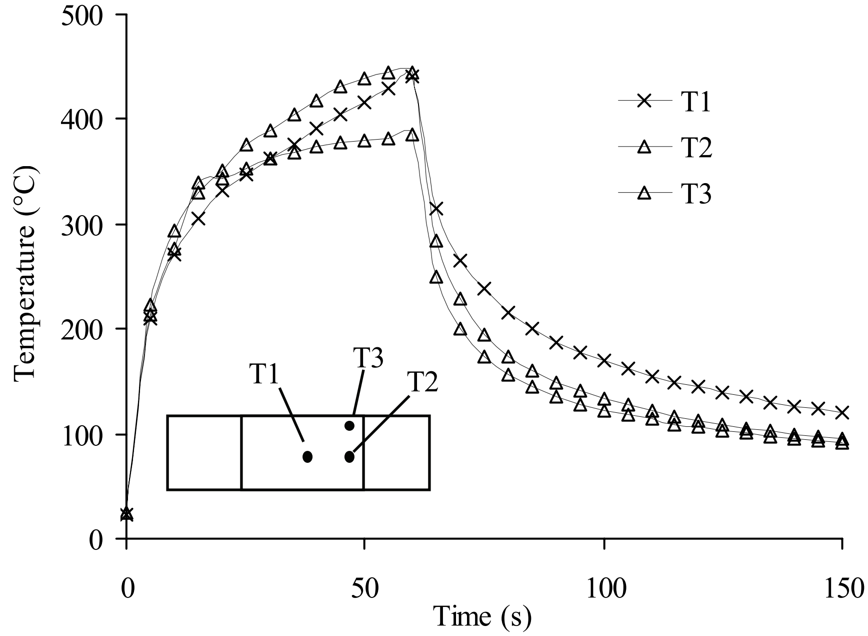

(a)

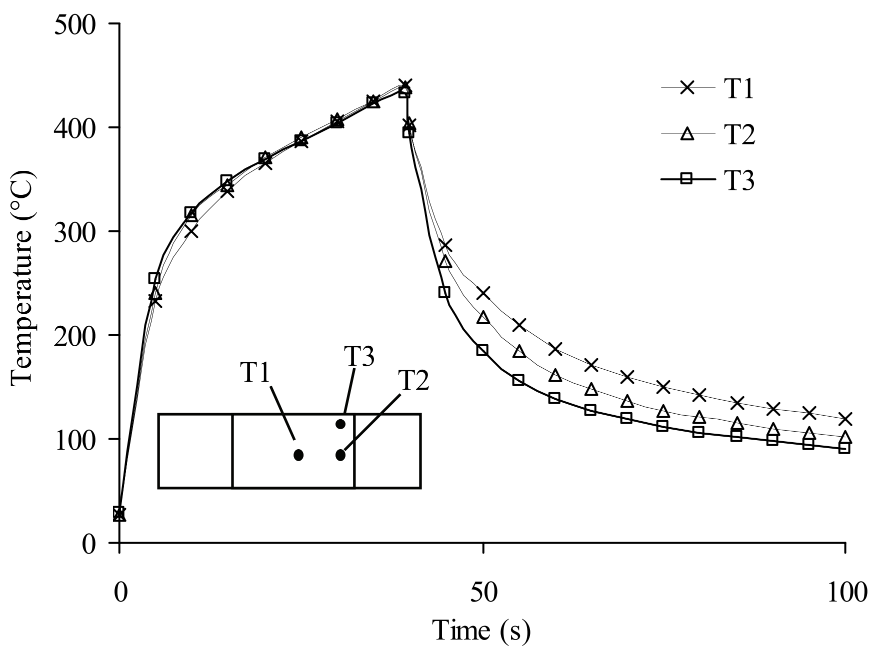

(b)

Fig. 4-8. Temperature profiles of quasi-isotropic APC-2/AS4 specimens welded using the conventional (a) and TiO2 (b) HE

Fig. 4-9 presents the temperature profile of the GF/PEEK specimens. The welding time of these specimens was around 40 seconds, just as for the UD and quasi-isotropic specimens welded using the TiO_2 HE. This confirmed the excellent electrical insulation provided by the TiO_2 HE. It is also worth noting that the temperature vs. time curve of the GF/PEEK specimens showed the same non-uniform temperature as the quasi-isotropic APC-2/AS4 specimens welded with the conventional HE. Since no current leakage could be blamed for these temperature gradients, it was concluded that they were the result of the edge effect only.

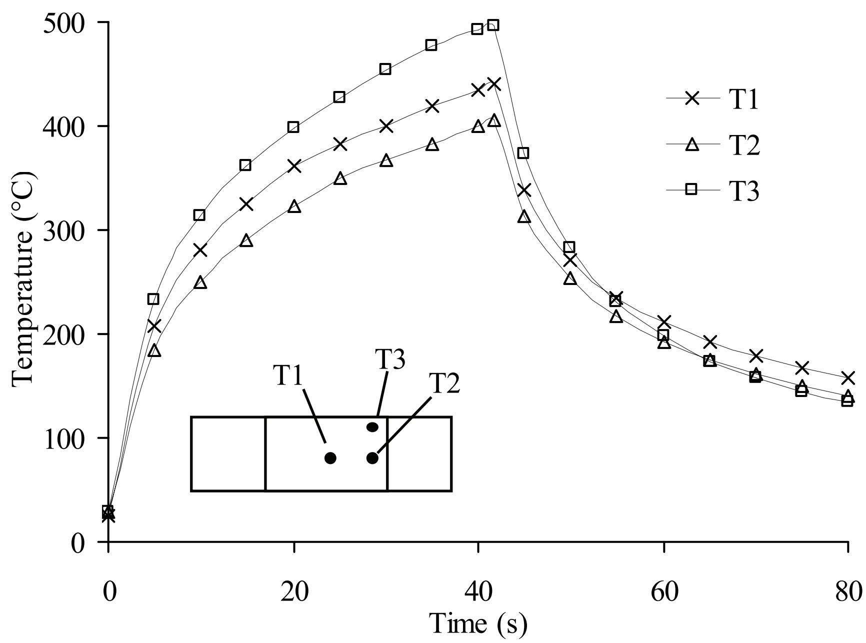

Fig. 4-9. Temperature profile of GF/PEEK specimens

4.5.3 Mechanical performance

The ILSS of the UD specimens welded using the TiO_2 HE and quasi-isotropic specimens welded using both the conventional and TiO_2 HE are presented in Fig. 4-10. The ILSS of the UD specimens was 99 N/mm^2 and the failure occurred at the weld interface. The ILSS of the quasi-isotropic specimens were 88 MPa and 94 MPa for the specimens welded using the conventional and TiO_2 HE, respectively. However, when considering the standard deviation, no difference is seen between the two results. In addition, in both cases the failure occurred in the laminates, at the 0° and 90° plies interface. As a reference, it was reported that the ILSS of the APC-2/AS4 quasi-isotropic laminates is 100 MPa [17].

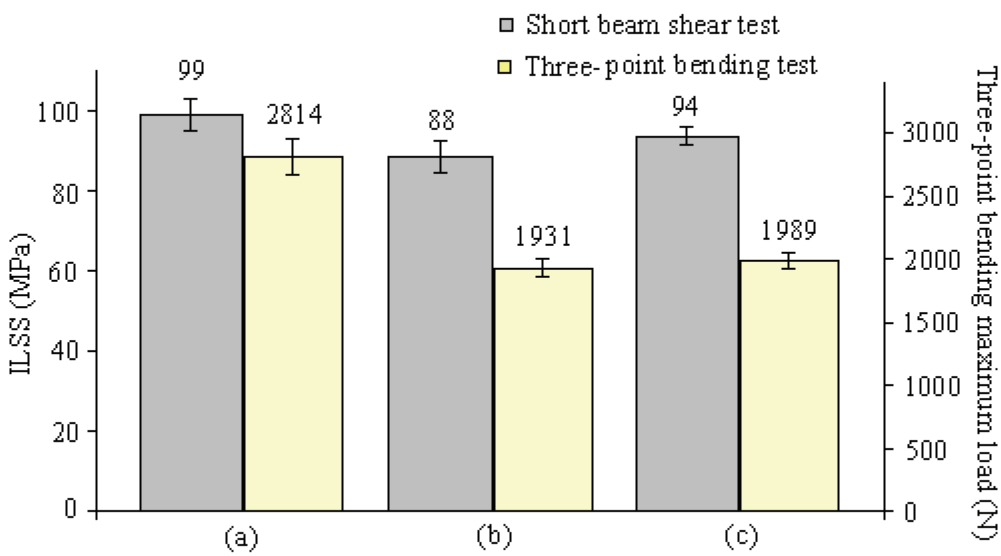

Fig. 4-10. Mechanical testing results of the UD specimens welded using the TiO_2 HE (a) and quasi-isotropic specimens welded using conventional (b) and TiO_2 (c) HE

The three-point bending tests results of the UD specimens (welded using the TiO_2 HE) and quasi-isotropic specimens (welded using the conventional and TiO_2 HE) are presented in Fig. 4-10 and Fig. 4-11. The maximum failure load of the UD specimens was 2814 N and the failure occurred at the weld interface. The first crack was located at the flange tip, between the skin laminate and the weld interface and then propagated in the weld, either between the skin laminate and the weld interface or in the weld itself, i.e., between the heating element wires and the TiO_2 coating. Comparison between the quasi-isotropic specimens welded with the conventional and TiO_2 HE revealed some discrepancies. Although the maximum failure loads were unchanged when considering the standard deviations, the load-deflection curves were different (Fig. 4-11). A rigidity increase of 20% was obtained for the TiO_2 HE, possibly due to the higher rigidity of the applied coating and its interfacial bond with the heating element. The failure modes were also different. As described in [15], the quasi-isotropic specimens welded with conventional HE showed a complex failure mode involving cracks at the weld interface and in the skin or flange laminates. However, when using the TiO_2 HE, the final failure of the specimens occurred in the weld itself, just as it was the case for the UD specimens. The first cracks were still located between the skin laminate and the weld interface, but the final delamination was in the weld, between the heating element wires and the TiO_2 coating. The fracture surfaces were observed under scanning electron microscopy to shade more light on the differences between the failure modes of the specimens welded with conventional and TiO_2 HE. For the specimens welded with conventional HE, no adherence was seen between the stainless steel wires and the PEEK polymer, due to low interfacial bonding between these two materials (Fig. 4-12 – a). The weld thus relied on mechanical interlocking between the polymer and the mesh. This lack of adherence between the stainless steel wires and the polymer was also observed for other polymers such as poly-ether-ketone-ketone (PEKK) and poly-ether-imide (PEI) [6]. However, the specimens welded using the TiO_2 HE, exhibited adherence between the PEEK polymer and the TiO_2 coating. As seen in Fig. 4-12 - b, the coating had a rough surface, which facilitated adherence with the polymer. On the other hand, the TiO_2 coating tended to debond from the stainless steel wires. That is, good adherence was obtained between the coating and the polymer but not between the coating and the wires. However, as stated previously, this lack of adherence did not induce any mechanical performance penalty for the three-point bending tests, nor for the short beam shear tests.

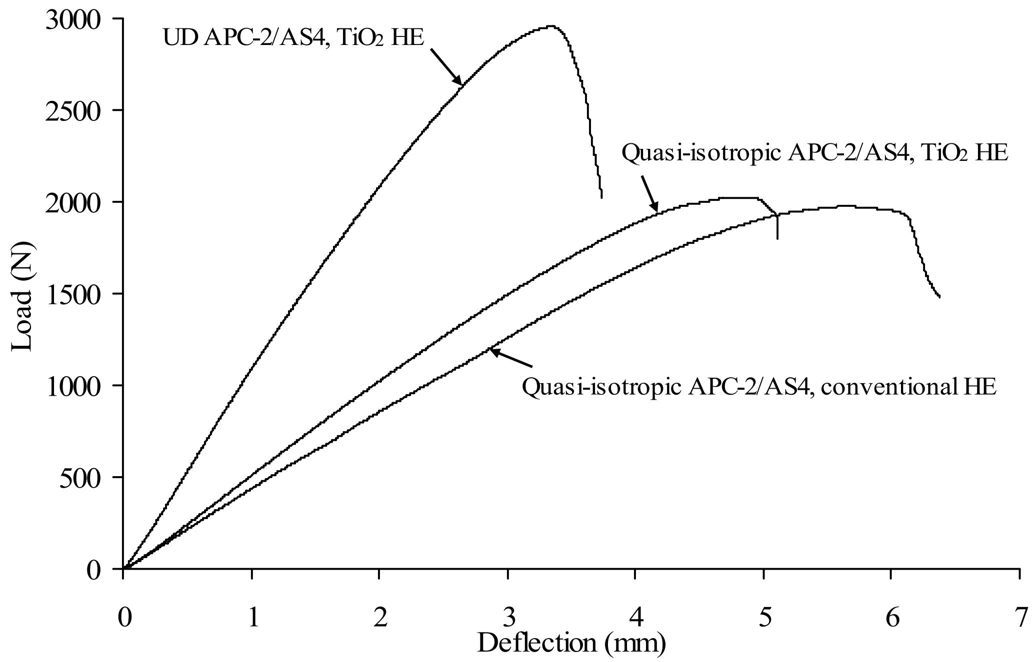

Fig. 4-11. Typical load-deflection curves under three-point bending

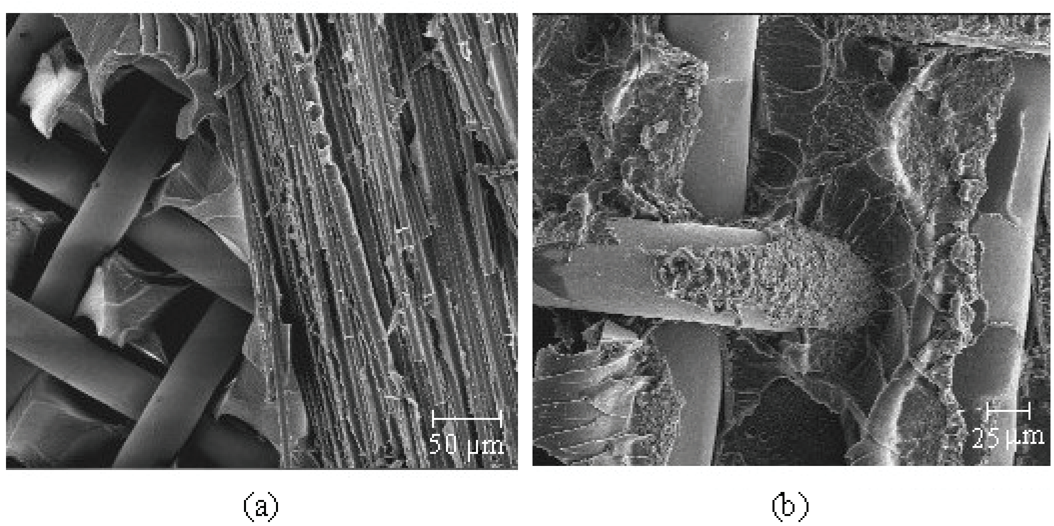

Fig. 4-12. Fracture surfaces of quasi-isotropic specimens welded using the conventional (a) [15] TiO_2 (b) HE, under three-point bending

4.6 Summary and conclusions

In this study, UD and quasi-isotropic APC-2/AS4 composite skin/stringer specimens were resistance-welded using a stainless steel mesh heating element. The electrical, thermal and mechanical behaviours of the welds were investigated. The mechanical performance was evaluated using short beam and three-point bending tests. Two methods were developed to prevent current leakage to the electrically conductive adherends and the following conclusions were drawn from the investigation:

1) Current leakage to the electrically conductive adherends was found to be a major issue to weld the UD specimens. After the polymer at the weld interface was melted, an electrical resistance drop was observed, due to the new electrical current paths created in the adherends.
2) The method consisting in applying two polymer films on each side of the heating element did not prevent current leakage. However, a new insulated heating element, consisting of a TiO_2-coated stainless steel mesh successfully prevented current leakage. No electrical resistance drop was observed when using this new method.
3) The TiO_2 HE improved the temperature uniformity in the welds and reduced the welding time by preventing power losses in the adherends. The better temperature uniformity was attributed to the thermal insulation provided by the coating on the exposed parts of the heating element, which reduced the edge effect.
4) The TiO_2 HE did not produce any mechanical performance drawback. The same ILSS was obtained as well as the same performance under three-point bending tests. However, the TiO_2 HE changed the failure mode of the quasi-isotropic specimens from delamination in the skin laminate to weld interface debonding.

Overall, the TiO_2 HE allowed the welding of UD specimens with good process control without affecting the static mechanical performance of the welds.

However, the fatigue properties of the welds and the impact of the TiO_2 coating on the fatigue performance are still unknown. Since resistance welding finds applications in the aerospace industry, where parts are subjected to cyclic loadings, the fatigue behaviour of the welds should be the subject of future investigations.

4.7 Acknowledgements

This work was supported by funding from the Natural Sciences and Engineering Research Council of Canada. The authors also greatly acknowledge Mr. David Leach from Cytec Engineered Materials Inc. for providing the materials used in this study, Dr. Rogerio Lima for technical advices concerning the TiO_2 deposition and Frédérick Belval for HVOF spraying.

4.8 References

1. Eveno, E., Gillespie, J.W.J. Resistance welding of graphite polyetheretherketone composites - An experimental investigation. Journal of Thermoplastic Composite Materials 1988;1:322-338.
2. Silverman, E.M., Griese, R.A. Joining Methods for Graphite/PEEK Thermoplastic Composites. SAMPE Journal 1989;25(5):34-38.
3. Stokes, V.K. Joining methods for plastics and plastic composites: an overview. Polymer Engineering and Science 1989;29(19):1310-1324.
4. Ageorges, C., Ye, L., Hou, M. Experimental investigation of the resistance welding of thermoplastic-matrix composites. II. Optimum processing window and mechanical performance. Composites Science and Technology 2000;60(8):1191-1202.
5. Ageorges, C., Ye, L., Hou, M. Experimental investigation of the resistance welding for thermoplastic-matrix composites. I. Heating element and heat transfer. Composites Science and Technology 2000;60(7):1027-1039.

6. Dubé, M., Hubert, P., Gallet, J.N.A.H., Stavrov, D., Bersee, H.E.N., Yousefpour, A. Heating Element Optimization in Resistance Welding of Semi-Crystalline and Amorphous Thermoplastic Composites. CANCOM, Winnipeg, Canada, 2007.

7. Hou, M., Friedrich, K. Resistance welding of continuous carbon fibre/polypropylene composites. Plastics Rubber and Composites Processing and Applications 1992;18(4):205-213.

8. Stavrov, D., Bersee, H.E.N. Thermal Aspects in Resistance Welding of Thermoplastic Composites. ASME Summer Heat Transfer Conference, Las Vegas, USA, 2003.

9. Stavrov, D., Bersee, H.E.N., Beukers, A. Experimental Investigation of Large-Scale Welding of Carbon Fiber Thermoplastic Composite Materials. International Conference on Composite Materials, San Diego, USA, 2003.

10. Stavrov, D., Bersee, H.E.N., Beukers, A. The Influence of the Heating Element on Resistance Welding of Thermoplastic Composite Materials. International Conference on Composite Materials, San Diego, USA, 2003.

11. Yousefpour, A., Simard, M., Octeau, M.-A., Hojjati, M. Process Optimization of Resistance-Welded Thermoplastic Composites Using Metal Mesh Heating Elements. SAMPE, Long Beach, USA, 2005.

12. Yousefpour, A., Simard, M., Octeau, M.-A., Lamarée, M., Hojjati, M. Effects of Mesh Size on Resistance Welding of Thermoplastic Composites Using Metal Mesh Heating Elements. SAMPE-Europe, Paris, France, 2004.

13. Stavrov, D., Bersee, H.E.N. Resistance welding of thermoplastic composites - an overview. Composites Part A: Applied Science and Manufacturing 2005;36(1):39-54.

14. Don, R.C., Gillespie, J.W., Lambing, C.L.T. Experimental characterisation of processing-performance relationships of resistance welded graphite/PEEK [polyetheretherketone] composite joints. Polymer Engineering and Science 1992;32(9):620-631.

15. Dubé, M., Hubert, P., Yousefpour, A., Denault, J. Resistance welding of thermoplastic composites skin/stringer joints. Composites Part A: Applied Science and Manufacturing 2007;doi:10.1016/j.compositesa.2007.07.014.

16. Minguet, P.J., O'Brien, T.K. Analysis of test methods for characterizing skin/stringer debonding failures in reinforced composite panels. Composite Materials: Testing and Design, Proceedings of the 12th Symposium, Montréal, Canada, 1996.

17. Dubé, M., Hubert, P., Yousefpour, A., Denault, J. Mechanical Performance of Resistance-Welded Thermoplastic Composite Skin/Stringer Specimen. SAMPE Fall Technical Conference, Seattle, USA, 2005.

18. Dubé, M., Hubert, P., Yousefpour, A., Denault, J. Fatigue performance of resistance-welded thermoplastic composite skin/stringer joints. SAMPE-Europe, Paris, France, 2007.

19. Dubé, M., Hubert, P., Yousefpour, A., Denault, J., Wadham-Gagnon, M. Resistance Welding of Thermoplastic Composites Skin/Stringer Specimens. SAMPE, Long Beach, USA, 2006.

20. Lima, B.S., Marple, B.R. Enhanced ductility in thermally sprayed titania coating synthesized using a nanostructure feedstock. Materials Science and Engineering A 2005;395:269-280.

CHAPTER 5. THIRD MANUSCRIPT

5.1 Preface

In the previous two chapters, the mechanical performance of resistance-welded thermoplastic composites skin/stringer joints was evaluated under static loading and a new insulation method was developed to prevent current leakage in the conductive adherends. The impact of this insulation method on the mechanical performance of the welds was investigated under static loading. In this chapter, the fatigue properties of the skin/stringer joints are evaluated. The fatigue performance and failure mechanisms are investigated for UD specimens as well as for quasi-isotropic specimens welded with and without the electrical insulation. The impact of the insulation method on the fatigue properties is investigated.

Fatigue failure characterisation of resistance-welded thermoplastic composites skin/stringer joints*

*Manuscript submitted to International Journal of Fatigue (August 2007)

Dubé, M. and Hubert, P.
McGill University, CREPEC, Department of Mechanical Engineering
817 Sherbrooke Street West, Montréal, Québec, H3A 2K6, Canada

Yousefpour, A.
Aerospace Manufacturing Technology Centre, National Research Council Canada
5145 Decelles Avenue, Montréal, Québec, H3T 2B2, Canada

Denault, J.
Industrial Materials Institute, National Research Council Canada
75 de Mortagne, Boucherville, Québec, J4B 6Y4, Canada

5.2 Abstract

An experimental investigation characterising the fatigue failure mechanisms of resistance-welded thermoplastic composites skin/stringer joints is presented. Unidirectional (UD) and quasi-isotropic carbon fibre/poly-ether-ether-ketone adherends were welded using stainless steel meshes as heating elements. The specimen geometry consisted of a flange laminate, representing a stringer, welded onto a skin laminate. In order to avoid current leakage to the electrically conductive adherends, a ceramic-coated heating element (TiO_2 HE) was used for welding the UD specimens and some of the quasi-isotropic specimens. The fatigue performance of the welded joints was investigated under three-point bending. An indefinite fatigue life was obtained at 40% and 35% of the static damage initiation load for the UD and quasi-isotropic specimens, respectively. The failure mechanisms were documented based on observation of the fatigue cracks initiation and growth. UD specimens failed at the weld interface while quasi-isotropic specimens showed delaminations both in the flange or skin laminates and at the weld interface. The TiO_2 HE did not show any fatigue mechanical performance reduction. However, debonding at the weld interface was shown to occur between the metal mesh wires and the TiO_2 coating instead of between the laminates and the weld.

Keywords: Polymer-matrix composites (PMCs); Resistance welding; Fatigue; Failure analysis; Crack growth rate.

5.3 Introduction

Resistance welding was the subject of several investigations in the past few years [1-16]. The interest for this joining method resides in its commonly cited advantages over other welding methods, i.e., the quickness, simplicity and low-cost of the technique [17]. Resistance welding implies entrapment of an electrically conductive heating element between two thermoplastic composite parts to be joined (adherends). An electrical current is applied to the heating element until the weld interface reaches the desired welding temperature. The electrical current is then stopped and the polymer cools down, under the application of pressure, resulting in a weld.

Most of the work done on the resistance welding process investigated the effects of the welding parameters such as the welding temperature, power level, welding pressure and heating element type on the weld quality and performance [1, 2, 9, 13, 15, 16, 18-20]. Simple lap shear and double cantilever beam (DCB) specimens are usually investigated [1, 2, 9]. These weld geometries are well suited to evaluate the shearing (lap shear) and toughness (DCB) properties of the welds and to optimise the welding parameters. However, these tests were conducted under static loading conditions and only little data are available in the literature about the fatigue properties of the welds.

One of the foreseen applications of resistance welding is in the aerospace industry. The now well-known J-nose leading edges of the Airbus A340-500/600 and A380 airplanes are the most cited examples of an application of the resistance welding technique. In this application, the glass fibre/poly-phenylene-sulfide (GF/PPS) ribs and stringers are resistance-welded to a GF/PPS skin laminate using a metal mesh heating element. The welded geometry of this type of application, i.e., a reinforced skin laminate, is thus completely different from the commonly studied lap shear and DCB specimens. For example, reinforced fuselages are subjected to out-of-plane loading due to the internal cabin pressure. This load case leads to complex failure modes involving damage in the skin and stringers [21]. These failure modes cannot be simulated by the usual lap shear and DCB specimens. In addition, it is well known that aerospace structures are subjected to cyclic loading due to the pressure cycles and aircraft manoeuvres. The study of these two parameters, i.e., the failure modes of the reinforced skin panel geometry and the weld fatigue properties, is of vital importance for the future of resistance welding.

Two previous investigations were reported on resistance welding of thermoplastic composites skin/stringer configurations [22, 23]. One of them analysed the mechanical properties of the resistance-welded skin/stringer configuration under static loading [23]. An optimisation of the welding parameters was performed and the failure modes of the resistance-welded skin/stringer specimens were discussed. The second investigation focused on one of the main issues of the resistance welding technique, which is current leakage from the heating element to the adherends [1, 2, 4, 9, 24, 25]. This phenomenon occurs when electrically conductive adherends, such as carbon fibre reinforced thermoplastics, are welded. This second investigation described the development of a new heating element consisting of a ceramic-coated stainless steel mesh (TiO_2 HE). The insulation provided by the TiO_2 coating prevented current leakage in the carbon fibre adherends and no mechanical performance penalty was reported under static loading [22].

The present study pursues two main objectives. The first objective is to characterise the fatigue failure mechanisms of a resistance-welded skin/stringer configuration made of APC-2/AS4 (carbon fibre/poly-ether-ether-ketone) composite material. Two laminate lay-ups were investigated: quasi-isotropic and unidirectional (UD). The second objective is to analyse the effect of the TiO_2 HE on the fatigue performance of the welds. It was already demonstrated that no mechanical performance penalty was obtained under static loading. However, the behaviour of this new heating element under fatigue loading is still unknown.

5.4 Experimental

5.4.1 Materials and specimen geometry

The adherends were 16 plies UD and quasi-isotropic $[\pm 45/90/0]_{2S}$ APC-2/AS4 laminates that were provided by CYTEC Engineered Materials Inc. They were compression-moulded at a processing temperature of 390°C, residence time of 20 minutes, moulding pressure of 0.7 MPa. and cool down rate of approximately

7°C/minute. The specimen geometry was the skin/stringer configuration with a square-ended flange (Fig. 5-1). The skin laminate was 130 mm long and 25.4 mm wide and the flange was 50 mm long and 25.4 mm wide. Both laminates were 2.2 mm thick.

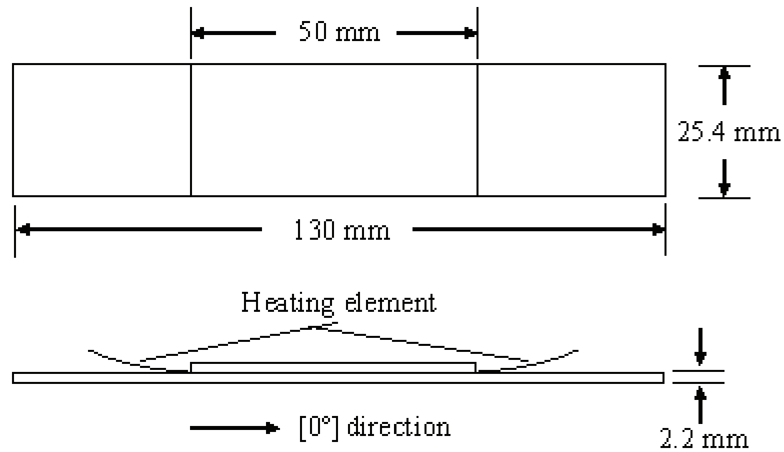

Fig. 5-1. Specimen geometry [22]

5.4.2 Heating element

Two types of heating elements were used. The first one was a 80 μm thick stainless steel mesh with a wire diameter of 40 μm and open gap width of 90 μm. A 127 μm thick neat PEEK polymer film was placed on each side of the metal mesh to provide a resin rich region at the weld interface. This first heating element, referred to as uncoated HE in the text, was used to weld one half of the quasi-isotropic specimens. The second heating element was the TiO_2 HE described in [22]. It consisted of the same metal mesh but it was coated with a 2 μm thick ceramic layer (TiO_2). The TiO2 HE was used to weld all the UD and one half of the quasi-isotropic specimens.

5.4.3 Resistance welding

The resistance welding set-up consisted of a DC power supply with maximum output of 40 A and 80 V, a pressure system, a computer/data acquisition system and a resistance welding rig. The computer/data acquisition system was used to monitor the temperature in the weld and the current and voltage in the heating element. A control system was developed using National Instruments Labview software to control the input power. The control system was designed in such a way that when temperature at the weld interface reached a pre-determined welding temperature of 440°C [23], the electrical current was turned off. A resistance welding rig, described in [23], was used to weld the skin/stringer specimens. The input power was applied to the heating element using the fixed voltage method [15]. A voltage of 9.0 V and welding pressure of 1.0 MPa were used for all welds.

5.4.4 Mechanical testing and characterisation methods

The mechanical performance of the welded skin/stringer specimens was first assessed using static three-point bending tests. A support span of 80 mm was used with the central load applied on the backside of the skin laminate. Specimens were tested at 23°C and at a relative humidity of 50% under a crosshead speed of 2.0 mm/min. Five replicated samples were welded and tested for each specimen lay-up and heating element. Based on the specimens static performance, load-controlled fatigue tests were then conducted using the same three-point bending fixture. Specimens were tested under a sinusoidal waveform at various loads between 35% and 80% of the static damage initiation load. The tests were conducted at room temperature under a load ratio R = 0.1 and a frequency f = 5 Hz. Between 10 and 15 specimens were tested for each laminate lay-up and heating element. The edges of the specimens were slightly polished prior to testing and the crack initiation and growth rate was documented using a travelling microscope. The load and deflection data were recorded at fixed intervals throughout the tests. The stiffness reduction of the specimens was obtained from these data. No significant heating was noticed during the fatigue testing. When a fatigue delamination could not be obtained within 1 million cycles, the test was terminated and an indefinite fatigue life was reported. The failure modes of the specimens were observed after fatigue testing using optical microscopy. Then, the flange and skin laminates of the tested specimens, which remained together after the fatigue testing, were taken apart using the same three-point bending fixture as the one used for testing and scanning electron microscopy (SEM) was used to observe the fracture surfaces and deepen the understanding of the fracture behaviour.

5.5 Results and analysis

5.5.1 Static tests

Typical load-deflection curves of the static three-point bending tests performed on UD and quasi-isotropic specimens are presented in Fig. 5-2 and Fig. 5-3, respectively. Average maximum loads were 2814 N and 1989 N for UD and quasi-isotropic specimens, respectively, with standard deviations of less than 5%. It was hard to determine the damage initiation loads from these curves since no load drop was observed before the maximum load was reached. However, the increasing non-linearity in the curves shows that damage was present in the specimens well before the maximum load. A reference damage initiation load was thus determined from the curves at 1% of non-linearity. The non-linear, maximum and reference loads are presented in Fig. 5-2 and Fig. 5-3 for the UD and quasi-isotropic lay-ups, respectively. Standard deviations of less than 5% were obtained in each case. The damage initiation loads that were used as a reference to design the fatigue testing were 2133 N and 1590 N for the UD and quasi-isotropic specimens, respectively. Failure of the UD specimens occurred at the weld interface. The failure modes of the quasi-isotropic specimens were described in [22, 23]. In the first failure mode, a crack was created at the weld interface and then propagated in the skin laminate, at the ±45° ply interface and at the -45°/90° ply interface. In the second failure mode, a crack was created in the skin laminate, at the ±45° ply interface and then propagated at the weld interface. The specimens welded using the TiO_2 HE failed at the weld interface.

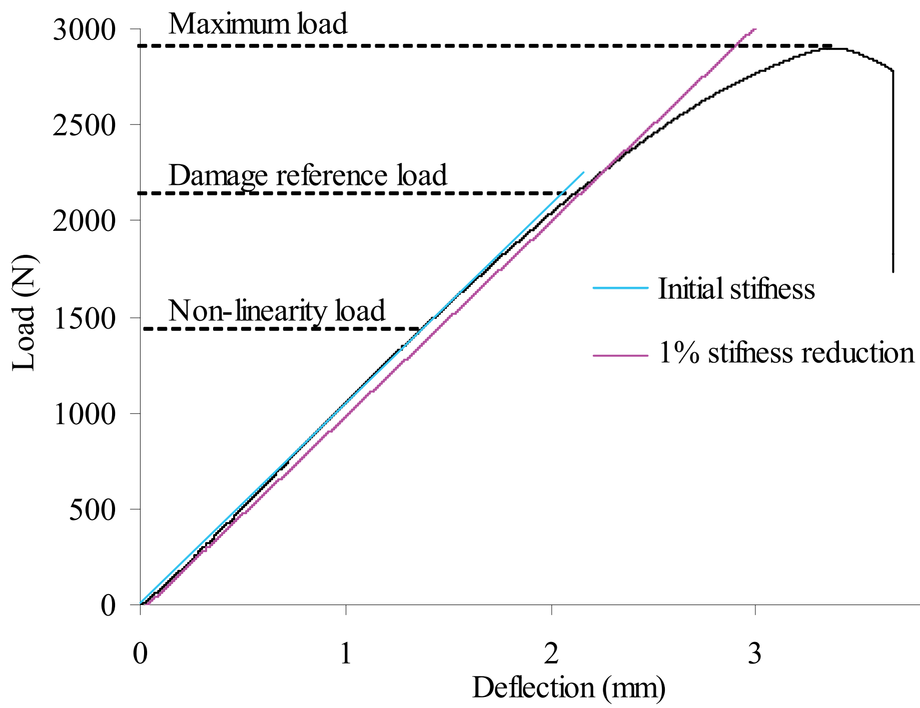

Fig. 5-2. Load-deflection curve of UD specimens

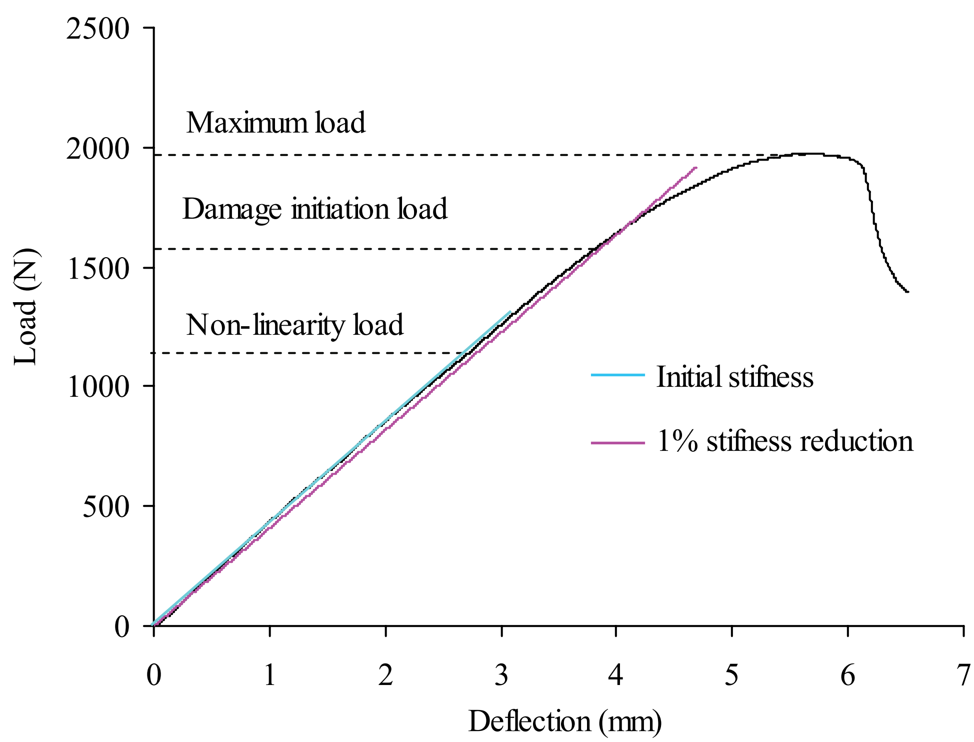

Fig. 5-3. Load-defection curve of quasi-isotropic specimens

The reported load-deflection curve of the quasi-isotropic specimens (Fig. 5-3) was based on the specimens welded using the uncoated HE. Previous work has shown that the coating has no effect on the welds static failure loads. However, a 20% stiffness increase was reported for the specimens welded using the TiO_2 HE, due to the high rigidity of the coating. Since the fatigue testing were load-controlled, the same loads were applied in both cases; however, it should be kept in mind that these loads corresponded to smaller deflections in the case of the specimens welded using the TiO_2 HE.

5.5.2 Fatigue tests

Fig. 5-4 summarises the fatigue testing results of the UD specimens as a plot of the number of cycles to crack initiation and subsequent delamination, for each load level (S-N curve). The crack onset event was defined as the number of cycles at which a crack could be detected for the first time using the travelling microscope installed on the test set-up. This crack onset event could not be identified precisely for all specimens, which explains the smaller number of crack onset points as compared to the number of points representing delamination. The delamination event was defined as the number of cycles at which the crack would reach the middle of the specimens. Although the specimens could still bear the applied load, the tests were terminated shortly after the delamination event occurred. An indefinite fatigue life was defined at a load level of 844 N. This load level represents 40% of the static damage initiation load, which is similar to the findings of previous studies on adhesive bonding of thermosetting composites [26]. No delamination growth was observed at this load level. At higher cyclic loads, the logarithm of the cycles to crack onset and delamination events presented a linear behaviour with the maximum cyclic load. At load level of 1690 N (80% of the damage initiation load), both events occurred within a few thousands cycles, showing a short fatigue life. In addition, as the load increased, the percentage of fatigue life required for the crack onset event to occur increased.

For example, at 80% of the damage initiation load, 75% of the fatigue life was required for the first crack onset to be detected while this event occurred within the first 10% of the fatigue life at a load level of 50%. At 40% of the damage initiation load, a crack onset was detected at approximately 80 000 cycles but this crack never propagated.

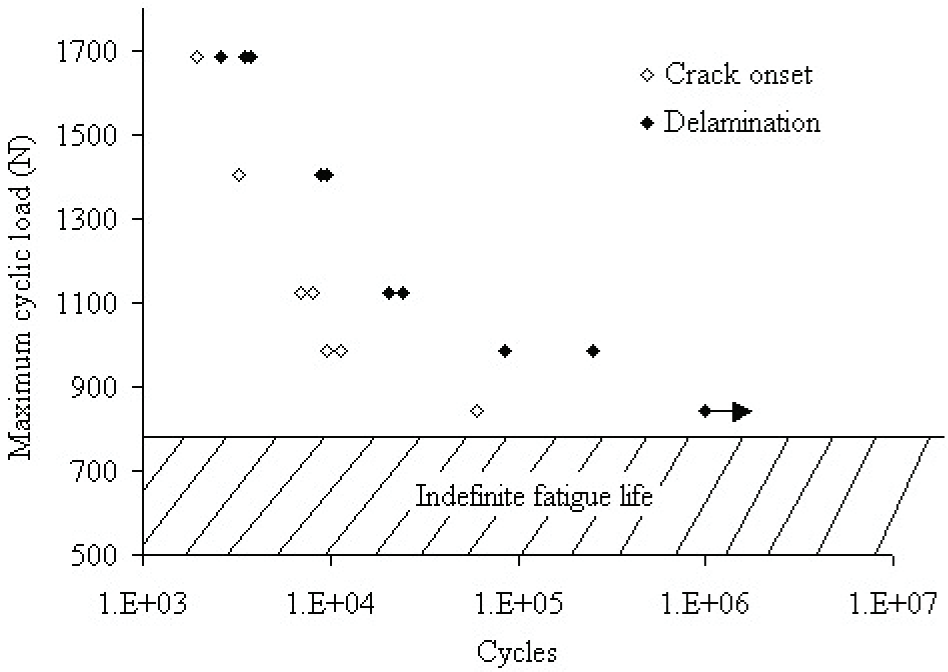

Fig. 5-4. Maximum cyclic load plotted against the number of cycles to crack onset and delamination for the UD specimens

Observation of the specimens during and after the tests revealed a delamination growing at the weld interface, either between the PEEK polymer and the first ply of the skin or flange laminate or at the actual weld interface, i.e., debonding between the heating element wires and the polymer. This last failure mode is shown in Fig. 5-5. The weld interfaces showed a good bonding between the ceramic coating and the PEEK polymer (Fig. 5-6). However, the ceramic coating tended to debond from the metal mesh wires. When the ceramic coating debonded, the polymer attached to it was stretched and finally ruptured (mechanical interlocking break). The failure mode of the UD specimens was therefore based on a ceramic debonding followed by a polymer mechanical interlocking rupture. This failure mode was also observed before under static loading [22].

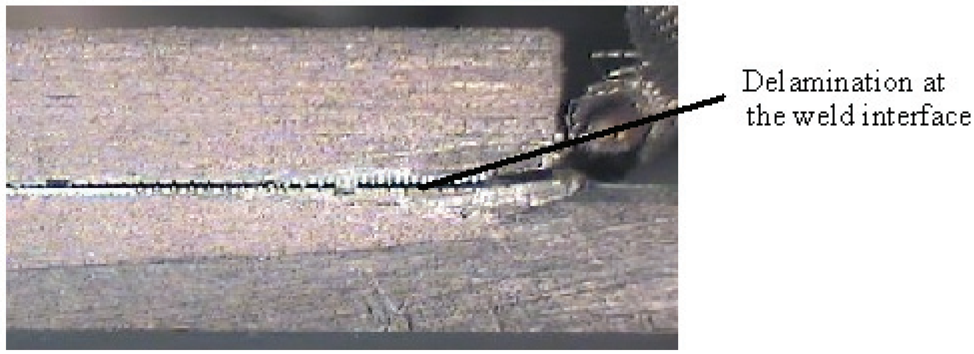

Fig. 5-5. Delamination at the weld interface (UD specimen)

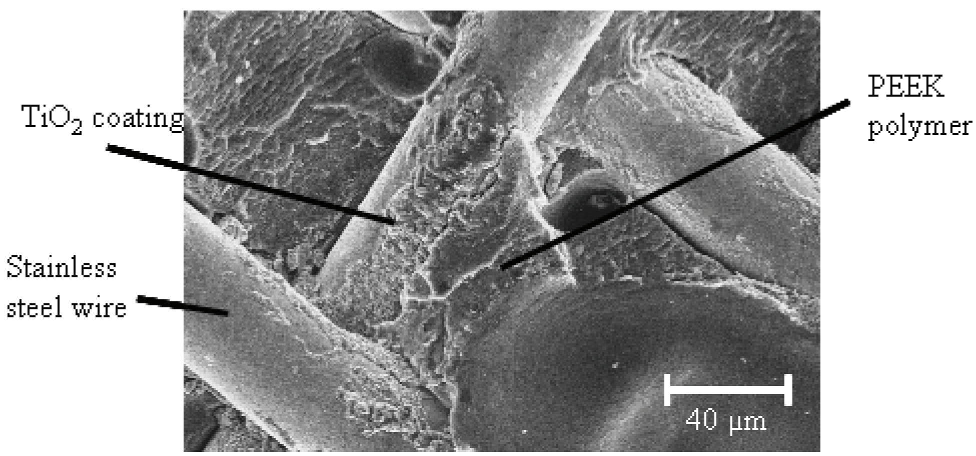

Fig. 5-6. Fracture surface of a UD specimen tested under cyclic three-point bending

The reduction of the normalised residual stiffness, defined as the stiffness of the specimen at cycle n divided by the stiffness at first cycle, is an indication of the damage evolution in the specimens [27, 28]. Fig. 5-7 depicts the evolution of the specimens normalised stiffness against the normalised cycles (n/N). A three-stage behaviour is seen for the loading cases of 55% and 65%. In stage I, a rapid stiffness reduction of 5% to 10% is observed. This reduction occurred in the first

3% of the fatigue life, independently of the applied load. A slightly decaying plateau is then observed. This second stage II lasted for 70% of the fatigue life after which the residual stiffness was 80% of its original value. The stage III shows an abrupt drop caused by the delamination at the weld interface. The tests were terminated shortly after this delamination occurred. This abrupt drop occurred approximately at 75% of the fatigue life, for all the load cases leading to a delamination at the weld interface. For the 40% of the damage initiation load case, which did not produce a weld interface debonding, the specimens exhibited a two-stage behaviour only, due to the absence of the final abrupt stiffness degradation. The stage I is the same as for the other loading cases. A reduction of approximately 5% of the initial stiffness at 3% of the fatigue life is observed. In stage II, the stiffness of the specimens decreased slowly with the loading cycles, indicating that some damage was being created in the samples. It is believed that this damage would eventually lead to a delamination in the specimens, which is in agreement with previous studies reporting that composite materials, as opposed to metals, do not have a real fatigue life limit [28]. Each load cycle should be considered as damaging. In addition, the residual strength of the samples that survived 1 million cycles was 65% of the initial strength. This reduced strength points out to the fact that a non-negligible damage has been induced to the specimens during the cyclic loading. This 35% strength degradation is similar to the findings of Whitworth [29] for adhesively-bonded lap shear thermosetting composites.

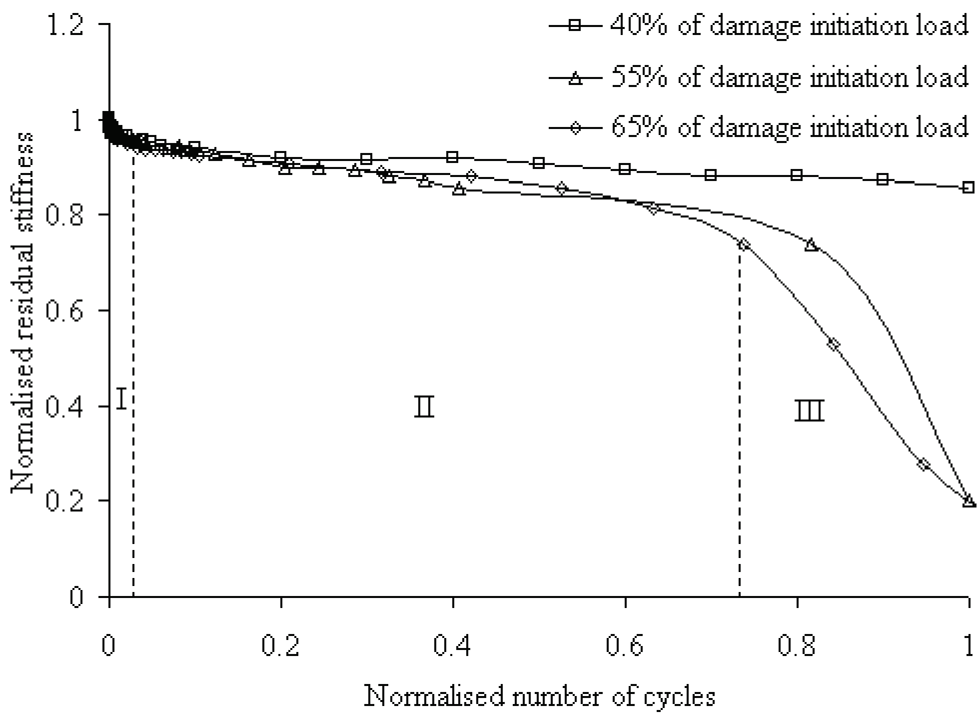

Fig. 5-7. Evolution of the specimens stiffness with cycles

Fig. 5-8 presents the S-N curves of the quasi-isotropic specimens welded using the uncoated and TiO_2 HE. The same fatigue behaviour is observed in both cases with indefinite fatigue lives obtained at 35% of the static damage initiation load. The specimens welded using the uncoated HE exhibited three different failure modes. In the first failure mode, a matrix crack was detected in the +45° ply of the skin laminate, at the edge of the weld. This crack propagated to the interface between the first two plies and produced a delamination at the ±45° plies interface, going towards the centre of the weld. One or two branches were then observed, going from the interlaminar delamination to the weld interface. A second delamination then propagated at the weld interface, between the polymer and the skin laminate, until the final failure of the specimens. This failure mode is illustrated in Fig. 5-9. In the second failure mode, the first crack was observed in the flange instead of the skin. It was still located at the ±45° interface and the same patterns, i.e., matrix crack branching to weld interface followed by a weld interface debonding, were observed. Both failure modes are schematically depicted in Fig. 5-10. The third failure mode was observed only once. In this case, the first crack initiated at the weld interface, between the skin laminate and the weld. The crack propagated in the weld towards the centre of the flange until one point where a matrix crack branching to the ±45° interface of the skin laminate appeared. A second delamination was then created at the ±45° interface of the skin laminate. All these failure modes were also observed under static loading [22, 23].

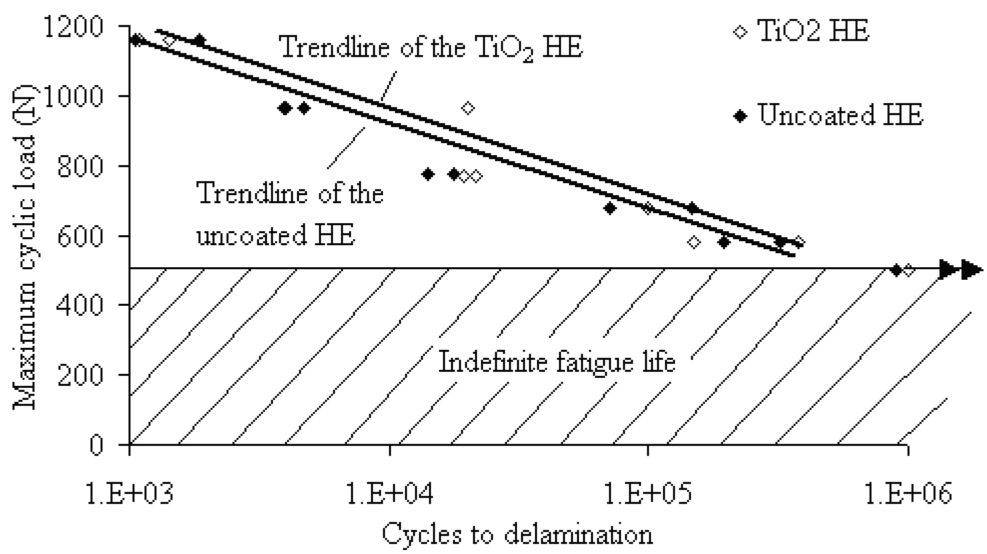

Fig. 5-8. Maximum cyclic load plotted against the number of cycles to delamination for quasi-isotropic specimens welded using the uncoated and TiO_2 HE

.

Fig. 5-9. Failure mode of the quasi-isotropic specimens welded using the uncoated HE

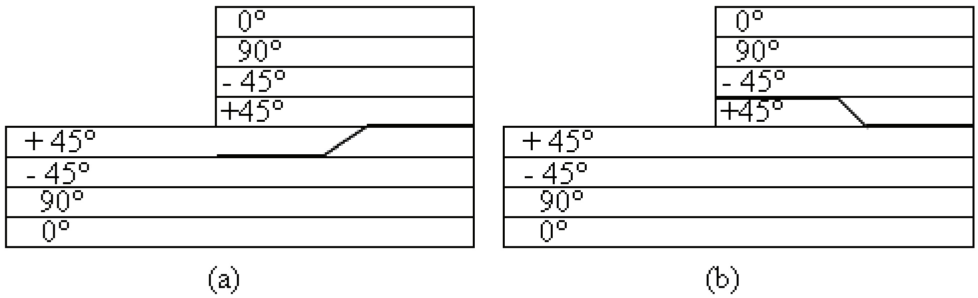

Fig. 5-10. Failure modes of quasi-isotropic specimens welded using the uncoated HE

It is interesting to compare the failure modes reported here with the ones of the adhesively bonded thermosetting composites [26]. The same specimen geometry was used for the adhesively bonded composites except that a taper angle was machined at the flange tip to reduce the stress concentration in this area [26]. In addition, the adhesively bonded specimens were tested under four-point bending instead of three-point bending. However, as reported in [21], the main factor contributing to matrix cracking and delamination is the bending moment at flange tip. No difference was observed between the static failure modes of the specimens under three- or four-point bending tests. It is thus assumed that the comparison with the failure mode under four-point bending is valid. One of the main findings of the reported studies on adhesively bonded skin/stringer composite is that the location of the 90° ply is the important feature determining the location of matrix cracking and delamination. For a stacking sequence similar to the one used here (skin lay-up $[45/-45/0/0/45/90/-45]_s$ and flange lay-up $[45/90/-45/0/90]_s$), three failure modes were reported. The first one was an initial matrix crack in the adhesive pocket, followed by a delamination at the weld interface (between the adhesive layer and the skin). The second failure mode was a first delamination at the –45°/90° interface of the flange, followed by a matrix branching and another delamination in the flange, at the 90°/45° interface. The last failure mode was based on an initial matrix crack in the adhesive pocket, followed by a delamination in the flange, at the 90°/45° interface. In all three cases, the final delamination always occurred either at the adhesive bondline or at the 90° ply interface. In the present case, the final delamination of the resistance-welded specimens was always at the weld interface or at the ±45° ply interface of the skin laminate. The fact that the 90° ply was further away from the bondline (third ply instead of the second) reduced the probability of having a matrix crack reaching this interface. The crack initiation and propagation for two loading cases, representing the two main failure modes of the resistance-welded specimens previously explained, are depicted in Fig. 5-11 as a plot of the crack length against the cycles.

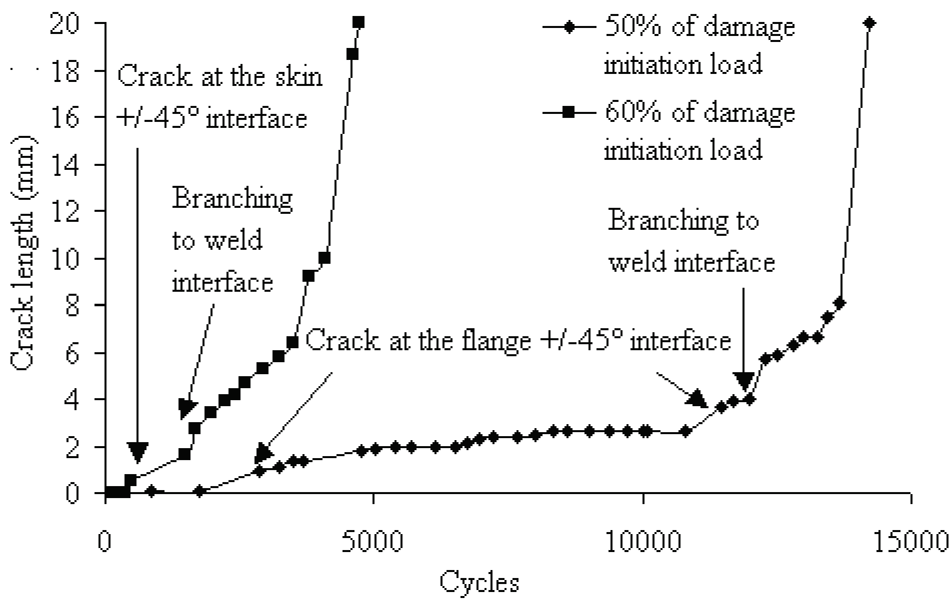

Fig. 5-11. Crack evolution as a function of cycles for quasi-isotropic specimens welded using the uncoated HE

The quasi-isotropic specimens welded using the TiO_2 HE showed certain differences in their failure modes (Fig. 5-12). The first cracks to be created were located in the skin, at the ±45° interface. A delamination running from this first crack towards the centre of the flange was then observed. However, no matrix crack branching to the weld interface was observed. The delamination at the weld interface was separated from the first crack and occurred between the metal mesh and the ceramic coating (as observed for the UD specimens) instead of between the polymer and the skin laminate. Once again, even though the failure mode was different, the fatigue performance was not affected by the use of the TiO_2 HE (Fig. 5-8).

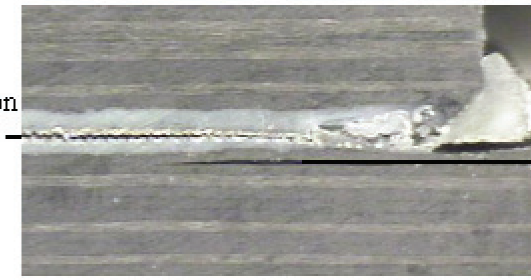

Fig. 5-12. Failure mode of the quasi-isotropic specimens welded using the TiO_2 HE

5.6 Summary and conclusions

In this study, the fatigue mechanical performance of resistance-welded UD and quasi-isotropic APC-2/AS4 skin/stringer specimens was investigated. A previously designed TiO_2 HE was used to weld the UD and some of the quasi-isotropic specimens. The following conclusions can be drawn from the investigation:

1) The UD and quasi-isotropic specimens showed a linear S-N curve in the region of intermediate fatigue life. The indefinite fatigue life was reported at 40% and 35% of the static damage initiation loads for the UD and quasi-isotropic specimens, respectively, which is similar to previous results on fatigue performance of adhesively bonded skin/stringer specimens [26].
2) The TiO_2 HE did not affect the fatigue mechanical performance of the specimens. The same linear S-N curve was obtained in the intermediate fatigue life region. The indefinite fatigue life was obtained at 35% of the static damage initiation load, as for the uncoated HE.

3) The delamination in the UD specimens was always located at the weld interface, between the metal mesh wires and the ceramic coating. A good adhesion between the TiO_2 coating and the polymer was observed. However, the TiO_2 coating tended to debond from the metal mesh, explaining the delamination at the weld interface.
4) The main failure modes of the quasi-isotropic specimens that were welded using the uncoated HE involved a first delamination at the ±45° interface, either in the skin or flange laminates. A matrix crack branching to the weld interface was then produced and the delamination then progressed at the weld interface, between the weld and the skin or flange laminates.
5) The failure mode of the quasi-isotropic specimens welded using the TiO_2 HE was similar to that of the uncoated HE. The main difference was that the delamination at the weld interface occurred between the metal mesh and the ceramic coating, just as it was observed for the UD specimens.

The failure modes of the skin/stringer specimens under static and fatigue loadings are important to investigate and characterise since they are the most likely to happen in a real-life-situation (where reinforced structure are very common). The description of these failure modes under static conditions was reported in [22, 23]. This present study completes the experimental work on the failure mechanisms of these types of structures by characterising the failure modes under fatigue conditions. The next step in the investigation of the resistance-welded skin/stringer configurations would be to develop a methodology for the cumulative fatigue life prediction using finite element analysis. Concerning the current leakage issue that is encountered in resistance welding of carbon fibre reinforced laminates, the new developed TiO_2 HE was shown to be a successful solution to it. No mechanical performance drawback was observed, either under static or fatigue loadings. However, since the delaminations in both cases occurred between the metal mesh wires and the TiO_2 coating, a special treatment of the metal mesh should be considered in order to improve the mechanical performance of the resistance-welded joints. This should be the focus of a future investigation.

5.7 Acknowledgements

This work was supported by funding from the Natural Sciences and Engineering Research Council of Canada. The authors also greatly acknowledge Mr. David Leach from Cytec Engineered Materials Inc. for providing the materials used in this study.

5.8 References

1. Ageorges, C., Ye, L., Hou, M. Experimental investigation of the resistance welding of thermoplastic-matrix composites. II. Optimum processing window and mechanical performance. Composites Science and Technology 2000;60(8):1191-1202.

2. Ageorges, C., Ye, L., Hou, M. Experimental investigation of the resistance welding for thermoplastic-matrix composites. I. Heating element and heat transfer. Composites Science and Technology 2000;60(7):1027-1039.

3. Ageorges, C., Ye, L., Mai, Y.W., Hou, M. Characteristics of resistance welding of lap shear coupons. Part I. Heat transfer. Composites Part A: Applied Science and Manufacturing 1998;29(8):899-909.

4. Ageorges, C., Ye, L., Mai, Y.W., Hou, M. Characteristics of resistance welding of lap shear coupons. Part II. Consolidation. Composites Part A: Applied Science and Manufacturing 1998;29(8):911-919.

5. Dubé, M., Hubert, P., Gallet, J.N.A.H., Stavrov, D., Bersee, H.E.N., Yousefpour, A. Heating Element Optimization in Resistance Welding of Semi-Crystalline and Amorphous Thermoplastic Composites. CANCOM, Winnipeg, Canada, 2007.

6. Dubé, M., Hubert, P., Yousefpour, A., Denault, J. Mechanical Performance of Resistance-Welded Thermoplastic Composite Skin/Stringer Specimen. SAMPE Fall Technical Conference, Seattle, USA, 2005.

7. Dubé, M., Hubert, P., Yousefpour, A., Denault, J. Fatigue Performance of Resistance-Welded Thermoplastic Composite Skin/Stringer Joints. SAMPE-Europe, Paris, France, 2007.

8. Dubé, M., Hubert, P., Yousefpour, A., Denault, J., Wadham-Gagnon, M. Resistance Welding of Thermoplastic Composites Skin/Stringer Specimens. SAMPE, Long Beach, USA, 2006.

9. Eveno, E., Gillespie, J.W.J. Resistance welding of graphite polyetheretherketone composites - An experimental investigation. Journal of Thermoplastic Composite Materials 1988;1:322-338.

10. Hou, M., Friedrich, K. Resistance welding of continuous glass fibre reinforced polypropylene composites. Composites Manufacturing 1992;3(3):153-163.

11. Hou, M., Friedrich, K. Resistance welding of continuous carbon fibre/polypropylene composites. Plastics Rubber and Composites Processing and Applications 1992;18(4):205-213.

12. Stavrov, D., Ahmed, J.T., Bersee, H.E.N. Resistance Welding of Thermoplastic Composites-The Influence of the Metal Mesh Heating Element. SAMPE-Europe, Paris, France, 2007.

13. Stavrov, D., Bersee, H.E.N. Experimental Investigation of Resistance Welding of Thermoplastic Composites with Metal Mesh Heating Element. SAMPE-Europe, Paris, France, 2004.

14. Yousefpour, A., Hojjati, M. Static and fatigue behavior of fusion bonded APC-2/AS4 thermoplastic composite joints. SAMPE-Europe, Paris, France, 2007.

15. Yousefpour, A., Simard, M., Octeau, M.-A., Hojjati, M. Process Optimization of Resistance-Welded Thermoplastic Composites Using Metal Mesh Heating Elements. SAMPE, Long Beach, USA, 2005.

16. Yousefpour, A., Simard, M., Octeau, M.-A., Lamarée, M., Hojjati, M. Effects of Mesh Size on Resistance Welding of Thermoplastic Composites Using Metal Mesh Heating Elements. SAMPE-Europe, Paris, France, 2004.

17. Yousefpour, A., Hojjati, M., Immarigeon, J.-P. Fusion Bonding/Welding of Thermoplastic Composites. Journal of Thermoplastic Composite Materials 2004;17(4):303-341.

18. Stavrov, D., Bersee, H.E.N. Thermal Aspects in Resistance Welding of Thermoplastic Composites. ASME Summer Heat Transfer Conference, Las Vegas, USA, 2003.

19. Stavrov, D., Bersee, H.E.N., Beukers, A. The Influence of the Heating Element on Resistance Welding of Thermoplastic Composite Materials. International Conference on Composite Materials, San Diego, USA, 2003.

20. Stavrov, D., Bersee, H.E.N., Beukers, A. Resistance Welding of Continuous Fibre Reinforced PPS Composites with Metal Mesh Heating Element. International Conference on Innovation and Integration in Aerospace Sciences, Belfast, Northern Ireland, UK, 2005.

21. Minguet, P.J., O'Brien, T.K. Analysis of test methods for characterizing skin/stringer debonding failures in reinforced composite panels. Composite Materials: Testing and Design, Proceedings of the 12th Symposium, Montréal, Canada, 1996.

22. Dubé, M., Hubert, P., Yousefpour, A., Denault, J. Current leakage prevention in resistance welding of carbon fibre reinforced thermoplastics. Accepted for publication in Composites Science and Technology (September 2007).

23. Dubé, M., Hubert, P., Yousefpour, A., Denault, J. Resistance welding of thermoplastic composites skin/stringer joints. Composites Part A: Applied Science and Manufacturing 2007;doi:10.1016/j.compositesa.2007.07.014.

24. Stavrov, D., Bersee, H.E.N. Resistance welding of thermoplastic composites - an overview. Composites Part A: Applied Science and Manufacturing 2005;36(1):39-54.

25. Stavrov, D., Bersee, H.E.N., Beukers, A. Experimental Investigation of Large-Scale Welding of Carbon Fiber Thermoplastic Composite Materials. International Conference on Composite Materials, San Diego, USA, 2003.

26. Cvitkovich, M.K., O'Brien, T.K., Minguet, P.J. Fatigue debonding characterization in composite skin/stringer configurations. Proceedings of the 7th Symposium on Composites: Fatigue and Fracture, St-Louis, USA, 1998.

27. Bureau, M.N., Denault, J. Fatigue Behavior of Continuous Glass Fiber Composites: Effect of the Matrix Nature. Polymer Composites 2000;21(4):9.

28. Nijssen, R.P.L., Beukers, A. Fatigue Life Prediction and Strength Degradation of Wind Turbine Rotor Blade Composites. Ph.D., Delft University of Technology, Aerospace Engineering, 2006.

29. Whitworth, H.A., Othieno, M., Yin, S.W., Sawicki, A., LIorente, G. Evaluation of composite bonded joints. ASME, Los Angeles, USA, 1995.

CHAPTER 6. FOURTH MANUSCRIPT

6.1 Preface

The fatigue properties of the skin/stringer joints made of APC-2/AS4 composites were investigated in the previous chapter. A fatigue performance investigation of other materials and weld geometry, i.e., CF/PEKK, CF/PEI and GF/PEI lap shear joints, is now needed. However, prior to this fatigue study, the metal mesh heating element size must be optimised. The effect of the mesh geometry on the static mechanical properties and the failure modes is presented in this chapter.

Metal mesh heating element optimisation in resistance welding of thermoplastic composites*

*Manuscript submitted to Composites Part A: Applied Science and Manufacturing (October 2007)

Martine Dubé and Pascal Hubert
McGill University, CREPEC, Department of Mechanical Engineering
817 Sherbrooke Street West, Montréal, Québec, H3A 2K6, Canada

Jan N.A.H. Gallet, Darko Stavrov and Harald E.N. Bersee*
Delft University of Technology, Faculty of Aerospace Engineering
Design and Production of Composite Structures
1 Kluyverweg, Delft, 2629 HS, The Netherlands

Ali Yousefpour
Aerospace Manufacturing Technology Centre, National Research Council Canada
5145 Decelles Avenue, Montréal, Québec, H3T 2B2, Canada

6.2 Abstract

Resistance welding of amorphous and semi-crystalline thermoplastic composites using various stainless steel meshes as heating elements was investigated. The adherends consisted of 16 plies of unidirectional carbon fibre/poly-ether-ketone-ketone (CF/PEKK), 16 plies of unidirectional carbon fibre/poly-ether-imide (CF/PEI) and 8 plies of 8-harness satin weave fabric glass fibre/PEI (GF/PEI). The objective of the work was to obtain an optimum mesh size in order to achieve the maximum lap shear strengths (LSS). LSS of 52 MPa, 47 MPa and 33 MPa were obtained for the CF/PEKK, CF/PEI and GF/PEI specimens, respectively, using the heating element with the optimum mesh size. Lap shear tests were also performed on compression-moulded GF/PEI lap shear specimens and LSS of 27 MPa, which was 18% lower than the LSS of the specimens welded using the optimum mesh size, was obtained. The metal mesh heating element, when adequately optimised, can thus reinforce the weld. Observations of the specimens fracture surfaces revealed an interlaminar failure mode involving damage of the laminates and tearing of the heating element. The CF/PEI specimens showed a linear load-displacement curve followed by a brittle fracture. The CF/PEKK specimens exhibited a non-linear behaviour and more ductility than the CF/PEI specimens. The lower LSS of the GF/PEI specimens was attributed to the different nature and architecture of the reinforcing woven glass fibres.

Keywords: A. Polymer-matrix composites (PMCs); A. Thermoplastic resin; E. Joints/Joining; Resistance welding

6.3 Introduction

Continuous fibre reinforced thermoplastic composites are increasingly used as structural components in automotive, marine and aerospace industries because of their commonly cited advantages over thermoset composites [1]. As the complexity of the parts made of these materials increases, development of efficient joining methods is becoming extremely important. Among the various joining methods available for thermoplastic composites, fusion bonding or welding has attracted most attention in the past few years [1]. Fusion bonding makes use of one of the main properties of thermoplastic polymers, which is their capability to be melted and subsequently cooled to regain their physical and mechanical properties. The interest for this joining method resides in its advantages over conventional joining methods such as adhesive bonding, in which extensive surface preparation and long curing times are involved and mechanical fastening, in which stress concentrations are induced by drilling holes.

The fusion bonding principle can be described as heating the surfaces of two adherends above their glass-transition temperature T_g (for amorphous polymers) or melting temperature T_m (for semi-crystalline polymers), fusing their interface and cooling them under the application of pressure for solidification and consolidation purposes [2]. Heat can be applied to the interface using direct heat sources (thermal welding), using linear, rotational or ultrasonic vibrations (vibration welding) or using electrical current or electromagnetic field (electromagnetic welding). Resistance welding is one of the electromagnetic welding techniques that showed a high potential to be implemented in industry [1]. It is a simple, inexpensive and fast process that requires simple tooling [1]. In this technique, a heating element is placed between the surfaces of two adherends and an electrical current is applied to the heating element. As the current passes into the heating element, the temperature rises due to the Joule heating effect and the adjoining polymer softens (amorphous polymer) or melts (semi-crystalline polymer). The softening or melting of the polymer is followed by a consolidating step in which the weld interface is cooled, under the application of pressure [3].

Recent investigations about resistance welding of thermoplastic composites include experimental and modelling works. The modelling works mainly focused on heat transfer, consolidation and crystallisation analyses while the experimental works investigated the effects of the welding parameters such as the input power level and heating element type on the weld quality and performance [3-10]. Three methods of applying the input power to the heating element were reported. In the first method, called constant input voltage, a fixed input voltage is applied to the heating element and remains constant over the entire welding process. The second method was proposed by Arias *et al.* [11] and is called the impulse power technique. In this method, power is applied in the form of intense pulses, followed by a pause of 1 to 3 seconds. It was claimed that this method could provide a better temperature homogeneity over the weld area as the heat can dissipate in the weld during the pauses. In the last method, called ramped voltage, the voltage applied to the heating element is increased at a fixed rate. The reported ramping rates vary from 1.5 V/min. to 9 V/min. [12-15]. This method was used to weld unidirectional and quasi-isotropic 16-ply APC-2/AS4 (carbon fibre/poly-ether-ether-ketone) adherends. The main advantage of this method is that a proper voltage ramping rate provides a linear heating rate which in turn facilitates the process control [14].

The heating element type is another resistance welding parameter that was extensively investigated in the past years. Since it is responsible for heating the weld interface and remains embedded in the weld after the welding operation, it is probably the most important parameter in the resistance welding process. In the eighties and nineties, carbon fibre prepreg plies were used as heating elements because of their compatibility with carbon fibre reinforced adherends [3, 16-18]. The heating elements consisted of a single unidirectional or fabric carbon fibre prepreg ply. In general, the unidirectional prepreg led to non-uniform heating due to the low thermal conductivity in the direction perpendicular to the fibres [4]. In addition, the brittleness of the carbon fibres reduced the connection efficiency with the power supply for both the unidirectional and fabric heating elements [4]. These problems arouse the interest of the researchers for a new type of heating element, which consisted of a stainless steel mesh. Although the stainless steel mesh induced a lack of resistance to galvanic corrosion, it improved the temperature homogeneity over the weld area and was more resistant to the pressure induced by the connectors, leading to an overall better weld performance, wider processing window and better process control and repeatability [2, 19]. Stainless steel meshes are available in different wire diameters and open gap widths. These parameters affect the electrical resistance of the meshes and consequently, the heat generation at the weld interface. The wire diameter and open gap width also affect the polymer diffusion and mechanical interlocking in the weld [15, 20, 21]. In order to come up with a good mechanical performance these two parameters need to be investigated and optimised.

The objective of the present study is to investigate the effects of the metal mesh heating element parameters on the general quality and mechanical performance of the welded joints. Five different stainless steel mesh heating elements were used to weld semi-crystalline (poly-ether-ketone-ketone - PEKK) and amorphous (poly-ether-imide - PEI) polymer composites. The effects of the heating elements wire diameter and open gap width on the weld quality and performance were investigated using static lap shear testing and optical microscopy. One optimal metal mesh size was selected and a comparison between the quality and mechanical performance of each welded material was performed.

6.4 Experimental

6.4.1 Adherends

The laminates used in this work consisted of unidirectional carbon fibre/PEKK (CF/PEKK), unidirectional CF/PEI and fabric GF/PEI. PEKK is a semi-crystalline polymer with a melting temperature of 310°C and PEI is an amorphous polymer with a glass-transition temperature of 218°C. The 2.2 mm thick $[0]_{16}$ CF/PEKK and CF/PEI laminates were supplied by Cytec Engineered Materials Inc. and were compression-moulded under the PEKK and PEI standard moulding conditions. The 2.0 mm thick GF/PEI laminates were provided by Ten Cate Advanced Composites and consisted of 8 plies of 8-harness satin weave. In order to perform lap shear testing, the adherends were cut off from the laminates to dimensions of 101.6 mm long and 25.4 mm wide before being joined by resistance welding.

GF/PEI benchmark laminates were made in order to compare the weld strength with the strength of the compression-moulded laminates. The GF/PEI benchmark laminates were made of 16 plies (twice the number of plies of the welded laminates) and were machined to the same lap shear geometry as the welded specimens.

6.4.2 Heating elements

Five woven stainless steel meshes were used as heating elements (Fig. 6-1). A description of each heating element is presented in Table 6-1 along with the materials that were welded with each mesh. The heating elements were cut to the exact width of the lap shear specimens overlap size, i.e., 12.7 mm. The electrical resistance values reported in Table 6-1 are thus for a width and length of 12.7 mm and 25.4 mm, respectively. A neat polymer film of the same polymer type as the adherends was placed on each side of the heating element prior to the welding operation in order to provide a resin rich region at the weld interface as well as to reduce the number of voids due to entrapment of air in the mesh.

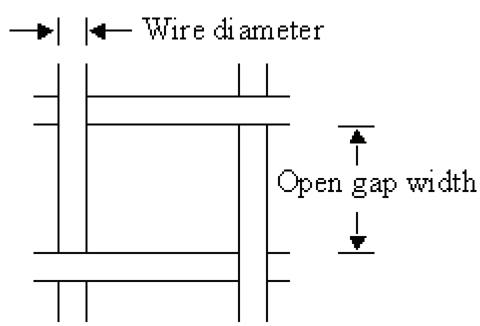

Fig. 6-1. Stainless steel mesh schematic

Table 6-1. Heating elements

Heating element	A	B	C	D	E
Wire diameter (mm)	0.114	0.066	0.041	0.036	0.025
Open gap width (mm)	0.152	0.104	0.089	0.043	0.038
Linear wire density (wires/mm)	3.9	5.8	7.7	12.5	14.3
Electrical resistance (Ω)	0.081	0.151	0.290	0.385	0.392
Welded materials	GF/PEI	GF/PEI CF/PEI CF/PEKK	GF/PEI CF/PEI CF/PEKK	GF/PEI CF/PEI CF/PEKK	GF/PEI CF/PEI

6.4.3 Resistance welding

The resistance welding set-up consisted of a DC power supply with maximum output of 40 A and 80 V, a computer/data acquisition system, a pressure system and a resistance welding rig. The resistance welding rig was specifically designed to weld a single lap shear sample. It consisted of a fibreglass plate on which ceramic block insulators were installed to provide thermal insulation against heat losses in the environment and apply the welding pressure. Copper electrical connectors were used to apply the current to the heating element. The ramped voltage method was used for all welds. A fixed initial voltage of 2.0 V was first applied to the heating element and the voltage was ramped at a rate of 9.0 V/min. A constant welding pressure of 1.0 MPa was applied during the process. The temperature was monitored using a K-type thermocouple located at the centre of the welds, between the polymer film and the adherend. When the monitored temperature reached a pre-determined welding temperature of 420°C for PEKK polymer and 400°C for PEI polymer, the current was stopped and the weld interface cooled down, under the application of pressure.

6.4.4 Mechanical testing and characterisation methods

The samples welded using each heating element and material were first analysed by optical microscopy to verify the quality of the weld interface. The samples were cut, polished and observed along both the length and width directions. The static lap shear tests were conducted according to the ASTM D1002 standard test method. The lap shear specimens were 190.5 mm long and 25.4 mm wide with an overlap length of 12.7 mm. The free length between the grips was 139.7 mm. The specimens were tested at 23°C and at a relative humidity of 50% under a crosshead speed of 1.27 mm/min. At least five replicated samples were welded and tested for each type of materials and heating element size. The fractured samples were observed visually to determine their failure modes.

6.5 Results

6.5.1 Thermal behaviour

The electrical resistance of the heating elements is a function of the wire diameter and the number of wires in the mesh. Thus for a given ramped voltage rate, the input power level and consequently the heating rate are functions of the heating element size. This behaviour was observed from the temperature profiles measured during the welding operation. An example is given in Fig. 6-2 for the GF/PEI specimens. The higher the electrical resistance was, the lower the input power, and the longer the welding time. This behaviour was observed for all three materials.

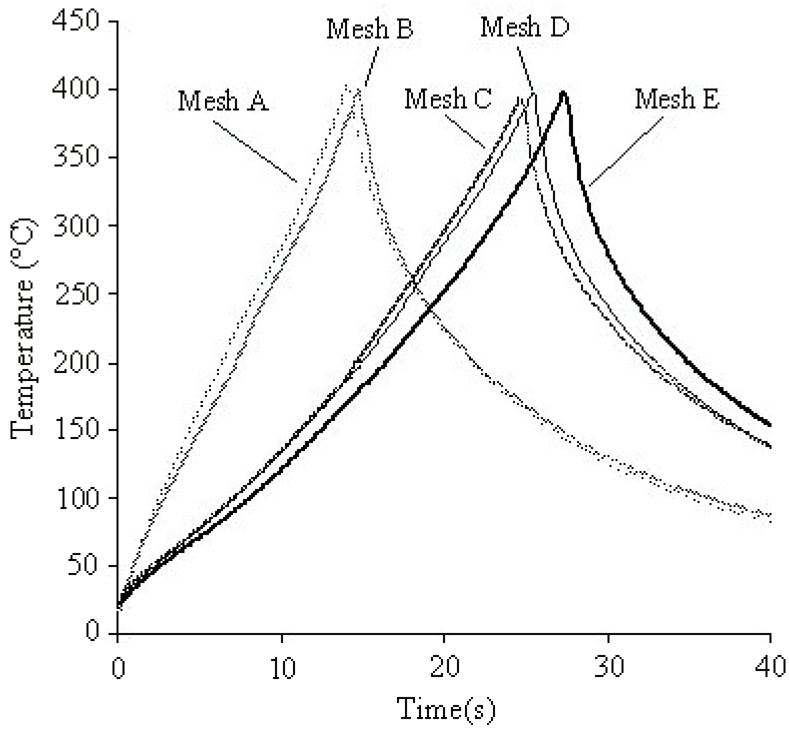

Fig. 6-2. Temperature profiles of the GF/PEI specimens welded using the five stainless steel heating elements

These variations in the heating rates were suspected to influence the microstructure of the polymer so that comparison between each heating element would not be reliable. However, looking carefully at the temperature profiles, one can see that the heating time, i.e. the time between the start of the welding process and the time at which current is switched off, was very short. It varied from 14 seconds only (heating element A) to 28 seconds (heating element E). Furthermore, the time spent above the glass-transition temperature varied from 14 to 16 seconds only. The difference between these periods of time was so short that its effect on the microstructure of the polymer was neglected. It should also be noted that although the PEI polymer was heated well above its glass-transition temperature, the time spent above that temperature was short and no polymer degradation was noticed.

6.5.2 Weld interface quality

Previous studies have shown that the weld quality is generally not uniform over the weld area. Therefore, microscopic observations were made both at the centre and edges of the welds. An example is given in Fig. 6-3 for a CF/PEKK sample welded using type B heating element. At the centre of the specimen (Fig. 6-3 – a), a good weld interface quality is observed without voids or porosities. Complete mesh impregnation and good polymer flow are observed, providing mechanical interlocking between the polymer and heating element. On the other hand, existence of voids was revealed at the edges of the weld (Fig. 6-3 – b). These voids reflected a lower weld quality that was attributed to two phenomena. The first one was the polymer squeeze out. When the polymer melted, the viscosity was reduced and it squeezed out of the weld at the edges of the adherends. Not enough polymer was left behind to fill the gaps in the heating element, explaining the voids located in the heating element. The second reason for the lower quality at the edges was a reduced welding pressure in this region. After the polymer squeezed out of the weld, only the remaining polymer, i.e., the polymer located at the centre of the welds, could sustain the applied welding pressure. The pressure at the edges was thus reduced explaining the existence of voids in the adherends (lack of consolidation pressure). The same behaviour, i.e., a good weld interface quality in the centre but some voids at the edges, was observed for the other heating elements used for the CF/PEKK specimens. The CF/PEI and GF/PEI samples revealed a different behaviour. Many defects were located at the weld interface and in the adherends, even in the centre of the welds (Fig. 6-4). The lower environmental resistance of the PEI polymer, compared to the PEKK polymer, can be partly responsible for those defects. It was shown that PEI does not have a good resistance to humidity absorption [22]. Since the PEI laminates were left at room conditions prior to welding, it is possible that they absorbed some humidity, which was released while heating the weld interface.

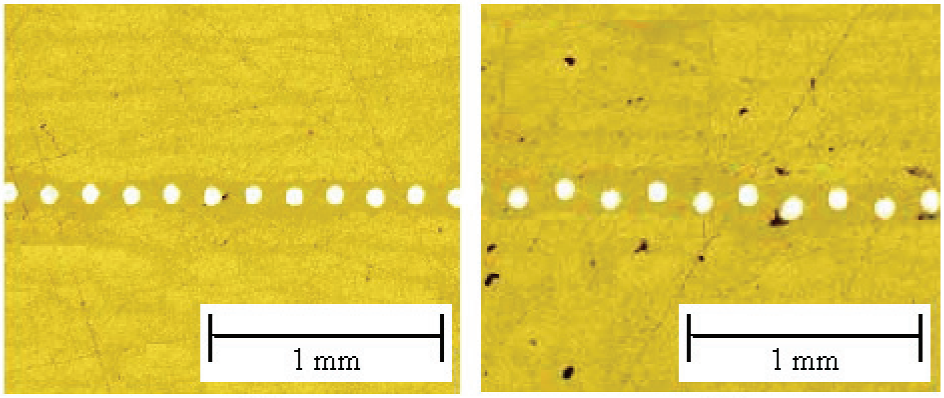

(a) (b)

Fig. 6-3. CF/PEKK weld interface at the centre (a) and edge (b) of the weld using type B heating element

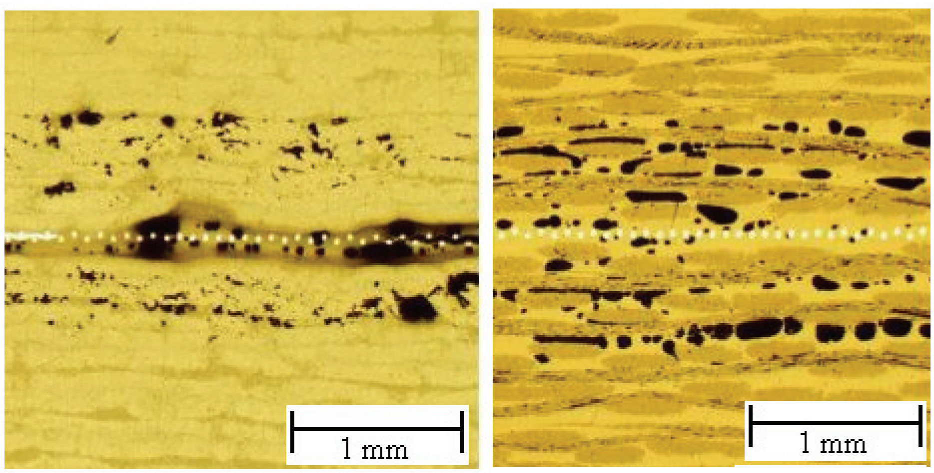

(a) (b)

Fig. 6-4. Micrographs of the weld interfaces at the centre of CF/PEI (a) and GF/PEI (b) specimens welded using type D heating element

6.5.3 Lap shear testing

Fig. 6-5 presents the lap shear strengths (LSS) of the tested specimens. The error bars on this figure correspond to two standard deviations. For all three materials, metal mesh C led to the highest LSS: 52 MPa, 47 MPa and 33 MPa for CF/PEKK, CF/PEI and GF/PEI, respectively. This was in accordance with a previous investigation on resistance welding of APC-2/AS4 material where it was shown that metal mesh C resulted in the best lap shear performance [15]. The reasons for this optimal mechanical performance reside in the metal mesh C wire diameter and open gap width. The metal meshes with larger wire diameters (A and B) reduced the LSS because the wires acted as inclusions (defects) in the weld. Furthermore, it was clear from the observations made by optical microscopy that the main mechanism contributing to the weld strength was mechanical interlocking between the metal mesh wires and the polymer. A small wire diameter implied that a large number of wires were present at the weld interface (Table 6-1). This large number of wires in turn provided the weld with more mechanical interlocking. This is what was observed between the heating elements A, B and C. By looking at the heating elements properties (Table 6-1), one can see that the main difference between those heating elements was the wire diameter. As the wire diameter decreased (from heating element A to heating element C), the linear density of wires increased and the LSS increased accordingly.

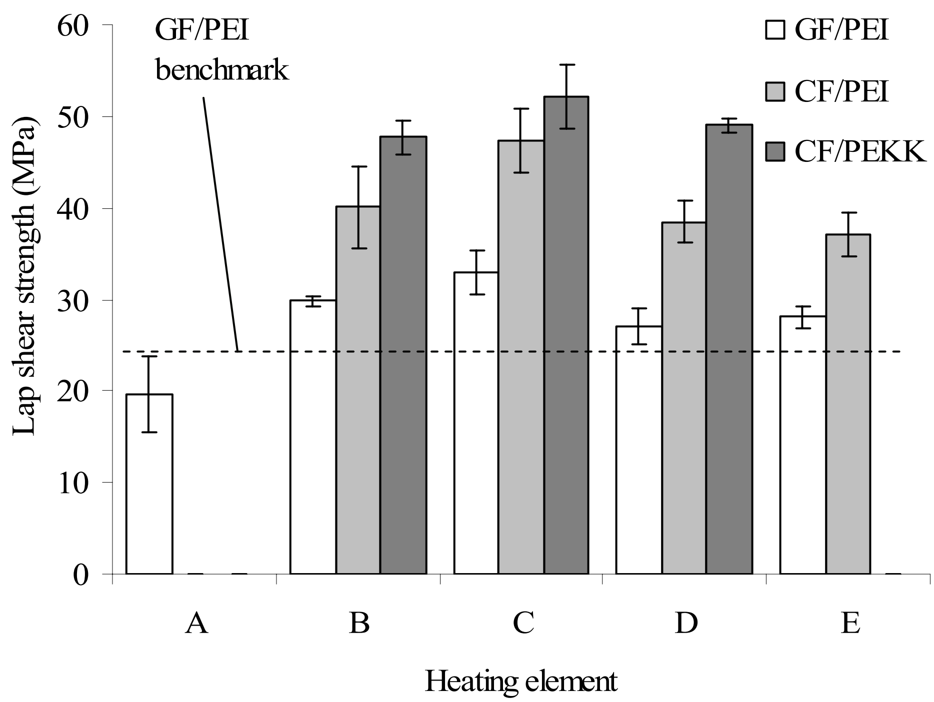

Fig. 6-5. Lap shear strengths

The number of wires cannot be increased indefinitely as the open gap width would be reduced and at some point, would become so small that the polymer on one side of the heating element could not inter-diffuse and mix with the polymer on the other side. The other important parameter affecting the LSS is thus the open gap width. The effect of the open gap width was investigated mainly by comparing the LSS of the specimens welded using heating elements C, D and E. As shown in Table 6-1, the main difference between those heating elements is the open gap width. As the open gap width decreased (from heating element C to heating element E), a reduction of the LSS was observed. One can also see that the strengths of the specimens welded using the heating elements D and E were quite similar. This behaviour was expected, since there was not much difference between these two heating elements (Table 6-1).

Fig. 6-5 also presents the results of the GF/PEI benchmark reference specimens. Average LSS of 27 MPa has been obtained for these specimens. This shows that the mesh can be seen either as a contaminant, e.g. metal mesh A that has a lower LSS than the benchmark specimens, or as a reinforcement, e.g. metal mesh C that has a higher LSS than the benchmark specimens. Optimising the metal mesh can thus change the mesh from a defect to reinforcement. The cause of this is the degree of mechanical interlocking, which improves the mechanical performance of the joint. Whitworth *et al.* [23] reported LSS of 48 MPa for compression-moulded CF/PEKK specimens, which is lower than the one reported here for the CF/PEKK specimens welded using type C heating element. This shows, once again, the reinforcing capabilities of the optimum metal mesh C.

The average LSS of the CF/PEKK and CF/PEI welds were similar when considering the standard deviations. However, the load-displacement curves and the fracture behaviours of the two materials were quite different. Fig. 6-6 shows a linear load-displacement curve for the CF/PEI material up to the maximum load. A brittle fracture follows the maximum load. The CF/PEKK specimens exhibited a different behaviour with a non-linear curve after 40% of the maximum load. A plateau was then observed just before the maximum load was reached. This plateau was due to a higher polymer ductility and damage progression in the weld. A higher force was required to break the CF/PEKK specimens. This behaviour was expected because of the excellent toughness properties of the PEKK polymer. The GF/PEI welds exhibited a lower strength and a much higher displacement to failure than the CF/PEI samples, even though the same heating element and polymer were used. The different nature and architecture of the reinforcing fibres (woven 8-harness glass fibre as opposed to unidirectional carbon fibre) were responsible for this lower strength and higher displacement to failure.

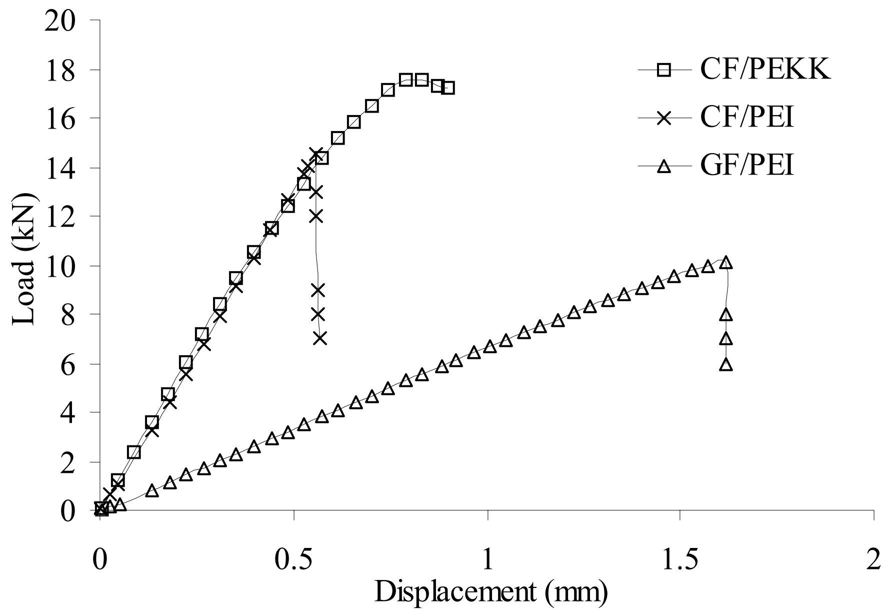

Fig. 6-6. Load-displacement curves of CF/PEKK, CF/PEI and GF/PEI specimens welded using type C heating element

The analysis of the fracture surfaces gave insight on the failure modes of the specimens. As explained in [2] the failure modes are generally classified into two categories: interfacial or interlaminar failure modes. Interfacial failure occurs at the interface between the heating element and adherend and leads to low LSS due to imperfect welding. The interlaminar failure mode, on the other hand, involves damage in the adherends or heating element or within both of them [2]. It generally leads to high LSS, especially if damage to the adherends is involved. Both the interfacial and interlaminar failure modes were observed in this investigation. For the CF/PEKK specimens, the heating element B led to an interlaminar failure, involving tearing of the heating element and debonding between the heating element and the polymer. No laminate damage was involved. Type C heating element also led to an interlaminar failure, but damage to both the heating element and adherend was involved. This failure required a higher force, explaining the higher LSS obtained in this case. Finally, heating element D showed a debonding between the heating element and the polymer. Some damage to the adherends was involved but not as much as for the heating element C.

The PEI specimens revealed the same failure modes as the CF/PEKK specimens. Debonding between the heating element and polymer interface was observed for the heating elements A and B. Tearing of the heating element was also observed, especially for the heating element B, but no damage to the laminates was involved. The heating element C showed a full layer of the laminate ripped off, which is an example of interlaminar failure without heating element tearing but a lot of laminate damage. The heating elements D and E showed weld interface debonding, involving little or no damage to the laminates. The same observations were made on the CF/PEI specimens. Examples of the various failure modes are given in Fig. 6-7.

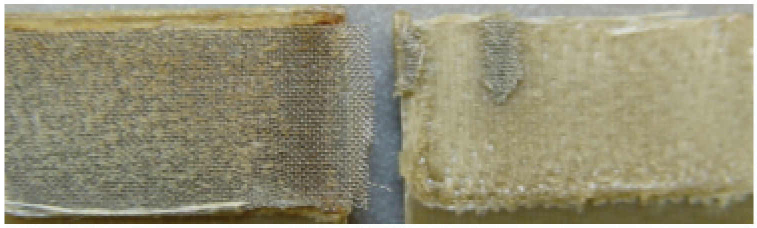

Heating element A

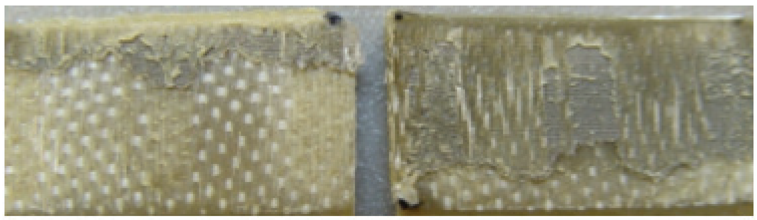

Heating element B

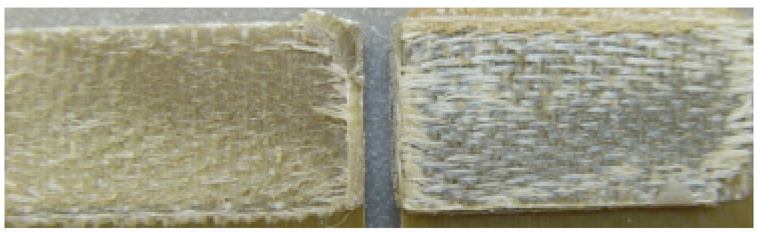

Heating element C

Fig. 6-7. Fracture surface of GF/PEI specimens showing interfacial failure (heating element A), interlaminar failure involving damage to the heating element (heating element B) and interlaminar failure with damage to the adherends (heating element C)

6.6 Conclusions

The heating element is a critical factor in resistance welding of thermoplastic polymers as it affects the heat generation at the weld interface and the mechanical properties of the weld. In this work, different stainless steel meshes were used as heating elements to weld semi-crystalline (PEKK) and amorphous (PEI) thermoplastic composites. It was found that the wire diameter and the open gap width had a great influence on the weld quality and performance. The metal mesh with a wire diameter of 0.04 mm and open gap width of 0.09 mm led to the best mechanical performances. LSS of 52 MPa, 47 MPa and 33 MPa were obtained for the CF/PEKK, CF/PEI and GF/PEI specimens, respectively, using this optimum mesh size. The LSS of the GF/PEI specimens welded using the optimum mesh size heating element is higher than the one obtained for the compression-moulded GF/PEI benchmark references. This shows the reinforcing properties of the metal mesh heating element when adequately optimised. Tested lap shear specimens exhibited interlaminar or interfacial failure modes, the latter leading to the best mechanical performances.

Although the LSS of the CF/PEKK and CF/PEI specimens were similar, different mechanical behaviours were observed. The CF/PEI samples showed a linear load-displacement curve, followed by a brittle fracture. The CF/PEKK specimens exhibited a non-linear behaviour, more ductility and a certain damage accumulation before the complete rupture of the specimens. A lower strength was obtained for the GF/PEI samples due to the reinforcing woven glass fibres.

This study showed that appropriate metal mesh size leads to good weld quality and mechanical performance, under static loading. As no data are available to date about the performance of the welds under cyclic loading, it is believed that the future investigations should focus on the fatigue behaviour of the resistance-welded joints. The behaviour of the welds in different environmental conditions should also be investigated.

6.7 Acknowledgements

This work was supported by funding from the Natural Sciences and Engineering Research Council of Canada. The authors would also like to gratefully acknowledge Mr. David Leach from Cytec Engineered Materials Inc. for providing the CF/PEKK and CF/PEI materials and Ten Cate Advanced Composites for providing the GF/PEI material.

6.8 References

1. Yousefpour, A., Hojjati, M., Immarigeon, J.-P., Fusion Bonding/Welding of Thermoplastic Composites. Journal of Thermoplastic Composite Materials, 2004;17(4):303-341.

2. Stavrov, D., Bersee, H.E.N., Resistance welding of thermoplastic composites - an overview. Composites Part A: Applied Science and Manufacturing, 2005;36(1):39-54.

3. Eveno, E., Gillespie, J.W.J., Resistance welding of graphite polyetheretherketone composites - An experimental investigation. Journal of Thermoplastic Composite Materials, 1988;1:322-338.

4. Ageorges, C., Ye, L., Hou, M., Experimental investigation of the resistance welding for thermoplastic-matrix composites. I. Heating element and heat transfer. Composites Science and Technology, 2000;60(7):1027-1039.

5. Ageorges, C., Ye, L., Mai, Y.W., Hou, M., Characteristics of resistance welding of lap shear coupons. Part I. Heat transfer. Composites Part A: Applied Science and Manufacturing, 1998;29(8):899-909.

6. Ageorges, C., Ye, L., Mai, Y.W., Hou, M., Characteristics of resistance welding of lap shear coupons. Part II. Consolidation. Composites Part A: Applied Science and Manufacturing, 1998;29(8):911-919.

7. Ageorges, C., Ye, L., Mai, Y.W., Hou, M., Characteristics of resistance welding of lap-shear coupons. Part III. Crystallinity. Composites Part A: Applied Science and Manufacturing, 1998;29(8):921-932.

8. Stavrov, D., Bersee, H.E.N. Thermal Analysis of Resistance Welding of Thermoplastic Composites. International Conference on Composite Materials, Durban, South Africa, 2005.

9. Talbot, E. Manufacturing Process Modelling of Thermoplastic Composite Resistance Welding. M.Sc. Thesis, McGill University, Department of Mechanical Engineering, 2005.

10. Talbot, E., Yousefpour, A., Hubert, P., Hojjati, M. Thermal Behavior During Thermoplastic Composites Resistance Welding. Annual Technical Conference (ANTEC) of the Society of Plastics Engineers, Boston, USA, 2005.

11. Arias, M., Ziegmann, G. Impulse resistance welding: a new technique for joining advanced thermoplastic composite parts. Proceedings of the 41st International SAMPE Symposium and Exhibition, Anaheim, USA, 1996.

12. Dubé, M., Hubert, P., Yousefpour, A. Mechanical Performance of Resistance-Welded Thermoplastic Composite Skin/Stringer Specimen. SAMPE Fall Technical Conference, Seattle, USA, 2005.

13. Dubé, M., Hubert, P., Yousefpour, A., Denault, J., Resistance welding of thermoplastic composites skin/stringer joints. Composites Part A: Applied Science and Manufacturing, 2007;doi:10.1016/j.compositesa.2007.07.014.

14. Yousefpour, A., Simard, M., Octeau, M.-A., Hojjati, M. Process Optimization of Resistance-Welded Thermoplastic Composites Using Metal Mesh Heating Elements. SAMPE, Long Beach, USA, 2005.

15. Yousefpour, A., Simard, M., Octeau, M.-A., Lamarée, M., Hojjati, M. Effects of Mesh Size on Resistance Welding of Thermoplastic Composites using Metal Mesh Heating Elements. SAMPE-Europe, Paris, France, 2004.

16. Hou, M., Friedrich, K., Resistance welding of continuous glass fibre reinforced polypropylene composites. Composites Manufacturing, 1992;3(3):153-163.

17. Hou, M., Friedrich, K., Resistance welding of continuous carbon fibre/polypropylene composites. Plastics Rubber and Composites Processing and Applications, 1992;18(4):205-213.

18. Hou, M., Ye, L., Mai, Y.W., An experimental study of resistance welding of carbon fibre fabric reinforced polyetherimide (CF fabric/PEI) composite material. Applied Composite Materials, 1999;6(1):35-49.

19. Stavrov, D., Bersee, H.E.N., Beukers, A. The Influence of the Heating Element on Resistance Welding of Thermoplastic Composite Materials. Proceedings of the ICCM-14 Conference, San Diego, USA, 2003.

20. Stavrov, D., Bersee, H.E.N. Experimental Investigation of Resistance Welding of Thermoplastic Composites with Metal Mesh Heating Element, 2004.

21. Stavrov, D., Bersee, H.E.N., Beukers, A. Resistance Welding of Continuous Fibre Reinforced PPS Composites with Metal Mesh Heating Element.

International Conference on Innovation and Integration in Aerospace Sciences, Berlfast, Northern Ireland, UK, 2005.

22. Lincoln, J.E., Morgan, R.J., Shin, E.E., Effect of Thermal History on the Deformation and Failure of Polyimides. Journal of Polymer Science Part B: Polymer Physics, 2001;39(23):2947-2959.

23. Whitworth, H.A., Othieno, M., Yin, S.W. Evaluation of composite bonded joints. Applied Mechanics and Materials Summer Meeting (ASME), Los Angeles, USA, 1995.

CHAPTER 7. FIFTH MANUSCRIPT

7.1 Preface

In the previous chapter, the optimisation of the heating element size was presented for three different materials: CF/PEKK, CF/PEI and GF/PEI. A stainless steel mesh with a wire diameter of 0.04 mm and open gap width of 0.09 mm was found be the optimum one, for all three materials. In the present chapter, the fatigue properties of the welded joints are studied using the optimum mesh size.

Fatigue performance characterisation of resistance-welded thermoplastic composites*

*Manuscript submitted to Composites Science and Technology (October 2007)

Martine Dubé and Pascal Hubert
McGill University, CREPEC, Department of Mechanical Engineering
817 Sherbrooke Street West, Montréal, Québec, H3A 2K6, Canada

Jan N.A.H. Gallet, Darko Stavrov and Harald E.N. Bersee*
Delft University of Technology, Faculty of Aerospace Engineering
Design and Production of Composite Structures
1 Kluyverweg, Delft, 2629 HS, The Netherlands

Ali Yousefpour
Aerospace Manufacturing Technology Centre, National Research Council Canada
5145 Decelles Avenue, Montréal, Québec, H3T 2B2, Canada

7.2 Abstract

This study investigates the fatigue performance of resistance-welded thermoplastic composites. Lap shear specimens consisting of carbon fibre/poly-ether-imide (CF/PEI), glass fibre/poly-ether-imide (GF/PEI) and carbon fibre/poly-ether-ketone-ketone (CF/PEKK) composites were resistance-welded using a metal mesh heating element. The specimens were fatigue-tested at various percentages of their static lap shear strengths at a load ratio of R = 0.1 and frequency f = 5 Hz. The fatigue performances of the resistance-welded semi-crystalline (PEKK) and amorphous (PEI) composites were compared and the failure modes of the specimens were described. The stiffness degradation was monitored during the tests in order to evaluate the damage accumulation in the specimens. Linear stress-life (S-N) curves were obtained for all three materials when plotted on a semi-log scale. Interlaminar failure modes, involving tearing of the heating element and damage to the adherends were observed. Indefinite fatigue lives were reported at 20% and 25% of the static lap shear strengths.

Keywords: A. Polymer-matrix composites (PMCs); A. Thermoplastic resin; E. Joints/Joining; Resistance welding

7.3 Introduction

Fusion bonding or welding of thermoplastic composites has attracted attention of researchers in the past few years [1, 2]. The advantages of welding over conventional joining methods such as adhesive bonding and mechanical fastening, and the increasing use of thermoplastic composites in the transportation industries are the main reasons for this growing interest. Among various welding techniques available for thermoplastic composites, resistance welding presents a number of advantages. It is a fast process, which requires simple equipment, and is adaptable to automation and on-line inspection [2]. In the resistance welding technique, an electrical conductive heating element is embedded between two thermoplastic composite parts to be welded (adherends). An electrical current is applied to the heating element using a direct electrical connection causing a temperature rise by Joule heating effect. As temperature reaches the polymer glass-transition temperature or melting temperature, the adjoining polymer matrix melts and flows. When a predetermined processing temperature is reached, the current is stopped and the weld interface cools down, under the application of pressure.

Both experimental and modelling investigations were conducted on resistance welding of thermoplastic composites [3-14]. The modelling works focused on the thermal, consolidation and crystallisation analyses of the welding process while the experimental works investigated the effects of the welding parameters on the weld quality. Among the main parameters influencing the weld quality, the heating element type is of particular importance as it is responsible for the heat generation at the weld interface [6, 13, 15-19]. In addition, since it remains trapped in the joint after the welding operation, it becomes part of the assembled structure and as such, has an influence on the physical and mechanical properties of the structure. Two materials are commonly used for the heating elements: carbon fibre prepreg plies and metal meshes. Research has shown that a metal mesh heating element facilitates the welding process and provides better mechanical performance with less scatter in the results [18, 20]. Metal meshes, which generally consist of stainless steel material, are thus used as heating elements in nearly all the recent studies.

Metal meshes are available in a wide range of wire diameter and open gap width. A previous investigation presented a metal mesh size optimisation for resistance welding of carbon fibre/poly-ether-ketone-ketone (CF/PEKK), carbon fibre/poly-ether-imide (CF/PEI) and glass fibre/poly-ether-imide (GF/PEI) [6, 15]. The metal mesh optimisation was based on qualitative evaluation of the welds as well as lap shear mechanical testing. Among five different stainless steel meshes, the one with a wire diameter of 0.04 mm and open gap width of 0.09 mm provided the best mechanical performance under static lap shear testing. In addition, a better weld quality was also obtained with this metal mesh size.

So far, a large number of investigations evaluated the static mechanical performance of the resistance-welded joints. However, only limited data about the fatigue properties of the thermoplastic composites welds are available in the literature [8, 21, 22]. The objective of the present study is thus to characterise the fatigue behaviour of resistance-welded thermoplastic composites. The same materials as the ones used for the heating element optimisation study were considered, i.e., CF/PEKK, CF/PEI and GF/PEI specimens. The optimal metal mesh size previously determined was used for all welds. The welded joints were characterised using optical and scanning electron microscopy (SEM) as well as fatigue lap shear testing. Emphasise was given to comparison between the fatigue behaviours of the semi-crystalline (PEKK) and amorphous (PEI) thermoplastic matrices. The damage accumulation during testing and the failure modes of the welded joints were also investigated.

7.4 Experimental

7.4.1 Materials

The adherends consisted of unidirectional CF/PEKK, unidirectional CF/PEI and fabric GF/PEI laminates. The CF/PEKK and CF/PEI laminates were supplied by Cytec Engineered Materials Inc. and were compression-moulded under standard moulding conditions. These laminates were made of 16 plies, which corresponded to a thickness of 2.2 mm. The GF/PEI material was provided by Ten Cate Advanced Composites. The laminates consisted of 8 plies of 8-harness satin weave, which corresponded to a thickness of 2.0 mm. In order to perform lap shear testing, 101.6 mm long and 25.4 mm wide specimens were cut off from the laminates before being joined by resistance welding.

The heating element was a stainless steel mesh with wire diameter of 0.04 mm and open gap width of 0.09 mm. The thickness of the heating element was 0.08

mm. One neat polymer film (same polymer as the adherends) was placed on each side of the heating element to provide a resin rich region at the weld interface.

7.4.2 Resistance welding

The resistance welding included a DC power supply with maximum output of 40 A and 80 V, a computer/data acquisition system, a pressure system and a resistance welding rig [6]. It consisted of. The lap shear samples were produced one at a time using a resistance welding rig specifically designed to weld this geometry. Ceramic block insulators were used to provide thermal insulation against heat losses in the environment and apply the welding pressure. Copper electrical connectors were used to make the connection between the heating element and power supply. The input power was applied to the heating element using a ramped voltage method. A fixed initial voltage of 2.0 V was first applied to the heating element and the voltage was ramped at a rate of 9.0 V/min. When the weld interface reached a pre-determined welding temperature of 420°C (PEKK) or 400°C (PEI), the current was stopped and the weld interface cooled down [6]. A constant pressure of 1.0 MPa was applied during the process.

7.4.3 Mechanical testing and characterisation methods

The lap shear specimens were 190.5 mm long and 25.4 mm wide with an overlap length of 12.7 mm. The tests were conducted using a servo-hydraulic MTS machine at standard room conditions. The free length between the grips was 139.7 mm. 25.4 mm long and 25.4 mm wide tabs were bonded on the specimens in order to reduce the bending moment in the welds. The static lap shear strengths of all three welded materials was determined in a previous investigation according to the ASTM D1002 standard test method [6]. Based on these results, load-controlled fatigue tests were designed. The specimens were tested under a sinusoidal waveform at various stresses between 20% and 70% of the previously determined lap shear strengths, under a load ratio $R = 0.1$ and a frequency $f = 5$ Hz. Between 11 and 18 specimens were tested for each material. The displacement data at maximum load were recorded at fixed intervals throughout the fatigue tests. The stiffness reduction of the specimens was obtained from these data. No significant heating was noticed during the fatigue testing. The tests were stopped when the specimens broke and could no longer sustain the applied load. When a specimen survived 1 million cycles, the test was terminated and an indefinite fatigue life was reported. The residual lap shear strengths of those samples were then obtained. The fracture surfaces of the broken specimens were observed visually and using scanning electron microscopy (SEM).

7.5 Results

7.5.1 Fatigue performance

Fig. 7-1 presents the fatigue performance of all three materials as a plot of the maximum cyclic stress versus the number of cycles to failure, on a semi-log scale (S-N plot). The static lap shear strengths, i.e., 52 MPa, 47 MPa and 33 MPa for CF/PEKK, CF/PEI and GF/PEI, respectively, are also reported on the graph. The fatigue performances of the CF/PEI and CF/PEKK were similar. However, since the static lap shear strength of the CF/PEKK was approximately 10% higher than the CF/PEI, the latter exhibited a slightly better fatigue performance when plotting the S-N curves in terms of the percentage of the static lap shear strengths (Fig. 7-2). Nevertheless, the indefinite fatigue lives of the two materials were both determined at 25% of their respective static lap shear strengths. These similar fatigue behaviours between the two materials were not expected since PEKK, which is a semi-crystalline polymer, should have a stronger interface with the metal mesh heating element or the fibres of the adherends than the amorphous PEI polymer. As pointed out by Bureau and Denault [23] and Gamstedt *et al.* [24], the strength of the interface between the fibres and polymer is controlled primarily by the polymer morphology, which in turn, is controlled by the processing temperature and cool down rate. Since the welding temperature and cooling rate were not varied and optimised in this study, the morphology of the PEKK polymer could not be controlled and hence, the interfacial bonding with the heating element or carbon fibres of the adherends could not improve the mechanical performance of the CF/PEKK specimens. For example, the cooling rate obtained during the welding of CF/PEKK was around 27°C/s, which corresponds to 1620°C/min. This cooling rate is extremely fast compared to the typical cooling rates of compression-moulded laminates, which are around 10°C/min [25]. The very fast cooling rate obtained here certainly resulted in a very low degree of crystallinity at the weld interface and hence, no interfacial bonding could be obtained between the polymer and the fibres or heating element surfaces. That is, although PEKK is a semi-crystalline polymer, the weld interface, which is the part of interest here, was amorphous, explaining the similarity between the CF/PEKK and CF/PEI performances.

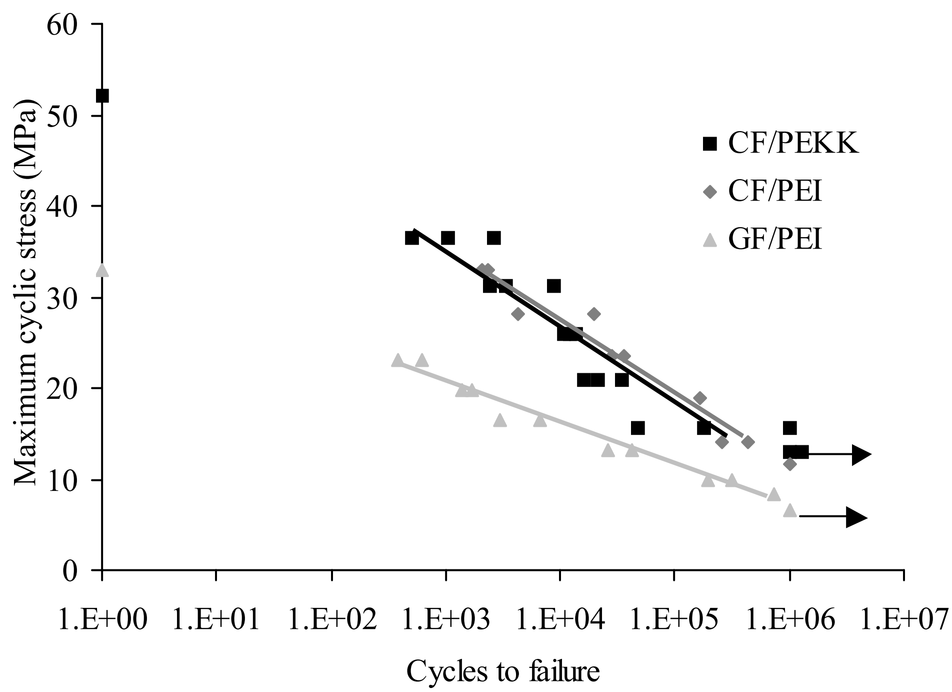

Fig. 7-1. S-N plot of CF/PEKK, CF/PEI and GF/PEI specimens

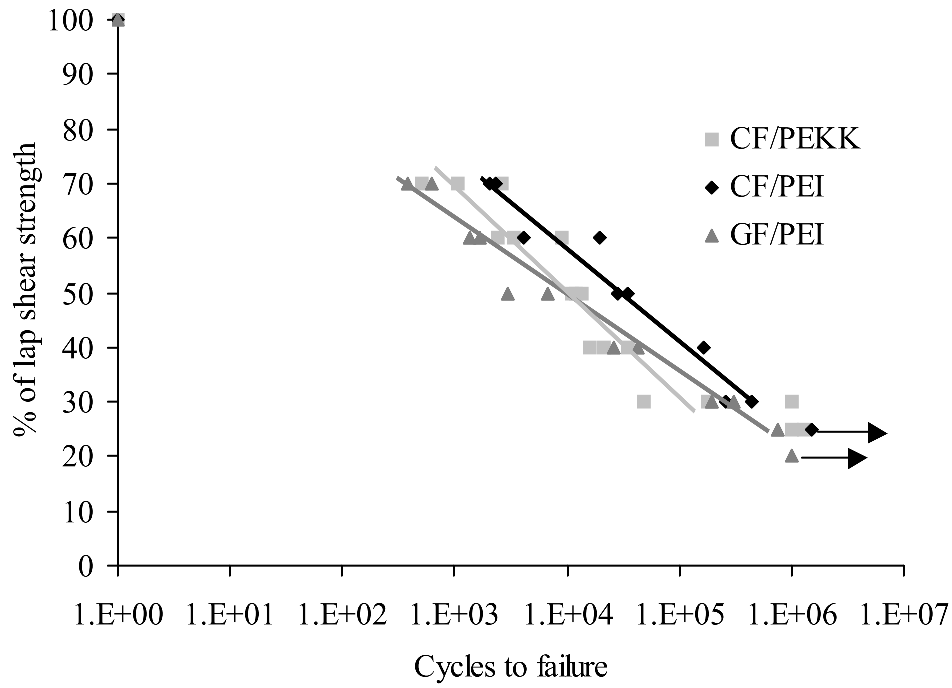

Fig. 7-2. S-N plot in percentage of the static lap shear strengths

For the same maximum cyclic stress, the GF/PEI exhibited a much shorter fatigue life than the CF/PEI or CF/PEKK welds. This behaviour was expected as the static strength of the GF/PEI was approximately 35% lower than the CF/PEI and CF/PEKK specimens. However, when plotting the fatigue lives as a function of the percentage of the static lap shear strength (Fig. 7-2), one can see that the GF/PEI behaved in a similar way as the CF/PEI and CF/PEKK specimens. The indefinite fatigue life of the GF/PEI specimens was obtained at 20% of the static lap shear strength. This lower percentage of the static strength was due to the GF/PEI lower stiffness. The Hart-Smith stress distribution for lap joints is increasingly unfavourable at lower stiffness [26].

The maximum cyclic stresses at which indefinite fatigue lives were obtained can seem to be quite low when compared to the generally reported results about thermoplastic composite materials. However, it should be kept in mind that the lap shear geometry is very poor in terms of load bearing capacity [27]. Under the fatigue testing, peel stresses are induced at the edges of the weld at each loading cycle (Fig. 7-3). Although only the shear stresses were considered and calculated in this study, the peel stresses were also partly responsible for the damage induced to the specimens. In addition, it is believed that the tested lap shear specimens do not have a real fatigue endurance limit as damage is constantly being created in the specimens, even at very low cyclic stresses. The specimens that survived one million cycles exhibited residual static lap shear strengths of approximately 65% of their initial strength values. These reduced strengths are an indication that damage was created in the samples and that the specimens would not survive an infinite number of cycles. These observations are in good agreement with the results of Whitworth *et al.* [28] who investigated the fatigue behaviour of adhesively bonded carbon fibre/epoxy (IM6/3501-6) and CF/PEKK and co-consolidated CF/PEKK lap shear specimens. The same type of fatigue behaviour was reported though the bonded or co-consolidated area was 25.4 mm X 25.4 mm instead of 12.7 mm X 25.4 mm as it is the case here. An indefinite fatigue life of the adhesively bonded IM6/3501-6 composites was reported at 30% of the static lap shear strength. The ones of the adhesively bonded and co-consolidated CF/PEKK were obtained at 25% of their static lap shear strengths, as it is the case here. In addition, the residual strength after the specimens survived one million cycles was reported to vary between 60% and 86% of the initial strengths, which is similar to the results reported here for resistance-welded thermoplastics. However, it should be noted that the static lap shear strength of the adhesively bonded IM6/3501-6 and CF/PEKK and co-consolidated CF/PEKK were 41, 40 and 48 MPa, respectively. That is, although the fatigue behaviours were similar when comparing in terms of percentages of the static lap shear strengths, the resistance-welded CF/PEKK specimens led to a better fatigue performance when comparing in terms of absolute stress values.

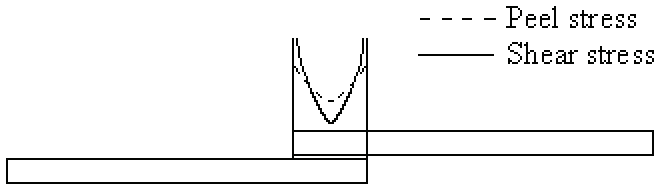

Fig. 7-3. Stress distribution in a lap shear specimen [26]

The stiffness degradation during fatigue testing is an indication of the damage accumulation in the specimens [29]. Fig. 7-4 shows the typical three-step curves commonly observed for the stiffness degradation in composite materials. This example is given for the GF/PEI specimens but the two other materials presented the same behaviours. A rapid stiffness reduction was observed early in the fatigue life followed by a more gradual linear reduction. Near the end of the fatigue life, the reduction rate increases again until failure. The stiffness degradation seems to be dependent upon the applied cyclic stress level. The higher the stress level, the lower the stiffness reduction. This is in agreement with the findings of Whitworth *et al.* for fusion and adhesively bonded lap shear composite specimens where it was shown that the loss of stiffness can be partly attributed to a reduction of the overlap area, due to a crack growth in the bonded region [30].

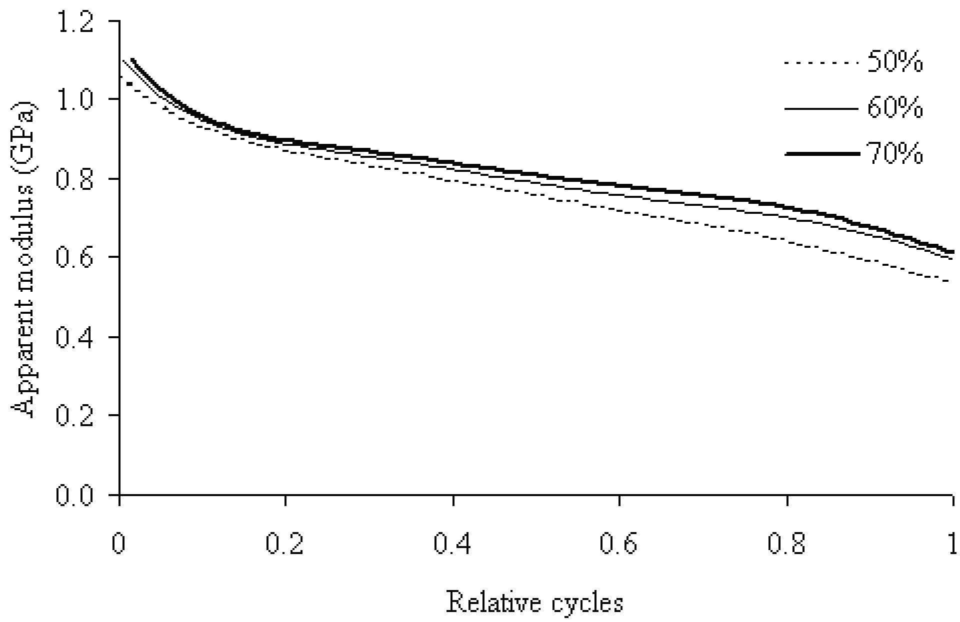

Fig. 7-4. Fatigue life as a function of the maximum applied stress in percentage of the static strengths

7.5.2 Failure behaviour

Two failure modes are typically observed for resistance-welded lap shear thermoplastic composites. The first one is called interfacial failure and occurs at the interface between the weld and the adherends. No damage to the adherends or heating element is observed. The second failure is called interlaminar failure and involves damage to the adherends, the heating element or both of them. A visual observation of the fatigue-tested specimens revealed an interlaminar failure mode, involving damage to the heating element and to the adherends (Fig. 7-5), for all materials and load levels. This failure mode is similar to the one previously-reported under static testing [6]. Fig. 7-6 presents SEM micrographs of the CF/PEKK fracture surfaces. Good fibre wetting is observed in Fig. 7-6 – a, showing that the welding condition allowed the polymer to flow and diffuse in the adherends, promoting good wetting of the fibres. On the other hand, Fig. 7-6 – b shows no significant adhesion between the stainless steel heating element and the PEKK polymer, due to weak interfacial bonding. The same observations were made for the CF/PEI and GF/PEI specimens. The weak interfacial bonding of both the CF/PEI and CF/PEKK is consistent with the similar fatigue performance of these specimens. Since the cooling rate of the CF/PEKK specimens was very fast, the polymer degree of crystallinity at the weld interface was very low and the polymer could be considered amorphous, just as the PEI polymer [25].

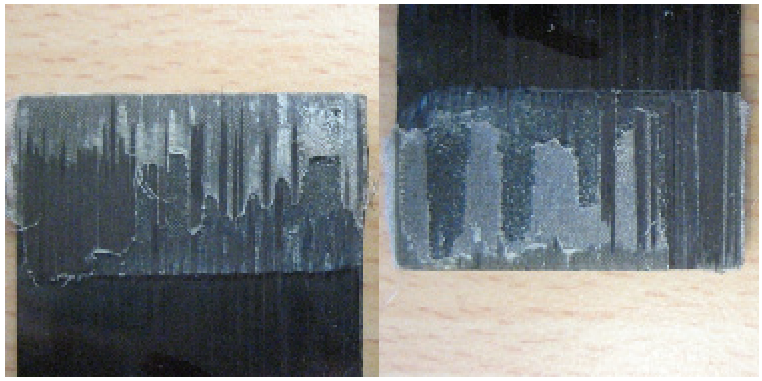

(a)

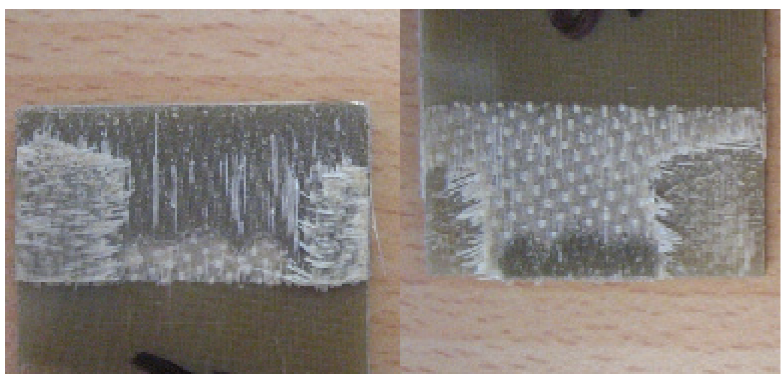

(b)

Fig. 7-5. Fracture surfaces of CF/PEI (a) and GF/PEI (b) specimens

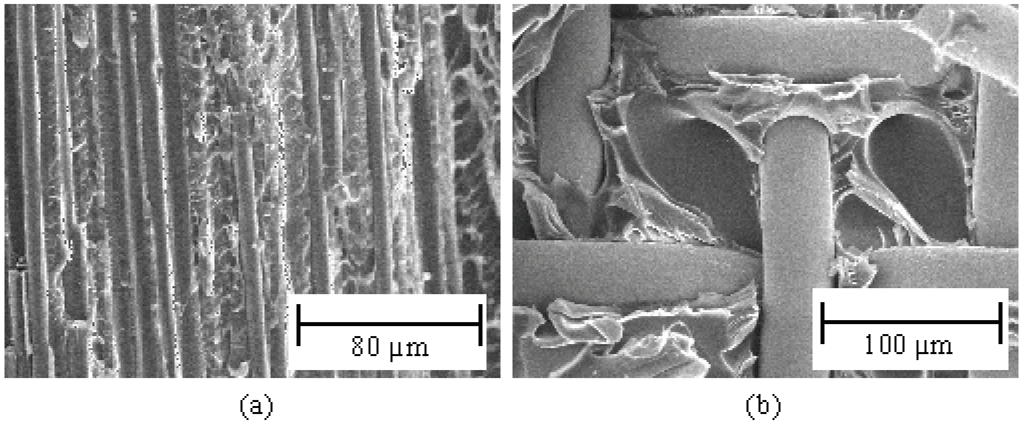

Fig. 7-6. SEM micrographs of the CF/PEKK specimens tested at 60% of the static lap shear strength, showing good wetting of the fibres (a) and poor adhesion with the heating element (b)

The cracks initiated at the edges of the weld and propagated towards the centre. Fig. 7-5 shows that large sections of the heating element were torn out. A deeper look at the fracture surfaces of the specimens using SEM revealed that the heating element tearing process produced striations on the wires surfaces (Fig. 7-7). Those striations were the effect of the peel stress rather than the shearing stress. A schematic of the failure behaviour is presented in Fig. 7-8 to clarify the location of the striations on the heating element wires. These striations could be observed for a large number of wires perpendicular to the load direction. No striations were observed on the wires parallel to the load direction. The pattern of the striations suggests a crack propagation in the z-axis of the wires (Fig. 7-7 and Fig. 7-8). This indicates that the peel stress, which acted perpendicularly to the load direction, was responsible for the crack propagation in the heating element wires (Fig. 7-9).

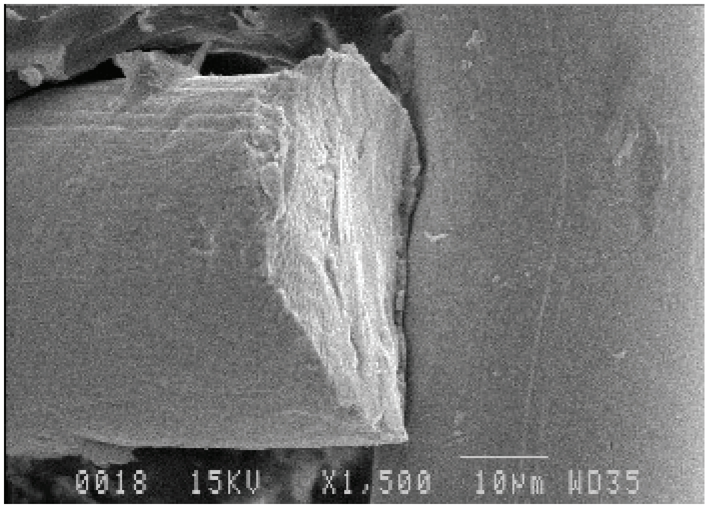

(a)

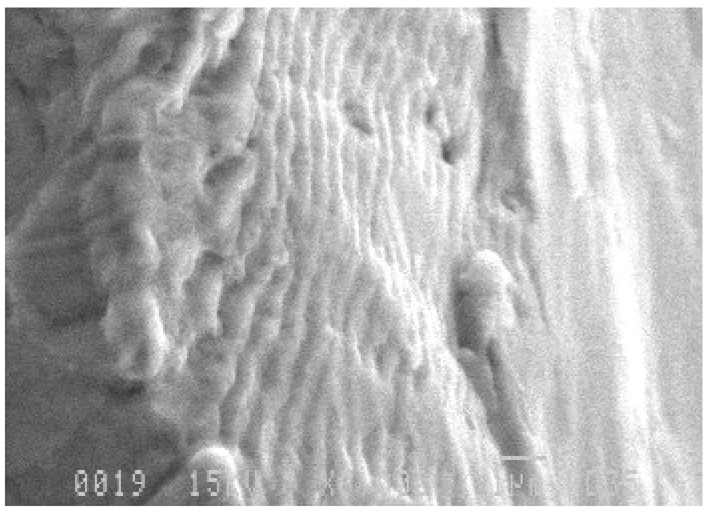

(b)

Fig. 7-7. Striations on stainless steel wires X 1500 (a) and X 8000 (b)

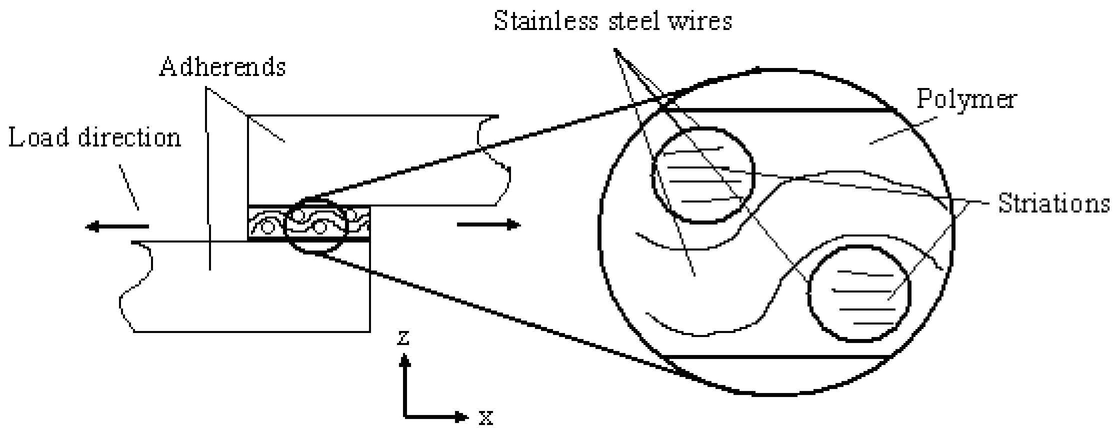

Fig. 7-8. Schematic of the fatigue failure behaviour

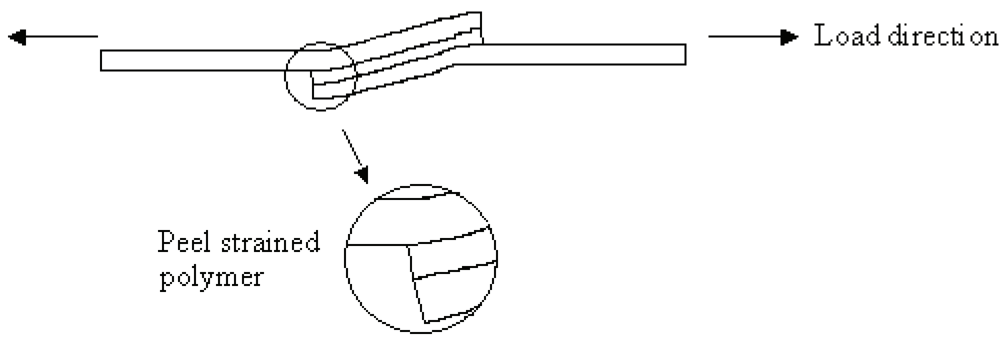

Fig. 7-9. Schematic of a deformed lap shear specimen [31]

7.6 Conclusions

The fatigue performance of resistance-welded CF/PEKK, CF/PEI and GF/PEI lap shear specimens was investigated. The S-N curves showed similar behaviours for all three materials when comparing in terms of percentage of the static lap shear strengths. Indefinite fatigue lives were obtained at 25% of the static lap shear strengths for both the CF/PEKK and CF/PEI specimens. The indefinite fatigue life of the GF/PEI specimens was obtained at 20% of the static lap shear strength. The fracture surfaces revealed a poor adhesion between the polymer and heating element, due to low interfacial bonding. This low interfacial bonding was the reason explaining the similar behaviours obtained for the semi-crystalline and amorphous thermoplastics; the semi-crystalline PEKK polymer did not produce a stronger interface with the stainless steel wires.

Peel stress was shown to have an important effect on the fatigue performance. The peel stress made the heating element debond from the adherends at the edges of the weld, tearing the stainless steel wires. Striations were observed on the stainless steel wires that were perpendicular to the load direction, suggesting a crack propagation through the thickness of the heating element.

Comparing the fatigue behaviour of the resistance-welded thermoplastic composites with the adhesively bonded thermosetting composites revealed the same behaviour when comparing in terms of the percentage of the static lap shear strengths. However, since the static lap shear strength of the resistance-welded thermoplastic was higher than the one of adhesively bonded IM6/3501-6 (52 MPa as opposed to 41 MPa), the fatigue performance of the resistance-welded CF/PEKK was better when comparing in terms of absolute stress values.

Although the heating element that was used in this investigation had been optimised using static lap shear testing, it may not be the optimal heating element to be used for fatigue testing. The effect of the metal mesh size on the fatigue properties of the welds should thus be investigated in a future study. In addition, solutions to improve the interfacial bonding between the heating element and the polymers should be investigated.

7.7 Acknowledgements

This work was supported by funding from the Natural Sciences and Engineering Research Council of Canada. The authors would also like to gratefully acknowledge Mr. David Leach from Cytec Engineered Materials Inc. for

providing the CF/PEKK and CF/PEI laminates and Ten Cate Advanced Composites for providing the GF/PEI material.

7.8 References

1. Stavrov, D., Bersee, H.E.N. Resistance welding of thermoplastic composites - an overview. Composites Part A: Applied Science and Manufacturing 2005;36(1):39-54.

2. Yousefpour, A., Hojjati, M., Immarigeon, J.-P. Fusion Bonding/Welding of Thermoplastic Composites. Journal of Thermoplastic Composite Materials 2004;17(4):303-341.

3. Ageorges, C., Ye, L., Mai, Y.W., Hou, M. Characteristics of resistance welding of lap shear coupons. Part I. Heat transfer. Composites Part A: Applied Science and Manufacturing 1998;29(8):899-909.

4. Ageorges, C., Ye, L., Mai, Y.W., Hou, M. Characteristics of resistance welding of lap shear coupons. Part II. Consolidation. Composites Part A: Applied Science and Manufacturing 1998;29(8):911-919.

5. Ageorges, C., Ye, L., Mai, Y.W., Hou, M. Characteristics of resistance welding of lap-shear coupons. Part III. Crystallinity. Composites Part A: Applied Science and Manufacturing 1998;29(8):921-932.

6. Dubé, M., Hubert, P., Gallet, J.N.A.H., Bersee, H.E.N., Stavrov, D., Yousefpour, A. Metal mesh heating element optimisation in resistance welding of thermoplastic composites. To be submitted to Composites Part A: Applied Science and Manufacturing (September 2007).

7. Dubé, M., Hubert, P., Yousefpour, A., Denault, J. Current leakage prevention in resistance welding of carbon fibre reinforced thermoplastics. Accepted for publication in Composites Science and Technology (September 2007).

8. Dubé, M., Hubert, P., Yousefpour, A., Denault, J. Fatigue failure characterisation of resistance-welded thermoplastic composites skin/stringer joints. Submitted to International Journal of Fatigue (August 2007).

9. Dubé, M., Hubert, P., Yousefpour, A., Denault, J. Resistance welding of thermoplastic composites skin/stringer joints. Composites Part A: Applied Science and Manufacturing 2007;doi:10.1016/j.compositesa.2007.07.014.

10. Eveno, E., Gillespie, J.W.J. Resistance welding of graphite polyetheretherketone composites - An experimental investigation. Journal of Thermoplastic Composite Materials 1988;1:322-338.

11. Hou, M., Friedrich, K. Resistance welding of continuous glass fibre reinforced polypropylene composites. Composites Manufacturing 1992;3(3):153-163.

12. Hou, M., Friedrich, K. Resistance welding of continuous carbon fibre/polypropylene composites. Plastics Rubber and Composites Processing and Applications 1992;18(4):205-213.

13. Stavrov, D., Ahmed, J.T., Bersee, H.E.N. Resistance Welding of Thermoplastic Composites-The Influence of the Metal Mesh Heating Element. SAMPE-Europe, Paris, France, 2007.

14. Stavrov, D., Bersee, H.E.N. Thermal Aspects in Resistance Welding of Thermoplastic Composites. ASME Summer Heat Transfer Conference, Las Vegas, USA, 2003.

15. Dubé, M., Hubert, P., Gallet, J.N.A.H., Stavrov, D., Bersee, H.E.N., Yousefpour, A. Heating Element Optimization in Resistance Welding of Semi-Crystalline and Amorphous Thermoplastic Composites. CANCOM, Winnipeg, Canada, 2007.

16. Hou, M., Yang, M.B., Beehag, A., Mai, Y.W., Ye, L. Resistance welding of carbon fibre reinforced thermoplastic composite using alternative heating element. Composite Structures 1999;47(1-4):667-672.

17. Stavrov, D., Bersee, H.E.N. Experimental Investigation of Resistance Welding of Thermoplastic Composites with Metal Mesh Heating Element. SAMPE-Europe, Paris, France, 2004.

18. Stavrov, D., Bersee, H.E.N., Beukers, A. The Influence of the Heating Element on Resistance Welding of Thermoplastic Composite Materials. International Conference on Composite Materials, San Diego, USA, 2003.

19. Yousefpour, A., Simard, M., Octeau, M.-A., Lamarée, M., Hojjati, M. Effects of Mesh Size on Resistance Welding of Thermoplastic Composites Using Metal Mesh Heating Elements. SAMPE-Europe, Paris, France, 2004.

20. Yousefpour, A., Simard, M., Octeau, M.-A., Hojjati, M. Process Optimization of Resistance-Welded Thermoplastic Composites Using Metal Mesh Heating Elements. SAMPE, Long Beach, USA, 2005.

21. Dubé, M., Hubert, P., Yousefpour, A., Denault, J. Fatigue Performance of Resistance-Welded Thermoplastic Composite Skin/Stringer Joints. SAMPE-Europe, Paris, France, 2007.

22. Yousefpour, A., Hojjati, M. Static and fatigue behavior of fusion bonded APC-2/AS4 thermoplastic composite joints. SAMPE-Europe, Paris, France, 2007.

23. Bureau, M.N., Denault, J. Fatigue Behavior of Continuous Glass Fiber Composites: Effect of the Matrix Nature. Polymer Composites 2000;21(4):9.

24. Gamstedt, E.K., Berglund, L.A., Peijs, T. Fatigue mechanisms in unidirectional glass-fibre-reinforced polypropylene. Composites Science and Technology 1999;59(5):10.

25. Yousefpour, A., Hojjati, M. Cooling Rate Influences on Crystallization of PEKK anb PPS Thermoplastic Polymers. CANCOM, Winnipeg, Canada, 2007.

26. Hart-Smith, L.-J., Analysis and design of advanced composites bonded joints. Vol. N.r. CR-2218. 1974.

27. Quaresimin, M., Ricotta, M. Fatigue behaviour and damage evolution of single lap bonded joints in composite material. Composites Science and Technology 2006;66:176-187.

28. Whitworth, H.A., Othieno, M., Yin, S.W., Sawicki, A., LIorente, G. Evaluation of composite bonded joints. ASME, Los Angeles, USA, 1995.

29. Whitworth, H.A. A stiffness degradation model for composite laminates under fatigue. Composite Structures 1997;40(2):7.

30. Whitworth, H.A. Fatigue Evaluation of Composite Bolted and Bonded Joints. Journal of Advanced Materials 1998;30(2):25-31.

31. Structural behavior of joints, MIL-Handbook, MIL-HDBK-17-3F, Vol.3.

CHAPTER 8. CONCLUSIONS AND FUTURE WORK

The static and fatigue behaviour of thermoplastic composite laminates joined by resistance welding was investigated. Two weld configurations, i.e., the skin/stringer and lap shear geometries and four composite materials, i.e., APC-2/AS4, CF/PEKK, CF/PEI and GF/PEI were investigated.

A more realistic specimen was proposed for the characterisation of aerospace skin/stringer welded joints. The effects of the input power level and clamping distance on weld quality were studied for a quasi-isotropic APC-2/AS4 skin/stringer configuration. The power level was found to have an effect on the temperature distribution at the weld interface and the weld static mechanical performance. An optimum clamping distance of 1.5 mm led to better temperature uniformity over the weld area. Failure modes similar to the ones of an adhesively bonded thermosetting composite skin/stringer configuration were obtained. The cracks initiated at the flange tip, either at the weld interface or in the skin laminate and then propagated towards the centre of the weld, either in the skin laminate or at the weld interface. In addition, two methods of reducing the stress concentration at the flange tips were investigated. The method consisting in tapering the edges of the flange after the welding operation led to a mechanical performance improvement of 25% compared to a square-ended flange.

An innovative solution to the current leakage problem was developed. A ceramic (TiO_2) coating was developed to insulate the heating element from the adherends. The coating was 2.0 µm thick and was deposited on the heating element using the high velocity thermal spraying method. The coating successfully prevented current leakage and did not lead to any mechanical performance penalty under static loading. In addition, the ceramic coating facilitated the welding process by shortening the welding time, improving the temperature homogeneity in the welds and improving the control of the welding process.

The fatigue properties for the skin/stringer joint were investigated. The fatigue performance of the skin/stringer joints was studied at levels varying between 35% and 80% of the static damage initiation load. The failure modes of APC-2/AS4 quasi-isotropic specimens were the same as the ones observed under static loading. In general, the first crack was located at the edge of the flange, at the ±45° plies interface. A matrix crack branching to the weld interface was then observed and the crack kept growing at the weld interface, towards the centre of the weld. This failure mode was also similar to previously reported studies on adhesive bonding of thermosetting composites. No impact of the ceramic coating on the fatigue properties of the welds was observed. Indefinite fatigue lives were obtained at 40% and 35% of the static damage initiation loads for the UD and quasi-isotropic specimens, respectively.

The mesh geometry was optimised for the lap shear strength of CF/PEKK, CF/PEI and GF/PEI adherends. The effects of the stainless steel heating elements wire diameter and open gap width on the mechanical performance of the welds under static loading were studied for CF/PEKK, CF/PEI and GF/PEI materials using the lap shear geometry. A heating element with a wire diameter of 0.04 mm and open gap width of 0.09 mm led to the best mechanical performance. This optimum heating element was then used to conduct the investigation of the fatigue properties of the lap shear welds. It was found that the fatigue performance of those materials, in terms of absolute loads or stresses, was superior to the performance of adhesively bonded thermosetting composites.

8.1 Future work

For future work in the development of the resistance welding of thermoplastic composites, a method of improving the interfacial bonding between the stainless steel heating element and the PEEK, PEKK and PEI polymers should be developed. It was shown that the weld strength relied primarily on mechanical interlocking at the weld interface. Having a good adherence between the heating element and the polymer should improve the weld strength and the fatigue behaviour.

The impact of environmental conditions on the mechanical performance of the welds should also be investigated. For example, airplanes are subjected to severe temperature gradients, ranging from –40°C to +30°C. These large gradients, as well as variable humidity conditions, may have an effect on the mechanical behaviour of the welds.

Finally, the possibility to use resistance welding for large-scale components should be investigated, as there is no information available in the literature on that topic. It was shown in the presented work that a uniform temperature distribution at the weld interface can be hard to achieve, even for small weld areas. The experimental and modelling studies on large-scale components should thus focus on the heat transfer phenomena in the welds, as a uniform temperature distribution on large components is expected to be even more difficult to achieve. Consolidation and crystallisation models of large-scale welding should also be included in the heat transfer model as those analyses were performed for small weld areas only. Those analyses are important in order to optimise the welding process, especially if semi-crystalline polymers are welded, as the welding parameters, e.g., the welding temperature and cooling rate, influence the polymer morphology, which in turn has an effect on the weld mechanical performance.

APPENDIX A. MATERIALS AND EXPERIMENTAL PROCEDURES

The details of the materials and experimental procedures that were used in this study are presented in this section.

A.1 Materials

A.1.1 Adherends

Five material systems were used as adherends in this work. The laminates were compression-moulded in a Wabash press and cut to the desired specimen geometry using a water-cooled diamond saw. The characteristics of each material system are presented in Table A-1.

Table A-1. Adherends

	Quasi-isotropic APC-2/AS4	UD APC-2/AS4	CF/PEKK	CF/PEI	GF/PEI
Supplier	CYTEC Engineered Materials, inc.	CYTEC Engineered Materials, inc.	CYTEC Engineered Materials, inc.	Ten Cate Advanced Composites	Ten Cate Advanced Composites
Polymer type	Semi-crystalline	Semi-crystalline	Semi-crystalline	Amorphous	Amorphous
T_g (°C)	143	143	156	218	218
T_m (°C)	343	343	310	-	-
Processing cycle	Processing temperature = 390°C Moulding pressure = 0.7 MPa Residence time = 20 min.	Processing temperature = 390°C Moulding pressure = 0.7 MPa Residence time = 20 min.	Processing temperature = 360°C Moulding pressure = 0.7 MPa Residence time = 20 min.	Processing temperature = 360°C Moulding pressure = 1.0 MPa Residence time = 15 min.	Processing temperature = 360°C Moulding pressure = 1.0 MPa Residence time = 15 min.
Lay-up	UD prepreg $[\pm45/90/0]_{2S}$	UD prepreg $[0]_{16}$	UD prepreg $[0]_{16}$	UD prepreg $[0]_{16}$	8-harness satin weave fabric $[0]_8$
Laminate thickness (mm)	2.2	2.2	2.2	2.2	2.0
Welded specimen geometry	Skin/stringer	Skin/stringer	Lap shear	Lap shear	Lap shear
Adherend dimensions (mm)	Flange: 25.4 X 50 Skin: 25.4 X 130	Flange: 25.4 X 50 Skin: 25.4 X 130	25.4 X 101.6	25.4 X 101.6	25.4 X 101.6

A.1.2 Heating elements

Five stainless steel meshes were used as heating elements. The heating elements were cut to dimensions of 25.4 mm X 75 mm (skin/stringer specimens) and 12.7 mm X 50 mm (lap shear specimens). The characteristics of each mesh are presented in Table A-2 along with the materials that were welded using each mesh. The electrical resistances were calculated experimentally using the following formula:

$$R = V/I$$

where R is the electrical resistance (Ω), V is the monitored voltage (V) and I is the monitored current (A).

Table A-2. Heating elements

Heating element	**A**	**B**	**C**	**D**	**E**
Wire diameter (mm)	0.114	0.066	0.041	0.036	0.025
Open gap width (mm)	0.152	0.104	0.089	0.043	0.038
Linear wire density (wires/mm)	3.9	5.8	7.7	12.5	14.3
Electrical resistance (Ω)	0.081	0.151	0.290	0.385	0.392
Welded geometry	Lap shear	Lap shear	Skin/stringer	Lap shear	Lap shear
Welded materials	GF/PEI	GF/PEI CF/PEI CF/PEKK	GF/PEI CF/PEI CF/PEKK APC-2/AS4	GF/PEI CF/PEI CF/PEKK	GF/PEI CF/PEI

A.1.3 Coating

A ceramic coating was applied on some of the stainless steel mesh heating elements. This coating was made of nanostructured titanium oxide (TiO_2) powders. This powder was produced by Altair Nanomaterials Inc. and was deposited on the mesh using the high velocity oxy-fuel (HVOF) thermal spraying method. The meshes to be coated were cut to the desired dimensions, cleaned with acetone and placed on an aluminium plate. HVOF spraying was then conducted on the meshes with special care not to coat the edges, which have to be connected to the copper electrical connectors. The TiO_2 layer applied on the heating element was 2 μm thick.

A.1.4 Polymer films

Neat polymer films, which were supplied by the same manufacturer as the adherends, were placed on each side of the heating element prior to the welding operation. The films were cut to dimensions of 25.4 mm X 50.0 mm and 12.7 mm X 25.4 mm for the skin/stringer and lap shear geometries, respectively and cleaned with acetone. The films were 0.127 mm thick.

A.2 Experimental procedures

A.2.1 Resistance welding

The welding operation was conducted using a DC power supply with maximum output of 40 A and 80 V. A Labview program was designed to control the welding process. The inputs of the program were the desired welding temperature or welding time and the input voltage or ramped voltage rate. The outputs of the program were the weld interface temperature as a function of time and the voltage and current, which were measured at the electrical connectors. Resistance welding rigs were designed and manufactured to weld the skin/stringer and lap shear specimens. The rigs consisted of fibreglass plates, ceramic block insulators and copper electrical connectors. The skin/stringer and lap shear rigs are shown in Figs. A-1 and A-2, respectively.

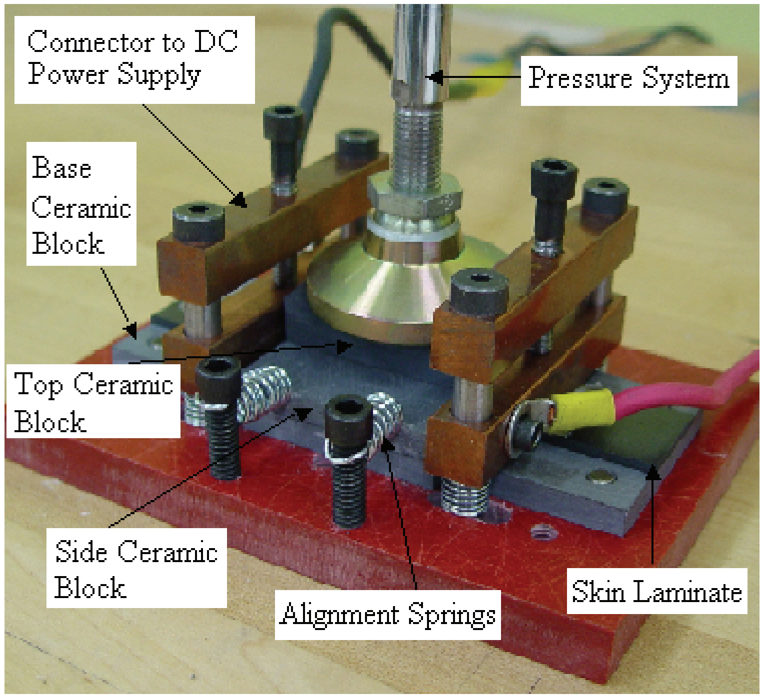

Fig. A-1. Skin/stringer resistance welding rig

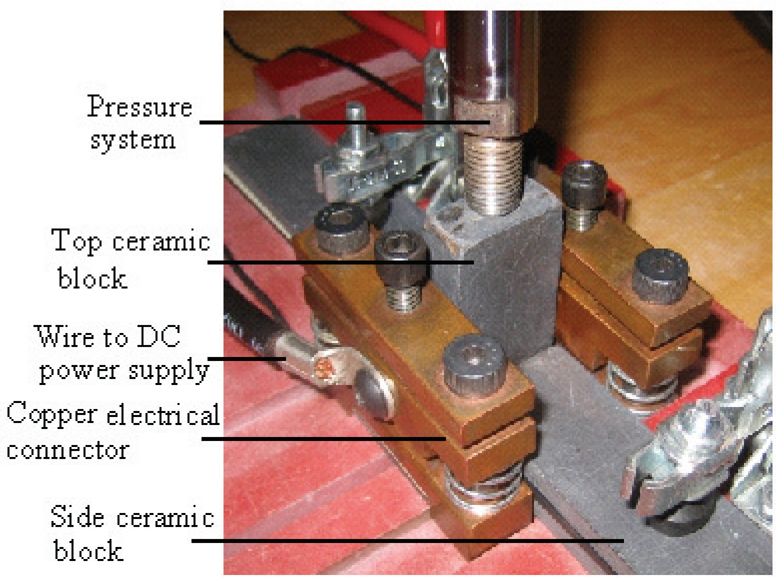

Fig. A-2. Lap shear resistance welding rig

The details of each component of the skin/stringer and lap rigs are presented in Tables A-3 and A-4.

Table A-3. Skin/stringer resistance welding rig components details

Component	Thickness (mm)	Width (mm)	Length (mm)
Base ceramic block	6.4	50.8	130.0
Side ceramic blocks	25.4	25.4	50.0
Top ceramic block	25.4	25.4	50.0
Copper electrical connectors	12.7	12.7	70.0

Table A-4. Lap shear resistance welding rig components details

Component	Thickness (mm)	Width (mm)	Length (mm)
Base ceramic block	6.4	25.4	200.0
Side ceramic blocks	6.4	25.4	100.0
Top ceramic block	12.7	25.4	50.8

The following steps were followed to weld the APC-2/AS4 skin/stringer specimens:

1) The skin laminate was placed on the base ceramic block insulator;
2) A neat PEEK polymer film was placed on the skin laminate, at the centre between the two electrical connectors;
3) The heating element was placed on the PEEK film and clamped under the two electrical connectors;
4) A second PEEK film was placed on the heating element;
5) The flange laminate was placed on the second PEEK film;
6) Pressure was applied using the top ceramic block insulator and a pneumatic pressure system;
7) The voltage was applied to the heating element.

To weld the APC-2/AS4 skin/stringer specimens, constant voltages of 9.0 V and 9.5 V were used, as well as three ramped voltages rates of 1.5 V/s, 3.0 V/s and 6.0

V/s. In all cases, the input voltage was stopped when the weld interface temperature reached 440°C. A constant welding pressure of 1.0 MPa was used during the welding operation. This pressure was released and the specimens were removed when the weld interface temperature was below 80°C.

The following steps were followed to weld the CF/PEKK, CF/PEI and GF/PEI lap shear specimens:

1) The first laminate was placed on the base ceramic block insulator, between the two electrical connectors;
2) A neat polymer film of the same polymer as the material to be welded was placed on the first laminate, at the centre between the two electrical connectors;
3) The heating element was placed on the polymer film and clamped under the two electrical connectors;
4) A second polymer film was placed on the heating element;
5) The second laminate was placed on the second polymer film;
6) Pressure was applied using the top ceramic block insulator and a pneumatic pressure system;
7) The voltage was applied to the heating element.

A ramped voltage rate of 9.0 V/s was used to weld the lap shear specimens. The input voltage was stopped after the weld interface temperature reached 420°C and 400°C for the CF/PEKK and PEI specimens, respectively. Again, a constant pressure of 1.0 MPa was used during the welding process. This pressure was released and the specimens were removed when the weld interface temperature was below 80°C.

A.2.2 Ultrasonic inspection

The ultrasonic inspection was performed on the skin/stringer specimens. The specimens were immersed in a multi-axes ultrasonic water bath, with the flange facing the bottom of the bath. The ultrasonic signal was sent on the backside of the skin laminate in both the length and width directions. C-Scan and B-Scan images were obtained from this inspection.

A.2.3 Optical microscopy

The specimens were cut using a water-cooled diamond saw at the desired locations to be observed. They were embedded in an epoxy resin and the faces to be observed were then polished using the method described in Table A-5.

Table A-5. Polishing method

Step	Abrasive	Lubrifiant	Rotating speed (RPM)	Polishing time
1	Sand paper (SiC) 800	Water	300	2 X 20 seconds
2	Sand paper (SiC) 1200	Water	300	2 X 20 seconds
3	Sand paper (SiC) 4000	Water	300	4 X 20 seconds
4	6 microns abrasive	DP red	150	1 X 360 seconds
5	3 microns abrasive	DP red	150	1 X 360 seconds

The specimens were observed using an Olympus microscope at magnitudes varying between 5 and 100 X.

A.2.4 Scanning electron microscopy

Scanning electron microscopy was used to observe the fracture surfaces of the tested specimens. The faces to be observed were first coated with a thin layer of gold-palladium using a Hummer V deposition instrument. The specimens were the observed using a Jeol JSM-6100 microscope at magnitudes varying between 100 and 5000 X.

A.2.5 Mechanical testing

All the mechanical tests were conducted at room conditions, i.e., temperature of 23°C and relative humidity of 50%.

A.2.5.1 Static three- and four-point bending tests

The three- and four-point bending tests were conducted on the skin/stringer specimens using an Instron 5500R testing machine and a load cell of 25 kN. They were tested under displacement control at a speed of 2.0 mm/min. The load was applied on the backside of the skin laminate. Various spans were used as depicted in Fig. A-3. The supports and loading nose had a 12.7 mm diameter. The load and displacement date were recorded during testing and the tests were stopped after a delamination could be observed in the specimens. In order to observe the fracture surfaces of the broken specimens, some tests were continued until the flange would completely debond from the skin laminate.

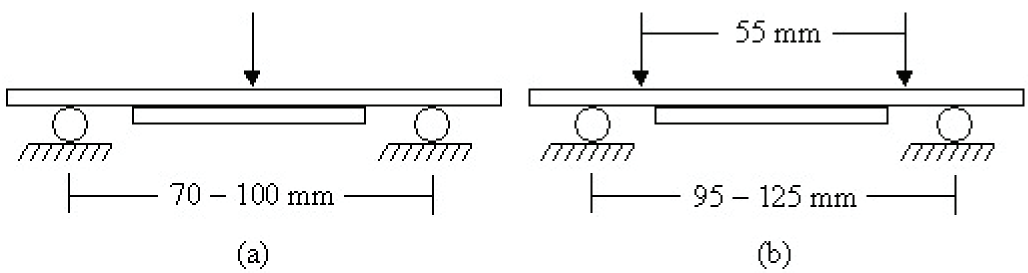

Fig. A-3. Three- (a) and four (b)-point bending tests

A.2.5.2 Short beam shear tests

The short beam shear tests were conducted according to the ASTM D 2344/D 2344 M standard testing method using a 25 kN load cell. The samples were cut from the skin/stringer specimens as shown in Fig. 4-4. The samples were first cut using a water-cooled diamond saw then polished to the exact desired dimensions of 4.6 mm thick, 9.2 mm wide and 25.4 mm long. A displacement-controlled speed of 1.0 mm/min. was used for all tests. The bottom support span was 18.4 mm long. The bottom supports had a 6.0 mm diameter and the loading nose had a 3.0 mm diameter. The ILSS was obtained from the following formula:

$$ILSS = 0.75 \times P_m / (b \times h)$$

where P_m is the maximum recorded load (N) , b is the sample width (mm) and h is the sample thickness (mm).

A.2.5.3 Static lap shear tests

The lap shear tests were conducted according to the ASTM D 1002 standard testing method. The specimens were 190.5 mm long and 25.4 mm wide with an overlap length of 12.7 mm (Fig. A-4). Tabs made of the same material as the material to be tested were bonded to the ends of the specimens in order to reduce the eccentricity in the load path. The tabs were 25.4 mm long and 25.4 mm wide. The ends the specimens were clamped in hydraulics grips and the tensile load was applied using a displacement-controlled crosshead speed of 1.27 mm/min. The LSS was obtained from the following formula:

$$LSS = P_m / (b \times h)$$

where P_m is the maximum recorded load (N), b is the welded area length (mm) and h is the welded area width (mm).

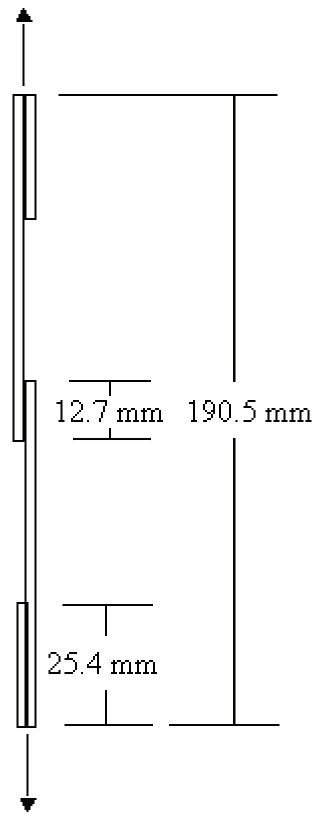

Fig. A-4. Schematic of lap shear test

A.2.5.4 Fatigue three-point bending tests

The fatigue three-point bending tests were conducted on the skin/stringer specimens using a MTS MVDT/244-22 testing machine and the same three-point bending set-up as the one used for the static tests. The specimens were tested under a sinusoidal waveform at various maximum loads between 35% and 80% of the static damage initiation loads. A load ratio (maximum load / minimum load) of R = 0.1 and frequency f = 5 Hz were used for all tests. Between 10 and 15 specimens were tested for each condition. The edges of the specimens were slightly polished prior to testing and the crack initiation and growth rate was documented using a travelling microscope. The maximum and minimum load and deflection data were recorded at fixed intervals throughout the tests, as shown in Table A-6. The stiffness reduction of the specimens was obtained from these data. Thermocouples were installed on some of the specimens and no significant heating was noticed during the fatigue testing.

Table A-6. Data recording schedule

	Data recorded at each N cycle
Between 1 and 10 cycles	1
Between 10 and 100 cycles	10
Between 100 and 10000 cycles	100
Between 1000 and 10 000 cycles	1000
Between 10 000 and 100 000 cycles	10 000
Between 100 000 and 1 000 000 cycles	100 000

A.2.5.5 Fatigue lap shear tests

The fatigue lap shear tests were conducted using a MTS mechanical testing machine and the same lap shear set-up as the one used for the static tests. The specimens were tested under a sinusoidal waveform at various maximum loads between 25% and 70% of the static failure loads. A load ratio (maximum load / minimum load) of R = 0.1 and frequency f = 5 Hz were used for all tests. Between 11 and 18 specimens were tested for each condition. The maximum and minimum load and displacement data were recorded at fixed intervals throughout the tests, as shown in Table A-6 (same schedule as for the fatigue three-point bending tests). The apparent modulus reduction of the specimens was obtained from these data. Thermocouples were installed on some of the specimens and no significant heating was noticed during the fatigue testing.